



EVALUATION OF A RIGID ELEMENT FOR OFFSHORE APPLICATIONS

JAN JERMAN

THESIS

Presented in partial fulfilment of the requirements for the degree of
Spécialité internationale “Géomécanique, Génie Civil et Risques”
(Geomechanics, Civil Engineering and Risks)

Université Joseph Fourier – Plaxis bv

June, 2014

Project Advisors:

- Ronald Brinkgreve (Plaxis bv)
- Richard Witasse (Plaxis bv)

Examiner at Home University:

- David Mašín (Charles University in Prague, Czech Republic)



ABSTRACT

In the latest version of finite element software Plaxis 3D kernel rigid bodies were implemented as a Plaxis 3D feature to enable the application of forces from offshore superstructures on the offshore foundation structure. A rigid body is an object without any change in shape during motion. Thus, the distance between every two point in the body remains constant and kinematics of rigid body motion is expressed in terms of translation and rotation. A driving force for implementation of rigid bodies was the fact, that the stiffness of the offshore foundations as suction piles compared to stiffness of the soil on the seabed is by many orders higher, thus the behavior of these structures can be modelled as behavior of a rigid body with six degrees-of-freedom and with forces applied to the reference point. In the project implementation of rigid bodies in Plaxis is validated for all the basic calculation options used in Plaxis. Then, a model of a suction pile. Computational times for models with rigid bodies and models with stiff structural elements are compared for both solver types in Plaxis -iterative solver Picos and direct solver Pardiso. A procedure how to determine single terms of soil response stiffness matrix from Plaxis computational results after applying the individual force components is created for two cases – environmental loading only and static loading by the structure with additional environmental loading. Then, the procedure is used to determine a stiffness matrix for full scale field test of a suction pile supporting jack-up structure obtained from a company manufacturing and designing suction piles. Coupling and evolution of stiffness matrix with change of load are studied using different material models- linear elastic, Mohr-Coulomb and Hardening soil model.

TABLE OF CONTENTS

Abstract	iv
Table of Contents	v
List of Tables	vii
List of Figures	viii
1 Introduction	1
1.1 Background Information	1
1.2 Problem description	1
1.3 Objectives.....	2
1.4 Report structure	2
2 Literature review	4
2.1 Offshore foundations	4
2.1.1 History of offshore geotechnics	4
2.1.2 Suction anchors.....	5
2.1.3 Other types of offshore foundations	10
2.1.4 Loading conditions of offshore foundations	15
2.1.5 Offshore foundations as rigid bodies	18
2.2 Plaxis Kernel and rigid body	20
2.2.1 Rigid body.....	20
2.2.2 Rigid body implementation in Plaxis 3D kernel	21
2.2.3 Solver types used in Plaxis	23
2.3 Conclusion	25
3 Comparison of Pardiso and Picos solvers and calculation times	26
3.1 Expected results	26
3.2 Performed calculations	27
3.3 Results	28
3.4 Conclusion	28
4 Case study – suction anchor	30
4.1 Problem description	30
4.2 Plaxis model.....	31
4.2.1 Model properties	31
4.2.2 Calculations.....	34
4.2.3 Results.....	35
4.3 Model with rigid body	36
4.4 Stiffness matrix determination.....	38
4.4.1 Description of the procedure.....	38
4.4.2 Validation of the procedure – environmental loading.....	40
4.4.3 Validation of the procedure – static loading.....	42
4.4.4 Stiffness matrix determination for the case study.....	47

4.5 Conclusion	50
5 Conclusions and recommendations.....	52
6 Bibliography.....	55
7 Appendix A: Verification of rigid body in Plaxis 3D	58
7.1 Basic rigid body validations	58
7.1.1 Interfaces	58
7.1.2 Model behavior with rigid bodies	62
7.1.3 Construction of an embankment – safety analysis	65
7.1.4 Consolidation	70
7.1.5 Dynamic calculations	73
7.2 Suction anchor bearing capacity	77
7.2.1 Basic model properties	77
7.2.2 Description of the model	80
7.2.3 Results	84
7.3 Conclusion	89
8 Appendix B:	91
8.1 Sign convention	91
8.2 Units used in Plaxis.....	91
8.3 Global iterative procedure used in Plaxis.....	91
8.4 Finite element calculation process based on the elastic stiffness matrix.....	92
9 Curriculum vitae.....	94

LIST OF TABLES

Table 1: Summary of expected results.	27
Table 2: Calculation times of Picos and Pardiso solvers (in seconds).	28
Table 3: Soil properties.	32
Table 4: Plate properties.	33
Table 5: Applied forces and displacements.....	41
Table 6: Material properties	59
Table 7: Maximum shear force applied to upper block	61
Table 8: Evolution of maximum shear force with stiffness difference of the two blocks.....	62
Table 9: Soil properties of embankment and subsoil (Plaxis, 2014)	66
Table 10: Footing material properties.....	68
Table 11: Footing material description	71
Table 12: Material properties	74
Table 13: Soil properties	78
Table 14: Plate properties	79
Table 15: Hypothetical capacity cases	79
Table 16: Mesh definitions – overall coarseness, coarseness factor (CF) and computation time	83
Table 17: Optimal load attachment point.....	84
Table 18: Combined loading - comparison of Plaxis results and results from Andersen (2005).	87
Table 19: Basic units used in Plaxis.	91

LIST OF FIGURES

Figure 1: Suction pile before installation with its load attachment point called pad-eye (Monajemi and Razak, 2009).....	6
Figure 2: Two types of mooring systems (Vryhof, 2014).	7
Figure 3: Two-point mooring system for a vessel (Narasimha et al, 2006).	7
Figure 4: Suction pile installation with shown loads applied to the anchor (Saito et al, 2004).	8
Figure 5: Catenary horizontal loading type on the left and taut legged vertical loading type on the right (Huang, 2003)	9
Figure 6: Failure modes for suction pile subjected to vertical tensile loads (Dang et al, 2003).	10
Figure 7: Mudmat at the bottom of the jacket structure (Advanced Geomechanics, 2012)..	11
Figure 8: Jacket structure, North Rankin platform, with piles used as foundations (Randolph et al, 2009).....	12
Figure 9: Spudcan foundation and the drilling rig (Lee and Randolph, 2011).	13
Figure 10: Jack - up rig installation, preloading and operation (Randolph et al, 2005).	14
Figure 11: Applications of shallow offshore foundations (Randolph et al, 2005).....	14
Figure 12: Comparison of offshore and onshore design loads showed at Taywood Seltrust offshore platform and One Shell Plaza skyscraper in Houston (Randolph et al, 2005).	16
Figure 13: Vertical, horizontal and moment loads applied to the pile foundation (Randolph et al, 2005).....	16
Figure 14: Combined loading applied to a spudcan footing (Randolph et al, 2005).....	17
Figure 15: Loading of spudcans during the storm conditions (Randolph et al, 2005).	17
Figure 16: Combined vertical, horizontal and moment loading applied to mudmat foundation (Randolph et al, 2005).	18
Figure 17: Deformed mesh and contour shadings during maximum wave loading of the Troll-A platform (Andersen et al, 2008).....	19
Figure 18: Solver type option in Plaxis 3D interface.	25
Figure 19: Suction pile (courtesy of E. Alderlieste).	30
Figure 20: Design of the suction pile and the jack-up structure (courtesy of E. Alderlieste).	31
Figure 21: Suction pile as modelled in Plaxis.	34
Figure 22: Final mesh of the model.....	34
Figure 23: Loading applied to the suction pile.	35
Figure 24: Resultant bearing capacity of the suction pile.	36
Figure 25: Comparison of rigid body and plate suction pile bearing capacity.	37
Figure 26: Performed calculations as shown in Plaxis Input program.	39

Figure 27: Load-displacement curve with highlighted secant stiffness matrices. The case of environmental loading in black and the case of static loading + environmental loading in red.	43
Figure 28: Reference point and forces and moments applied to the rigid body.	44
Figure 29: All calculation phases carried out in Staged construction.	45
Figure 30: Mohr - Coulomb model.	48
Figure 31: Model definition in Plaxis 3D.	59
Figure 32: Calculation phases.	60
Figure 33: Comparison of evolution of force/displacement curve for prescribed surface displacement (red) and rigid body (pink) for internal friction angle of interface 30°. In red are shown the same curves for internal friction angle 0° for both rigid body and prescribed surface displacement.	60
Figure 34: Convergence of interface stiffness for rigid body a prescribed surface displacement.	62
Figure 35: Model to test symmetry.	63
Figure 36: Two rigid bodies in model.	63
Figure 37: Plate elements rigid body.	64
Figure 38: Comparison of soil volume rigid body and plate rigid body	64
Figure 39: Model geometry definition	67
Figure 40: Position and geometry of the footing with interfaces.	67
Figure 41: Calculation phases of the whole project.	68
Figure 42: Failure mechanism evolution after footing installation.	69
Figure 43: Evolution of $\sum Msf$ with deformation, the reference point for the deformation is at the tip of an embankment.	70
Figure 44: Model definition.	71
Figure 45: Generated mesh.	72
Figure 46: Calculation phases.	72
Figure 47: Consolidation beneath the footing	73
Figure 48: Model definition.	74
Figure 49: Generated mesh.	75
Figure 50: All carried out calculation phases	75
Figure 51: Free vibration of the upper soil layer after release of a surface load.	76
Figure 52: Soil layers as used in C3 and C4 on the left and C1 and C2 on the right.	80
Figure 53: The suction pile geometry of the models using soil body and soil rigid body81	81
Figure 54: The suction pile geometry in models using plates and plate rigid bodies81	81
Figure 55: Generated mesh.	82
Figure 56: Bearing capacity for different meshing, C3 case with soil rigid body82	82

Figure 57: Mesh coarseness factor changes	83
Figure 58: Horizontal bearing capacity (C3)	85
Figure 59: Combined loading of C3 case. In blue are shown results for very stiff soil body and in red for rigid body.....	86
Figure 60: Comparison of Plaxis result with FEM results from (Andersen et al, 2005), C3 case.	87
Figure 61: Plate/surface rigid body comparison with plate suction pile	88
Figure 62: Plate and soil rigid bodies with reference point at the same position.	89
Figure 63: Coordinate system and indication of positive stress components.	91

1 INTRODUCTION

1.1 BACKGROUND INFORMATION

Offshore geotechnical engineering is closely connected to onshore practice, but it tended to diverge due to different scale of the foundations and to fundamental differences in installation techniques. As examples, we can mention a shift from many small size piles in onshore practice to few large diameter piles used offshore, replacing excavations of shallow soft sediments with use of skirts penetrating deeper into soil beneath the soft soils or use of under-pressure (suction) to aid the installation (Randolph et al., 2005).

The history of offshore geotechnics is closely related to that of gas and oil production. The persistent rise in world energy consumption has led to oil and gas exploration and production in new environments and regions, extending onshore oil fields offshore, then to deeper and deeper waters and to less suitable and geotechnically more challenging conditions. Example of recent installations is the foundation in 2000 m of water in the Gulf of Mexico. This rapid increase in water depths from 200 m in 1980s to more than 2000 m now has necessitated in the development of new foundations designs and anchoring systems (Randolph, 2010). This change of environment has led to evolution of facilities used: from fixed steel or concrete platforms to floating moored facilities, as well as types of foundations used: from particular types of shallow foundations to anchoring systems.

For similar reasons as in case of oil and gas industry, where energy demand has been continuously increasing, wind renewable energy has grown intensively last decade, but due to noise and aesthetic issues, further wind turbine expansion is limited mostly to offshore regions to offshore wind parks. This change has also other advantages: higher wind speeds off the coast and large areas available compared to land. In any case moving offshore brings new challenges to geotechnics as it is necessary to prepare sufficiently stiff foundations to support the structure loaded by persistent cyclic wind and wave forces in the harsh sea environment. The most frequently used structure is the large diameter monopile (de Vries, 2007).

1.2 PROBLEM DESCRIPTION

Concerning the stiffness of the structure compared to the stiffness of the soil is by many orders higher in case of offshore foundations – mudmats, suction piles, spudcans and large monopiles. It is possible to define the behavior of these structures as behavior of a rigid body with six degrees-of-freedom and to apply forces to the reference point. A rigid body is an object of finite dimensions and negligible change in shape during motion. It is a collection of nodes and elements whose motion is governed by the motion of a single reference node and any body or part of a body can be defined as a rigid body. Kinematics of rigid body motion is expressed in terms of translation and rotation.

In the latest version of finite element software Plaxis 3D kernel rigid bodies were implemented as a Plaxis 3D feature to enable the application of forces from offshore

superstructures on the offshore foundation structure (such as a suction pile or a spudcan) in order to calculate soil response stiffness matrix. The main purpose of this thesis is to validate rigid body elements in Plaxis 3D, to evaluate result for cases using rigid bodies and to determine soil response stiffness matrix by applying the individual force components, thus obtain single components of the matrix from the computational results.

1.3 OBJECTIVES

The first objective is to gain insight into offshore geotechnics – types of foundations used, its important differences to onshore geotechnics followed by study of rigid bodies and rigid body elements used for the modelling of offshore foundations in Plaxis.

The second objective of the thesis is to validate rigid body elements in Plaxis 3D 2014. The validation is carried out by solving problems in Plaxis using rigid body elements and by comparison of these results with:

- Plaxis results with structural elements with a high stiffness.
- Solutions obtained “*by hand*” for less complicated problems.
- Results obtained from published scientific articles.
- Case study of interaction between soil and structure (suction pile) using data from company manufacturing suction piles for the full scale field tests.

The third objective following the validation is to create a procedure, how to determine single terms of soil response stiffness matrix from Plaxis computational results after applying the individual force components. Then, the procedure is used to determine a stiffness matrix for full scale field test, while coupling and evolution of stiffness matrix with changing load is studied.

Fourth objective is to give recommendations for use of rigid bodies in Plaxis 3D – for what kind of offshore structures they could and should be used and with what limitations they can be used. Then, computational times for different solver times are studied, as with the implementation of rigid bodies, different computational times are expected compared to structural elements.

1.4 REPORT STRUCTURE

The report starts with Introduction followed by Literature review. In Literature review are described all necessary topics of theory needed for the main research part of the report – theory for offshore foundations, rigid bodies, their implementation in Plaxis and solver types used in Plaxis.

Then, verification of rigid body feature is described. It starts with basic validations as behavior of interfaces or stability of the whole model. The second part of verification is dedicated to

model of a suction anchor and to comparison of different rigid body types to the results with typical stiff structural elements and results from the literature.

In the next section a full scale field test obtained from a company manufacturing and designing suction piles is described, then modelled with stiff structural elements and rigid bodies. When the model is finished, a procedure how to build soil response stiffness matrix from Plaxis results is created. At the end, the procedure is applied to the field test results.

Then, as the rigid bodies are implemented and validated in Plaxis, calculations of the same model with rigid bodies and stiff structural elements with Pardiso and Picos solvers are used and calculation times are compared. With implementation of rigid bodies different calculation times for rigid bodies and structural elements are expected.

2 LITERATURE REVIEW

In this section will be described literature review performed in order to gain information according main topics of this report – validation of rigid bodies in Plaxis 3D 2014, using rigid body elements for the case study of full scale field test of suction anchor and comparison of calculation types of two basic solvers in Plaxis – direct solver Pardiso and iterative solver Picos.

It will be focused on theoretical background of offshore foundations, their types, the most typical application and the loading conditions, then rigid bodies and rigid body elements in Plaxis are described. At the end iterative and direct solvers are described with detailed description of Pardiso and Picos solvers used in Plaxis.

2.1 OFFSHORE FOUNDATIONS

Offshore geotechnical practice has tended to diverge from onshore practice, both in terms of types of foundations or anchoring systems and in the geotechnical specialists who service the industry. Even in areas such as site investigation, where similar field and laboratory testing techniques are used, strategies, implementation methods and types of tests are often very different (Randolph et al., 2005). The energy demand of the society led to development of offshore geotechnical engineering, at the beginning it was hydrocarbon exploration and production, later followed by boom of renewable energy – in case of offshore engineering, development of offshore wind turbines and offshore wind farms. Generally, we can say that the evolution and history of offshore geotechnics is very closely connected to oil and gas production with all the innovations such as types of mooring and foundations developed for use in this particular industry.

In the last 50 years, there has been an inevitable progression from shallow to deep water within oil and gas industry. As the energy demand escalated and oil and gas reserves became depleted in shallow waters, offshore engineering had to move beyond the immediate continental shelf into deeper waters and untested environments. In Gulf of Mexico, West Africa, offshore Brazil and more developments have proceeded into water depths in excess of 2000 m. This kind of deep water structures mostly consists of floating structures moored to the seabed via an anchoring system. These complex deep sea offshore structures comprises of integrated network of wells, manifolds and pipelines, all of which has to be supported by foundations (Randolph et al., 2010). Another very important structures besides offshore engineering are offshore wind turbines, which registered very fast grow in last two decades in shallower waters along the coasts all over the world. Most of the already existing offshore wind energy converters are founded on monopiles (Achmus, 2009).

2.1.1 History of offshore geotechnics

The first offshore soil borings were drilled in the 1940s. By the 1960s, steel jacket or template structures became common and in this decade oil and gas exploration expanded to Arctic waters, which posed a new set of challenges related to harsher weather conditions. Major hydrocarbon production expanded from the Gulf of Mexico to the North Sea and other

significant offshore fields around the world. In the 1970s the productions started to expand beyond the continental shelf leading to evolution of new foundation types as gravity, tension – leg and moored structures. This evolution still continues and now hydrocarbons are being recovered from waters exceeding 2000 m with deeper fields being planned. As the easily extractable fields were mostly drained, the industry had to move to more and more complex and complicated ones. This rapid increase in water depths from under 200 m in 1980s to more than 2000 m now has led to another evolution of design of anchoring systems, because deep water systems rely heavily on mooring systems. The new types of anchors are suction caissons, plate anchors and dynamically penetrated anchors. This progression has also encompassed changing of type of facilities evolving from fixed steel or concrete platforms to floating facilities as well as changing of soil types with softer and more clayey soils in deep water in contrast with prevalent sandy soils in shallow waters.

2.1.2 Suction anchors

At the beginning it is important to point out, that there is no exact transition between suction anchors and shallow skirted foundations, as the working principle is exactly the same for both foundations types and the difference lies only in geometry of the construction. For example Tjelta (2001) states that the transitions should be: if length/diameter (L/D) ratio of the foundation is lower than 1, the foundation should be called skirted foundation and the term suction anchor should be used for foundations with larger L/D ratio. Special attention will be paid to the suction anchors, as this particular type of foundation is mostly used in practical part of the thesis. In the literature, the terms suction pile and suction caisson are often used, meaning exactly the same as suction anchor.

Suction anchors are gaining more attention in last two decades and have proven to be an economical and reliable solution for many types of offshore structures such as jackets, tension leg platforms, gravity based structures, deep-water subsea structures, subsea well manifolds, single buoy mooring and deep-water platforms (Huang, 2003).

Suction anchor is a large diameter steel hollow cylinder, open at the bottom and closed at the top. Valves are fitted to the top of the pile to allow escape of the water from inside the anchor during the installation. It is installed to the seabed at the beginning by the self-weight of the steel pile to provide a seal between the soil and the tip of the skirt of the pile. Later the installation is finished by pumping out the water from the inside of the skirt creating a suction inside and pushing the pile into the seabed (Monajemi and Razak, 2009). Typical appearance of a suction pile is shown in Figure 1.

Figure 1: Suction pile before installation with its load attachment point called pad-eye (Monajemi and Razak, 2009).



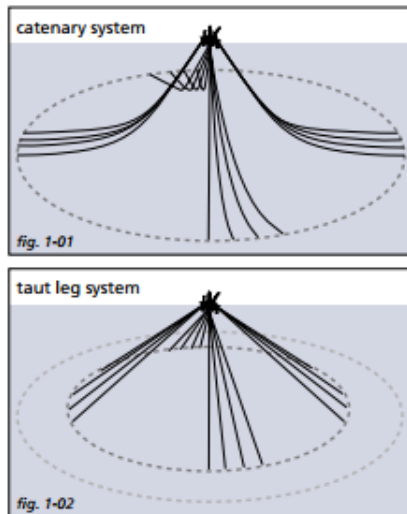
Typical suction anchors possess very high ratios of diameter to wall thickness (d/t) ranging from 100 to 250. In the skirt wall, internal stiffeners are included to prevent buckling of the structure during the installation and due to mooring loads during operation (Randolph et al, 2005).

Mooring

However, the main use of the suction anchors is for mooring, where we recognize two main types of mooring:

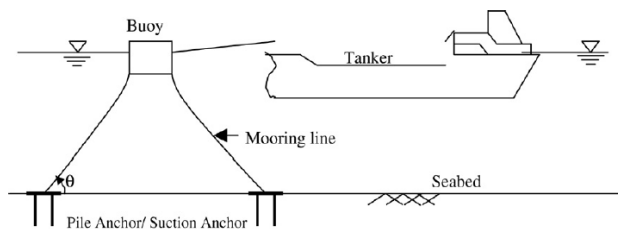
1. Catenary mooring, where the load from the mooring line is horizontal or nearly horizontal, although load inclination at the attachment point (pad-eye) to the anchor may be inclined due to location of the point at the lower part of the anchor. The static load in the mooring line is not present or is negligible close to the anchor.
2. Taut mooring, which is used in deep water applications – the load inclination is mostly around 30-40 degrees and part of the load is static and permanent (Tjelta, 2001). In special conditions, the load inclination can grow up to 90 degrees.

Figure 2: Two types of mooring systems (Vryhof, 2014).



In addition, single point mooring systems are often used for loading and unloading of crude oil and bulk cargo in marine transport operations. In these mooring systems, load inclination may vary significantly between 0 and 90 degrees (Narasimha et al, 2006). The example of a two – point mooring system for a vessel is shown in Figure 3.

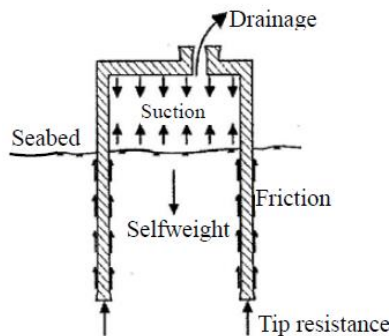
Figure 3: Two-point mooring system for a vessel (Narasimha et al, 2006).



Suction effect

By definition, “active suction” and “passive suction” can occur during the caisson installation and operation phases, respectively. “Active suction” is used to install the pile by pumping out water to create underpressure inside the pile top (Huang, 2003). The underpressure inside the pile sets up seepage flow that reduces tip resistance together with internal friction and the suction provides a downward load during the second phase of the installation. In addition the pile inclination during installation in heterogeneous soils can be controlled by adjusting hydrostatic pressure in the compartments (Saito et al, 2004). “Passive suction” develops when the valves are closed and underpressure is generated at the bottom of the caisson under cyclic tension loading during storms (Huang, 2003). Schematic view of suction pile installation is shown in Figure 4.

Figure 4: Suction pile installation with shown loads applied to the anchor (Saito et al, 2004).



As the evolution of suction inside the pile is the main feature of the foundation, it is impossible to use it in certain soil conditions such as gravel and boulder beds, very hard clays and strongly cemented soil, but these types of soil are not frequently found offshore (Tjelta, 2001).

Loading types and holding capacity

For suction anchors used as anchor foundations, the loading can be classified into three groups: permanent (static) loads applied by the structure above (as the loads from the hull buoyancy), low frequency loads – mean wind and current loads, and high frequency cyclic loads as hurricane and storm wave loads (Huang, 2003). These distinct types of loading have significantly different loading durations, which in result leads to different drainage type. Static load has as expected very long durations and can be assumed as drained loading, on the other hand hurricane loads are applied very quickly, so the soil undergo undrained loading.

Holding capacity of a suction pile is influenced at first by soil conditions, other important factors are: anchor geometry and position of the load attachment point.

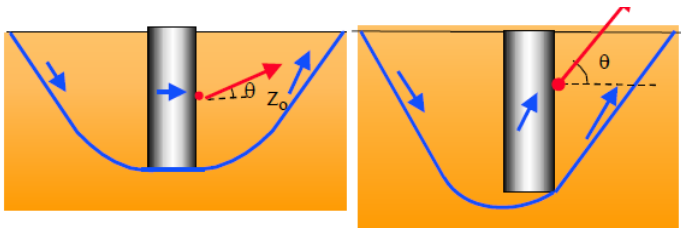
Optimal d/t ratio for a suction pile with inclined load is when the failure mode is a combined vertical and horizontal translation with no rotation. This requires the ratio to be at least around 2-3 (Tjelta, 2001). To obtain only translational failure, the load has to be applied at a depth that gives no resultant moment loading. The depth of this optimum load attachment point (position of the pad-eye) depends on shear strength profile of the soil, the shear strength at the outside of the pile skirt wall, the load inclination and the d/t ratio. The imaginary optimal load attachment point at the centerline of the anchor lies typically about 0.67 to 0.7 of the anchor penetration depth (Andersen et al, 2005). Randolph et al (2005) places the optimal load attachment point to depth from 0.6 to 0.7 of the penetration depth. From this information we can conclude, that the finding of maximal bearing capacity of the suction pile is very complex problem with many variables.

The main advantage of a suction anchor is that it can provide sufficient resistance to uplift loading. This resistance cannot be achieved by any other offshore foundation to an extent of a suction pile. The total uplift capacity depends upon passive suction under sealed cap, self-weight of caisson, frictional resistance along the soil-caisson interface, submerged weight of the soil plug inside the anchor and reverse end bearing of the caisson (Samui et al, 2011).

Soil failure modes

For suction anchors, Huang (2003) describes two examples of translation (i.e., without rotation) failures, as shown in Figure 5, depending on the loading directions. For taut leg moorings, suction anchors are primarily subjected to tension loads acting at large loading angles relative to the seabed. Therefore, the axial uplift capacity of suction anchors is usually the controlling factor in suction anchor design.

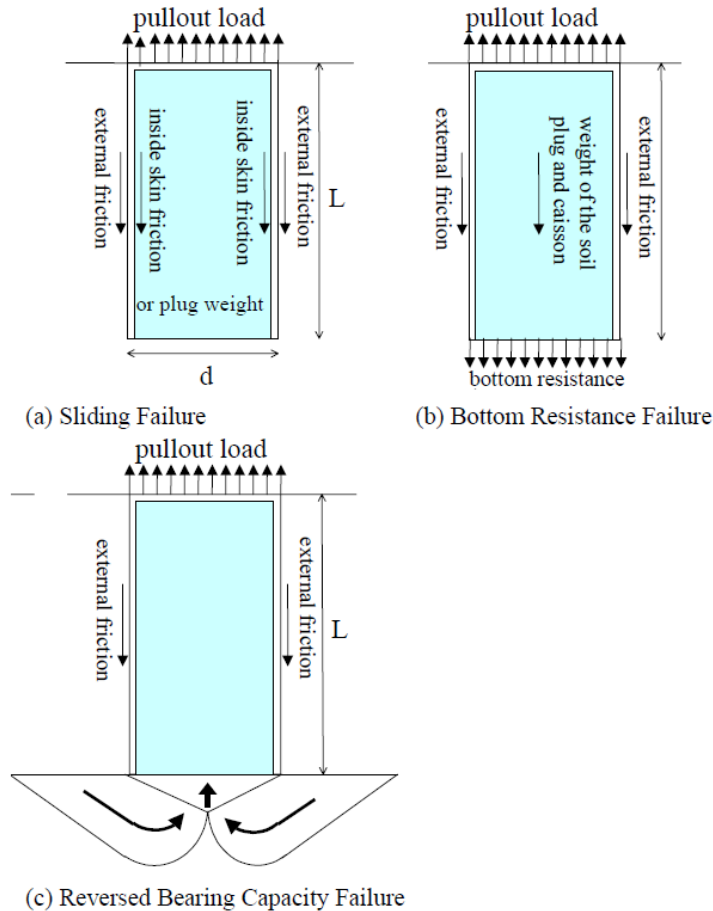
Figure 5: Catenary horizontal loading type on the left and taut legged vertical loading type on the right (Huang, 2003)



Deng et al. (2001) developed failure models for suction piles subjected to vertical tensile loads, as this is the most typical loading type for the suction anchors. All the modes are illustrated in Figure 6. The failure mode is determined by different drainage conditions at the pile top and the pile base. The failure modes are:

- a) Sliding failure – this failure mode is predominant, if the valves on the top of the caisson are not sealed. The capacity is equal to sum of the internal wall friction, submerged weight of the soil plug and the external wall skin friction, as the suction is not developed in the anchor.
- b) Bottom Resistance failure – this mode is active, if the reverse end bearing at the bottom of the pile is limited due to existence of drainage paths and pore pressure dissipation. The capacity is equal to internal and external frictions and reduced reverse end bearing capacity.
- c) Reversed Bearing Capacity Failure – this mode is valid, if the valves on the top are well sealed and full reverse end bearing is developed at the bottom under the tension. The capacity can be calculated as sum of the reverse end bearing and the external friction resistance. This failure mode is characteristic for storm and hurricane loading.

Figure 6: Failure modes for suction pile subjected to vertical tensile loads (Dang et al, 2003).



2.1.3 Other types of offshore foundations

As offshore geotechnics is an extremely wide fields of interest, the literature review of foundations types will focus only on the most widely used types and on the types of foundations modelled by Plaxis in the thesis with other foundations just briefly described. In addition, the reason for it lies in quite similar behavior of many foundations types with only different manufacturing and construction, but with the same type of soil – structure interaction.

2.1.3.1 Mudmats

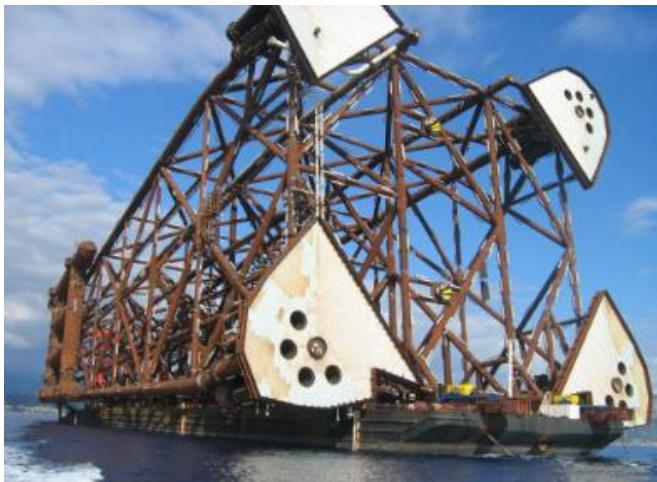
Mudmats are subsea shallow raft foundations systems typically supporting subsea structures (Gazis, 2013). They are used for temporary support during piling for jackets and in deep water oil and gas fields to support deep water pipelines, manifolds and well heads (Chen et al, 2012). In harsh conditions and in deep waters, the mudmats are often designed with additional skirts around their perimeters to resist tension, either through direct uplift (such as when used as part of a tripod support for a fixed structure or through buoyancy of a floating structure) or more commonly because of high overturning moments on a foundation (Acosta-Martinez et al, 2008). In the fine-grained soils of deep water seabeds, the uplift capacity of a mudmat may be amplified by the development of suction at the interface between the mudmat and the underlying seabed.

Skirted mudmats for subsea structures, which are by far the largest application nowadays for such foundations, generally have relatively low embedment ranging from 5% to 30% of the foundation diameter or breadth, while embedment of 20% to 50% of the foundation diameter or breadth is typical for gravity bases, jackets or floating structures (Gouvernec et al, 2003).

Mudmats for jacket foundations

An offshore jacket is comprised of three or four legs forming a triangular or rectangular base with a leg disposed at each corner of the base. The legs are resting on the sea floor or slightly penetrating into the soil. The jacket is secured to the sea floor with piles (Oksuzler, 1987).

Figure 7: Mudmat at the bottom of the jacket structure (Advanced Geomechanics, 2012).



An offshore jacket is comprised of three or four legs forming a triangular or rectangular base and a leg is disposed at each corner of the base. The legs are resting on the sea floor or slightly penetrating into the soil. The jacket is secured to the sea floor with piles (Oksuzler, 1987).

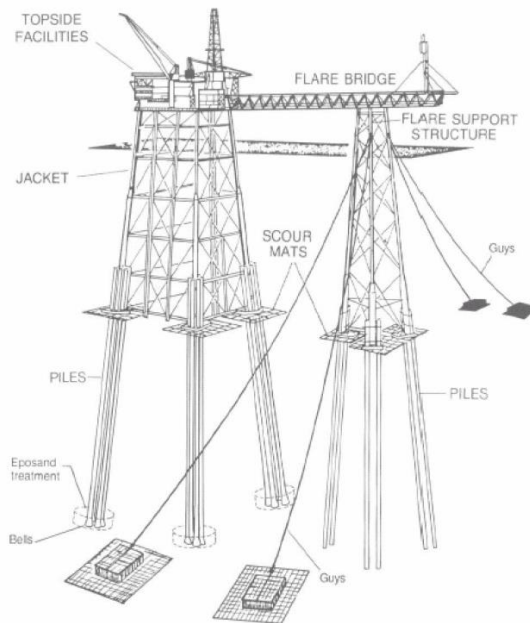
In many areas of the world, the soil of the sea floor is unconsolidated and very soft, which leads to very low bearing capacities creating jacket support problems during installation of offshore platforms? In this cases as a pile is driven into the sea bed through the sleeves the legs of a jacket can sink into the soft soil at the sea floor, causing the jacket to either fall onto its side or settle lower than design specifications.

The solution to this issues with very soft sea floors is to create a structure that spreads the downward forces applied to the jacket over a larger area of the sea floor. The most common structure with this function is a mudmat. A mudmat with much larger area than a leg of a jacket is distributing the load of a jacket over the seabed providing stability during pile driving operations (Haas, 1999).

2.1.3.2 Pile foundations

Offshore monopiles are used as common foundation for steel jacket structures, which still are the most common form of fixed offshore platform. The platforms are attached to the seabed by piles inserted through sleeves attached to the jacket. The example of jacket structure with piles is shown in Figure 8.

Figure 8: Jacket structure, North Rankin platform, with piles used as foundations (Randolph et al, 2009).



Offshore monopiles have been receiving increasing attention of scientists and engineers since offshore renewable energy gained global popularity in the last few decades. Generally, embedded in shallow waters with a depth of no more than 50 m, offshore monopiles typically have a much larger diameter than those of other pile foundations (Li et al, 2011). These two are the most typical applications of pile foundations in offshore engineering, even though there is more possibilities of their use such as for mooring tension leg platforms etc.

In offshore geotechnical engineering two basic types of piles are used:

Driven piles

Most of the piles used offshore are of this type: steel pipes driven open ended into the seafloor. The diameter of typical piles ranges from 0.5 to 2.5 m. In exceptional cases of large wind turbines installed in depths around 30 m with rated power of 5MW it is required to install piles with a diameter between 5 and 7.5 m (Chums et al., 2009). The wall thickness of the pile usually vary along the length with thicker walls used near the pile head, where bending moments are maximum. The typical diameter to wall thickness ratios (d/t) are around 40, giving a net steel area of 10% of the overall pile cross-section (Randolph et al., 2009).

Grouted piles

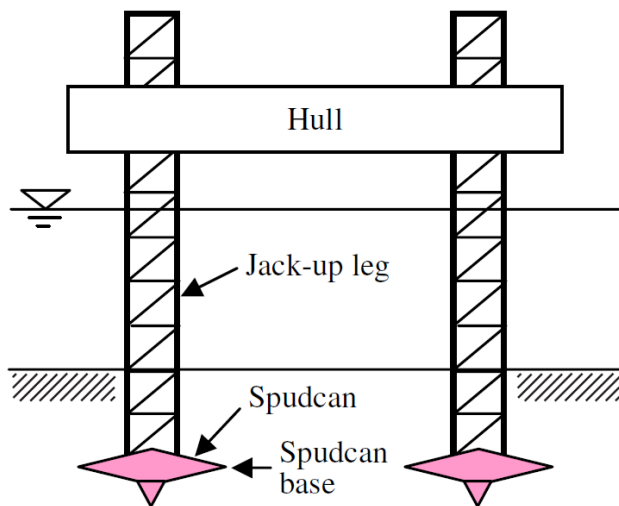
Grouted piles are an offshore equivalent of a bored pile and they comprise a steel tubular section grouted into a pre-drilled hole.

Drilled and grouted piles are usually more expensive to install than driven piles, because of longer construction period required. They are worth installing in cases, when a drilling barge is already in the area. They are also preferred in calcareous sediments, and potentially other crushable material, where shaft friction obtained with driven piles can be extremely low (Randolph et al., 2009).

2.1.3.3 Foundation for mobile drilling units – spudcans

Most of the offshore drilling activities in shallow to moderate water depths is performed by self-elevating mobile jack-up drilling rigs. The reason for their use is long term proven mobility and cost-effectiveness and the operation depth of the rigs is up to 150 m (Zhang et al, 2010). The typical rig consist of a buoyant hull and three or four independent latticework legs with conical spudcan foundations at the bottom. The process of installation of a drilling rig is as following: the rig is towed to site, after which legs are lowered and the spudcans penetrated in the seabed to provide bearing resistance to allow the drilling rig to be jacked upwards from the wave zone (Lee and Randolph, 2011). The schematic view of typical drilling jack-up rig with spudcan foundation is shown in following Figure 9.

Figure 9: Spudcan foundation and the drilling rig (Lee and Randolph, 2011).

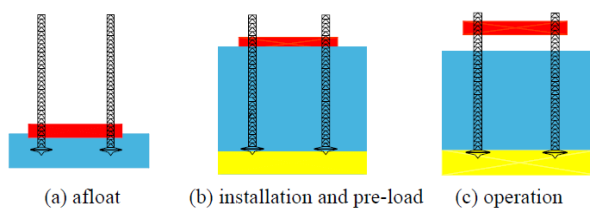


The foundation itself is circular in plan, has a shallow conical underside (around 15 degrees) and sharp protruding spigot at the bottom. The diameter of spudcans ranges up to 20 m with height of up to 4 m.

Installation and “punch-through”

At the beginning, jack-ups are floated to the site on a hull with its legs elevated. Then, the spudcan foundation penetrates into the seabed under the weight of the jack-up rig, augmented by ballasting the hull of the rig. After the installation the foundation is preloaded by pumping sea water into ballast tanks in the hull to expose it to higher pure vertical load than would be expected during the service to ensure that they have sufficient reserve capacity in any extreme storm event that the structure might need to withstand. The procedure is summarized in Figure 10.

Figure 10: Jack - up rig installation, preloading and operation (Randolph et al, 2005).

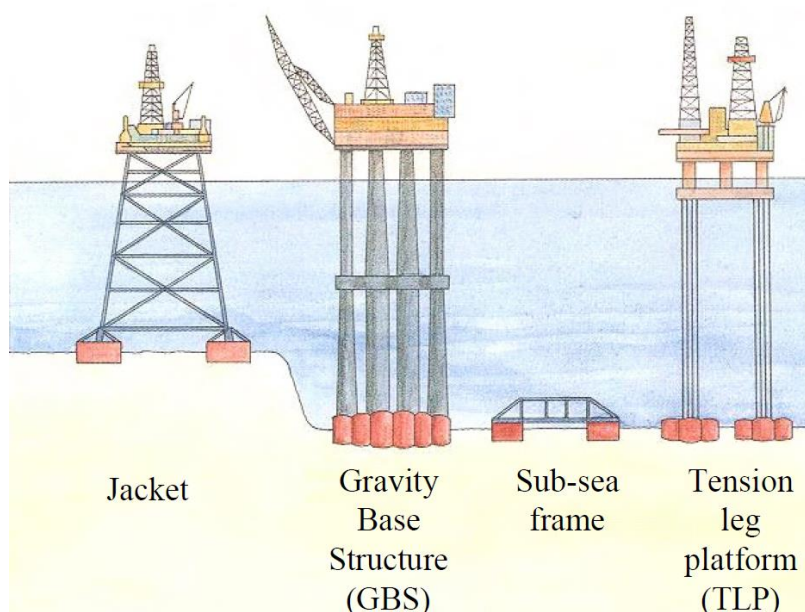


The most common geotechnical failure within jack-up rigs is so called “punch through” of a spudcan (Lee and Randolph, 2011). The process typically occurs in a particular soil conditions – when a thin sand layer overlies a weaker clay stratum. This can lead to overestimating the bearing capacity of the soil and then to rapid uncontrolled penetration. Such failures can be followed by buckling of the leg or even toppling of the unit (Qui and Henke, 2011).

2.1.3.4 Shallow foundations

Offshore shallow foundations comprise more types of structures: large concrete gravity bases supporting fixed structures, steel mudmats and concrete and steel bucket foundations.

Figure 11: Applications of shallow offshore foundations (Randolph et al, 2005).



Design practice and loading

There is lot of important differences between onshore and offshore shallow foundations:

- Offshore foundations are typically much larger than the ones used onshore
- Offshore foundations are required to withstand much higher horizontal and moment loading
- Cyclic loading is very important in offshore design
- Soft soils on the seabed are not removed, but they are incorporated into the foundation, on the other side onshore undesirable soils are commonly removed prior to construction of the foundation
- In projecting offshore foundations there is more emphasis placed on capacity than on displacements (Randolph et al, 2005).

Types of foundations

The most common type is concrete or steel bucket foundations used as anchors for floating platforms or as permanent supports for jacket structures instead of piles. The concrete buckets are no longer used in new offshore projects and are in general replaced by steel buckets. The use of skirts possess lots of advantages and functions:

- Incorporating soft soils into the foundation
- Assisting the penetration of the foundation into the soil
- Reducing the scour around the foundation, which leads to reducing ultimate bearing capacity of the foundation
- Balancing irregularities in seabed
- The most important point in construction of skirted offshore foundations is that the skirts provide transient uplift capacity to the foundations during undrained loading

Skirtless gravity base foundations are lying on the seabed, but in case of worse quality of soils, skirts are added to them as well to transform the loads to deeper and stronger soil.

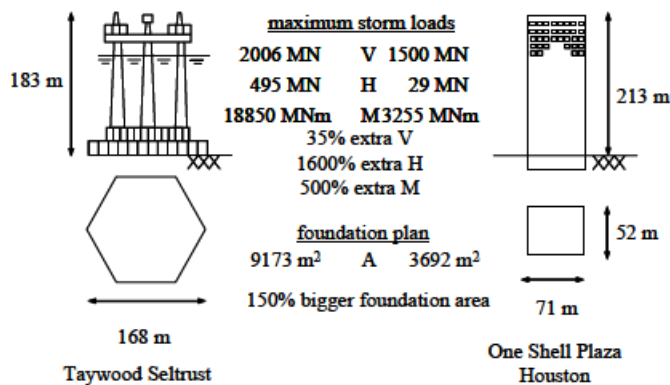
2.1.4 Loading conditions of offshore foundations

It is important to point out, that the seabed in deep water is typically composed of normally consolidated or lightly overconsolidated fine-grained very soft sediments with a strength profile that increases with depth (Chen et al, 2012). On the other hand, the seabed in shallow waters consists mostly of sands and sandy soils.

For offshore structures a dominance of environmental loading is typical and the influence of cyclic loading on the soil response is much more important than for a typical onshore structure. Environmental forces, as wind, current and wave loading, impose significant cyclic horizontal, vertical and moment loads and generate excess pore water pressures in the surroundings of the foundation reducing the effective stresses in the seabed (Randolph et al, 2005). Thus, while designing an offshore structure, besides the design for the maximum static load, fatigue design is a very important aspect for offshore structures. The effect of cyclic loading of the soil has to be considered, since the number of loads due to wind and wave could exceed 10^8 over the lifetime of the structure (Achmus et al, 2009).

(Randolph et al, 2005) states, that the horizontal load is 1600% larger and moment 500 % larger for offshore foundations, which is reflected in an increased foundation area typical for offshore structures and foundations. This fact is shown in Figure 12.

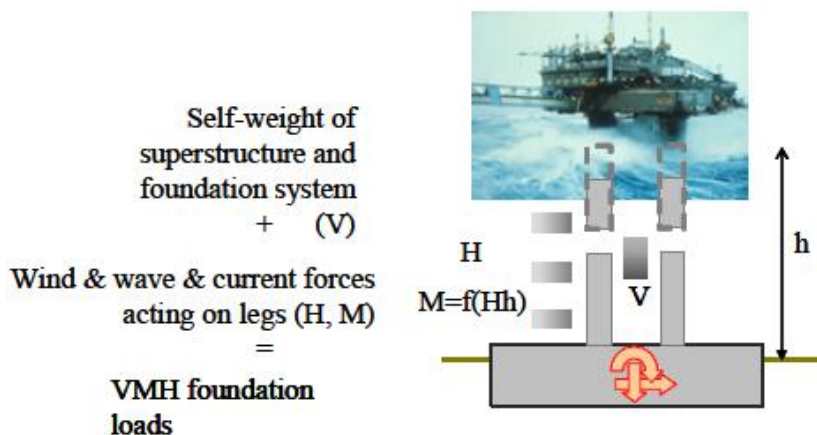
Figure 12: Comparison of offshore and onshore design loads showed at Taywood Seltrust offshore platform and One Shell Plaza skyscraper in Houston (Randolph et al, 2005).



Loading conditions - piles

Piles have to be designed to resist the total weight of the structure, but in addition to this, they are loaded by significantly high environmental loading, which is in case of offshore foundations much higher than for most of onshore structures. The piles are subjected to cyclic loading and often to both compressive and tensile loading as well. While used for mooring, they are also subjected to mainly horizontal loading or to higher angles up to 45 degrees, depending on tethering system.

Figure 13: Vertical, horizontal and moment loads applied to the pile foundation (Randolph et al, 2005).



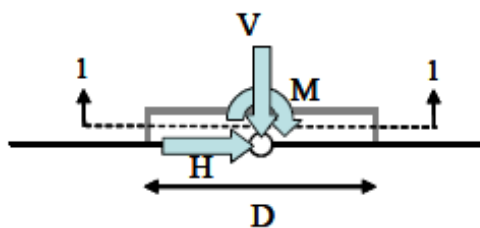
The vertical loads are transferred to the soil through wall friction and tip resistance, while the lateral loads, which are especially in case of wind turbines much larger, are conveyed to the foundation through bending. The loads are subsequently transferred laterally to the soil. To provide enough stiffness the diameter of the monopile has to be large enough (de Vries, 2007). This is the reason, why in the last decades we can see monopiles with diameter up to 7.5 m.

compared to the time required for dissipation of the suction developed in the pore water under the foundation. Cyclic uplift loads from waves may be resisted even on relatively pervious sand deposits and uplift loads over much longer durations may be carried by skirted foundations on clays with lower permeability (Randolph et al, 2005).

In case of skirted mudmats, if no suction is generated, the uplift resistance is essentially the internal and external friction along the skirt, which is an order of magnitude lower than the foundation self-weight for skirt lengths used offshore. If suction is generated at the mat invert, the failure mechanism is expected to be either a reverse end bearing mechanism or a breakout hemispherical contraction-type mechanism (Chen et al, 2012).

For non-uniform shear strength profiles classical bearing capacity theory will underpredict the capacity even for simple eccentricity with no lateral load. The breakdown of classical bearing capacity theory under combined loading is particularly significant in offshore shallow foundation design due to the large components of horizontal load and moment from the harsh environmental conditions (as wind, wave and current forces) and the normally consolidated seabed deposits. The applicability of classical bearing capacity theory to offshore design is also questionable as the approach neglects tensile capacity, which in reality can be mobilized by some offshore shallow foundations provided they are equipped with skirts (Randolph et al, 2005).

Figure 16: Combined vertical, horizontal and moment loading applied to mudmat foundation (Randolph et al, 2005).

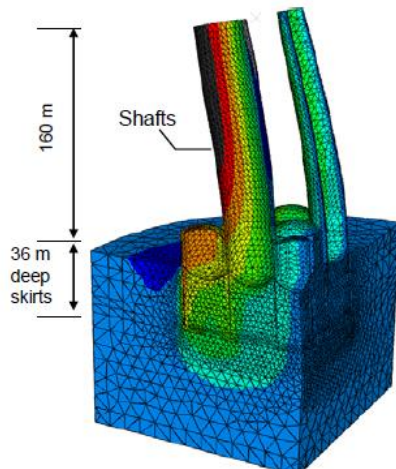


2.1.5 Offshore foundations as rigid bodies

In the interests of simplicity and computational efficiency, researchers have tended to concentrate on models that idealize the offshore foundations as spudcans and suction piles as rigid bodies (Martin and Houlsby, 2001). In the offshore practice, the foundations as mudmats, spudcans, piles and suction anchors are made of steel and they are installed into the seabed, which consists of mostly sandy soils in shallow waters and soft clays in deep water applications. As Andersen et al (2008) states in some cases the foundation may be regarded as rigid compared to the soil stiffness and those cases do not require any sophisticated modelling of the structure. However, in other cases there may be considerably flexibility in the structure and in its foundations. In these cases it may be necessary to perform a more sophisticated Soil-Structure-Interaction (SSI) analysis with realistic representation of the structure geometry and stiffness. A deformable structure model of an oil platform is shown in following Figure 17.

For the purpose of modeling of soil response, the foundation can be regarded as rigid, on the other hand, this procedure is not common for structural engineers interested in deformation of the structure itself, even though the deformation can be insignificant compared to the deformation of the soil.

Figure 17: Deformed mesh and contour shadings during maximum wave loading of the Troll-A platform (Andersen et al, 2008).



Rigid bodies compared to standard models are computationally efficient:

- Their motion is described completely by no more than six degrees of freedom at the reference node.
- A rigid body is a collection of nodes and elements whose motion is governed by the motion of a single reference node.
- Any body or part of a body can be defined as a rigid body.

From this we can conclude, that the model can be significantly simplified, when the whole structure typically comprised by thousands of nodes can be modelled by simple rigid body with one reference point and 6 degrees of freedom instead of sophisticated model of the structure. Thus, the computational efficiency can be much higher in a models using rigid bodies and the attention can be fully paid to the response of a soil.

2.2 PLAXIS KERNEL AND RIGID BODY

Plaxis 3D is a three-dimensional finite element software used specifically for the analysis of the deformation and stability in various types of geotechnical engineering projects. The program includes a graphical user interface, in which geometry of the model and finite element mesh can be generated. The graphical input part of the program enables a quick generation of finite element models, and the output part provides a detailed presentation of computational results. Even though Plaxis is equipped with features to deal with various and complex geotechnical aspects, the accuracy at which reality is approximated depends highly on the expertise of the user regarding the modeling of the problem, the understanding of the soil models and their limitations, the selection of model parameters, and the ability to judge the reliability of the computational results (Brinkgreve et al, 2013). The simulation by finite elements implicitly contains some unavoidable numerical and modelling errors that can be significant if the program is not used correctly. It is necessary to point out, that the reality is often much more complicated than the finite element method (FEM) model itself, and this fact has to be taken into account while interpreting results of the models. Plaxis can simulate very complicated subsoil, combined with boundary conditions, large deformations, updated mesh and many more complex phenomena. In general, soil behavior is complex and it tends to be highly non-linear under load. This non-linear stress-strain behavior can be modeled at several levels of sophistication, while the number of the parameters in the model increases with the level of sophistication. In Plaxis a wide range of material models can be used, all the models with their parameters are described in detail in the Material Models Manual (Brinkgreve et al, 2013). Especially in Plaxis 3D it is very important to distinguish between features, which should be necessarily used in the particular model, and which are not important for the results and will only cause extremely long calculation times with more or less identical results. This leads to another very important point – the user has to understand what kind of information he wants to obtain from the program. For example while solving stability problems, Plaxis is prescribing very large displacements to obtain a safety factor, but it is necessary to know, that these displacements are not real and the user should be interested only in deformation mechanism and resulting safety factor.

2.2.1 Rigid body

A *Rigid body* is an object of finite dimensions and negligible change in shape during motion. That is where the distance between every two points on the body remains constant. A rigid body is assumed to have a continuous mass distribution although in reality matter is quantized at small scales. Kinematics of rigid body motion is expressed in terms of translation and rotation. Forces are sliding vectors - they can slide on their line of action without their mechanical effects being altered. Model equations are balance of energy, linear momentum and angular momentum (Hackl et al, 2010). On opposite lies the *deformable body*, it is a mechanical object of continuous mass distribution, whose relative distance of points can change. This is officially the starting point of continuum mechanics, although a rigid body has a continuous mass distribution too. Continuum mechanics deals with the length scales large enough to neglect all the molecular effects and, at the same time, small enough to observe the shape changes in the body. Together with translations and rotations we have deformation

in kinematics study of deformable bodies. As the point of action of forces is important here, forces are fixed vectors. Balance equations of linear and angular momentum and energy are not sufficient to model deformation (Huckl et al, 2010).

The rigid body displacement is one consisting of a simultaneous translation and rotation, which produces a new configuration, but causes no changes in the size or shape of the body, only changes in its position and/or orientation. On the other hand, an arbitrary displacement will usually include both a rigid body displacement and a deformation, which results in a change in size, or shape, or possibly both (Mase and Mase, 2010). The force acting on a rigid body has two effects:

- It tends to move the body
- It tends to rotate the body.

2.2.2 Rigid body implementation in Plaxis 3D kernel

The idea in the implementation of rigid body lies in defining a master point (a reference point of the rigid body) with the other soil or plate elements within the body rigidly connected to that particular point. The motion of a single material point is governed by only 6 degrees of freedom (DoF's): 3 displacement DoF's u_x , u_y , u_z and three rotational DoF's ϕ_x , ϕ_y and ϕ_z . Having the body and the master node, a list of slave nodes can be created that refer to the master node.

The displacements of the slave nodes can be described in a simple way:

$$\begin{Bmatrix} u_x \\ u_y \\ u_z \end{Bmatrix}_{slave} = \begin{Bmatrix} u_x \\ u_y \\ u_z \end{Bmatrix}_{master} + \begin{bmatrix} 0 & z_s - z_m & y_m - y_s \\ z_m - z_s & 0 & x_s - x_m \\ y_s - y_m & x_m - x_s & 0 \end{bmatrix} \begin{Bmatrix} \phi_x \\ \phi_y \\ \phi_z \end{Bmatrix} \quad (1)$$

While for rotations:

$$\begin{Bmatrix} \phi_x \\ \phi_y \\ \phi_z \end{Bmatrix}_{slave} = \begin{Bmatrix} \phi_x \\ \phi_y \\ \phi_z \end{Bmatrix}_{master} \quad (2)$$

The displacements of the node are defined as:

$$\begin{Bmatrix} dx \\ dy \\ dz \end{Bmatrix} = \begin{Bmatrix} x \\ y \\ z \end{Bmatrix}_{slave} - \begin{Bmatrix} x \\ y \\ z \end{Bmatrix}_{master} \quad (3)$$

By combining (1) and (3) we obtain the following form:

$$\begin{Bmatrix} u_x \\ u_y \\ u_z \end{Bmatrix}_{slave} = \begin{Bmatrix} u_x \\ u_y \\ u_z \end{Bmatrix}_{master} + \begin{bmatrix} 0 & dz & -dy \\ -dz & 0 & dx \\ dy & -dx & 0 \end{bmatrix} \begin{Bmatrix} \varphi_x \\ \varphi_y \\ \varphi_z \end{Bmatrix} \quad (4)$$

Thus, from (4) can be built the relationship for the slave node degrees of freedom in a more robust form using one single transformation matrix:

$$\begin{Bmatrix} u_x \\ u_y \\ u_z \\ \varphi_x \\ \varphi_y \\ \varphi_z \end{Bmatrix}_{slave} = \begin{bmatrix} 1 & 0 & 0 & 0 & dz & -dy \\ 0 & 1 & 0 & -dz & 0 & dx \\ 0 & 0 & 1 & dy & -dx & 0 \\ 0 & 0 & 0 & 1 & 0 & 0 \\ 0 & 0 & 0 & 0 & 1 & 0 \\ 0 & 0 & 0 & 0 & 0 & 1 \end{bmatrix} \begin{Bmatrix} u_x \\ u_y \\ u_z \\ \varphi_x \\ \varphi_y \\ \varphi_z \end{Bmatrix}_{master} \quad (5)$$

In the same manner, relationship for the master node degrees of freedom is:

$$\begin{Bmatrix} u_x \\ u_y \\ u_z \\ \varphi_x \\ \varphi_y \\ \varphi_z \end{Bmatrix}_{master} = \begin{bmatrix} 1 & 0 & 0 & 0 & -dz & dy \\ 0 & 1 & 0 & dz & 0 & -dx \\ 0 & 0 & 1 & -dy & dx & 0 \\ 0 & 0 & 0 & 1 & 0 & 0 \\ 0 & 0 & 0 & 0 & 1 & 0 \\ 0 & 0 & 0 & 0 & 0 & 1 \end{bmatrix} \begin{Bmatrix} u_x \\ u_y \\ u_z \\ \varphi_x \\ \varphi_y \\ \varphi_z \end{Bmatrix}_{slave} \quad (6)$$

The relationship between force vector of the master node and the force vector of the slave node can be expressed and formed in the same way as was built (6), the final matrix is:

$$\begin{Bmatrix} F_x \\ F_y \\ F_z \\ M_x \\ M_y \\ M_z \end{Bmatrix}_{master} = \begin{bmatrix} 1 & 0 & 0 & 0 & 0 & 0 \\ 0 & 1 & 0 & 0 & 0 & 0 \\ 0 & 0 & 1 & 0 & 0 & 0 \\ 0 & -dz & dy & 1 & 0 & 0 \\ dz & 0 & -dx & 0 & 1 & 0 \\ -dy & dx & 0 & 0 & 0 & 1 \end{bmatrix} \begin{Bmatrix} F_x \\ F_y \\ F_z \\ M_x \\ M_y \\ M_z \end{Bmatrix}_{slave} \quad (7)$$

All the equation above can be simplified:

$$\begin{Bmatrix} u \\ \varphi \end{Bmatrix}_S = \begin{bmatrix} I & R \\ 0 & I \end{bmatrix} \begin{Bmatrix} u \\ \varphi \end{Bmatrix}_M \quad \begin{Bmatrix} u \\ \varphi \end{Bmatrix}_M = \begin{bmatrix} I & R^T \\ 0 & I \end{bmatrix} \begin{Bmatrix} u \\ \varphi \end{Bmatrix}_S \quad (8)$$

and

$$\begin{Bmatrix} F \\ M \end{Bmatrix}_M = \begin{bmatrix} I & 0 \\ R^T & I \end{bmatrix} \begin{Bmatrix} F \\ M \end{Bmatrix}_S \quad (9)$$

with

$$\begin{aligned} dx &= x_s - x_M \\ dy &= y_s - y_M \\ dz &= z_s - z_M \end{aligned} \quad , \quad R = \begin{bmatrix} 0 & dz & -dy \\ -dz & 0 & dx \\ dy & -dx & 0 \end{bmatrix} \quad , \quad R^T = \begin{bmatrix} 0 & -dz & dy \\ dz & 0 & -dx \\ -dy & dx & 0 \end{bmatrix} = -R \quad (10)$$

2.2.3 Solver types used in Plaxis

In the geotechnical problems, for which the Plaxis software is generally used, the model typically involve a volume of soil and various structural objects. In addition the soil often consists of many soil layers with different material properties and the structural objects, as steel or concrete walls, foundations, piles and anchors, are embedded in the soil or are located on top of the soil (Lingen et al, 2012).

Finite element models are used to compute the deformation of the soil and the structural objects. In the models are two basic types of objects – volume elements modelling the soil and thick structural objects as shell elements for plates and thin – called structural objects, line elements for anchors and piles and interface elements for modelling interaction between the soil and structures in the model. The displacement field u in an element e is approximated by

$$u(x) = N_e(x)a_e \quad (11)$$

in which N_e is a matrix containing the element shape functions and a_e is a vector containing the degrees of freedom in the nodes of the element. The second one are 3 displacements: u_x , u_y and u_z , and three rotations: ϕ_x , ϕ_y and ϕ_z . Substitution of the approximate displacement field into the constitutive equations yields a non-linear system of equations that is solved with a Newton method. Newton iteration requires the solution of a non - linear system of equations of the form

$$K a = f \quad (12)$$

in which K is the tangent stiffness matrix (or an approximation thereof), a is a vector containing the incremental degrees of freedom in all the nodes, and f is a vector containing the unbalanced forces and moments in the nodes. The solution of this linear system can be approximated with moderate accuracy because it is only an intermediate of the non-linear system to be solved (Lingen et al, 2012). Mostly, the K is large, sparse and ill-conditioned.

There are two basic classes of algorithms that are used to solve above described problems: Direct or Iterative method.

2.2.3.1 Direct methods

Direct methods attempt to solve the problem by a finite sequence of operations. In the absence of rounding errors, direct methods would deliver an exact solution. The sparse direct solver is based on a direct elimination of finite sequence of equations. Direct methods are not appropriate for solving large number of equations in a system, particularly when the coefficient matrix is sparse, i.e. when most of the elements in a matrix are zero. A typical direct method is Gaussian Elimination Method (Jamil, 2012).

All the direct methods comprise three phases: an analysis of the sparsity pattern with a view to reordering the variables to reduce fill-in, a (static or dynamic) factorization of the

reordered matrix, and a solution of the given system using forward- and back-substitution. The interaction between all three phases is crucial for a reliable and fast solution.

2.2.3.2 Iterative methods

Contrary to direct solvers, iterative methods approach the solution gradually, rather than in one large computational step (it is starting with initial guess x_0 and continues iterations until an absolute error is less than the pre-defined tolerance, then, it returns a final guess x_k). Therefore, when solving a problem with an iterative method, the error estimate in the solution can be observed to decrease with the number of iterations. For well-conditioned problems, this convergence should be quite monotonic. If the problem is not well-conditioned, then the convergence will be slower.

Iterative methods are suitable for solving systems of equations when the number of equations in a system is very large and iterative methods are very effective concerning computer storage and time requirements. One of the advantages of using iterative methods is that they require fewer multiplications for large systems (Jamil, 2012).

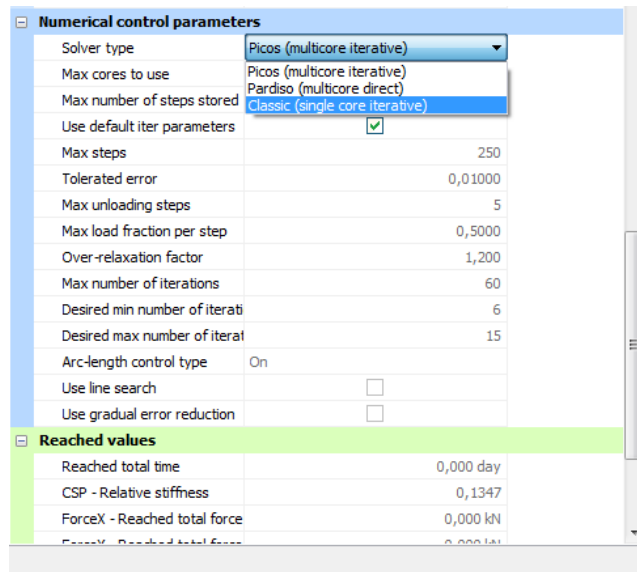
2.2.3.3 Solvers used in Plaxis

In Plaxis the assembly and solution of sparse linear equation systems is carried out by solvers. The available solvers used in Plaxis are:

- **Picos (Plaxis Iterative Concurrent Solver)** – It is a multicore iterative solver. It is efficient iterative solver that solves the system of equations in parallel on multi-core processors. It is generally the fastest way to perform calculations.
- **Pardiso (Parallel Sparse Direct Solver)** – It is a direct solver, that solves the system of equations in parallel on multi-core processors. It is generally the most robust way solve equations, but it has also the highest memory consumption (Brinkgreve et al, 2013). The package PARDISO is a high-performance, robust, memory-efficient and easy to use software for solving large sparse symmetric and nonsymmetric linear systems of equations on shared-memory and distributed-memory architectures (Schenk and Gartner, 2001).
- **Classic** – It is single core iterative solver, which has been used in previous Plaxis 3D versions. It solves the system of equations using only a single core on the processor (Brinkgreve et al, 2013).

In the following is shown the Solver type option in the Numerical control parameters subtree:

Figure 18: Solver type option in Plaxis 3D interface.



The user may also set the Max cores to use. This number specifies how many cores will be used per phase calculation. If the number is larger than the number of available cores in the computer, the calculation will only use the available physical cores. E.g. on a quad core PC using the default 256 Max cores to use, the program will use 4 cores for the phase calculation in a multi-core calculation (Picos or Pardiso solver).

2.3 CONCLUSION

A literature study was performed in this chapter. At the beginning types of offshore foundations were described with their typical geometry and use in offshore practice, then, typical loading conditions were examined for offshore foundations generally and then for every particular type. Special attention was paid to suction piles, as this particular type of foundation was used in the validation of implementation of rigid bodies in Chapter 7.2 and in the full scale field test in Chapter 4. In the second part of literature study rigid body was defined, the implementation of rigid body into Plaxis kernel was described and at the end two types of solvers used in Plaxis – Picos as iterative solver and Pardiso as direct solver – were described. The validation of rigid bodies in described in Chapter 7. The comparison of computation times of Pardiso and Picos solvers, for the stiff structural element models versus rigid body models, is described in Chapter 3 in order to show expected changes of computation times for solvers with different models.

3 COMPARISON OF PARDISO AND PICOS SOLVERS AND CALCULATION TIMES

In this chapter is described comparison of Picos and Pardiso solvers used in Plaxis. The reason why these calculations were performed is that after implementation and validation of rigid bodies in Plaxis kernel, different calculation times were expected for rigid bodies and for typical stiff structural elements as plates, surfaces and soil volumes.

The comparison was performed for a model of a suction anchor described and evaluated in Chapter 7.2. The basic theory for solvers used in Plaxis is described in Chapter 2.2.3. The two solver types used in the calculations are

- **Picos (Plaxis Iterative Concurrent Solver)** – It is a multicore iterative solver

and

- **Pardiso (Parallel Sparse Direct Solver)** – It is a multicore direct solver.

For the comparison of the solver types, calculations with stiff soil body and volume rigid body were performed.

3.1 EXPECTED RESULTS

The sparse direct solver is based on a direct elimination of finite sequence of equations, as opposed to iterative solvers, where the solution is obtained through an iterative process that successively refines an initial guess to a solution that is within an acceptable tolerance of the exact solution. Direct elimination requires the factorization of an initial very sparse linear system of equations into a lower triangular matrix followed by forward and backward substitution using this triangular system. The space required for the lower triangular matrix factors is typically much more than the initial assembled sparse matrix, hence the large disk or in-core memory requirements for direct methods. Because the sparse direct solver is based on direct elimination, poorly conditioned matrices do not pose any difficulty in producing a solution (although accuracy may be compromised) (Gould et al, 2007).

An iterative solver assembles the full global stiffness matrix and calculates the degrees of freedom solution by iterating to convergence (starting with initial guess solution for all degrees of freedom and continues iterations until an error is smaller than tolerance, then the final guess is returned). Because they take fewer iterations to converge, well-conditioned models perform better than ill-conditioned models. The approximate solution is computed in every step: $u^k = A^{-1}f$.

Direct solvers are using much bigger amount of memory than iterative solvers, while rigid bodies will use less memory than structural elements in both cases, because many degrees of freedom are condensed out of the system. Pardiso is more robust than Picos, while rigid body models should be more robust than structural elements as well. It was expected that for a rather small model with structural elements and less elements Pardiso should perform better. For the models with a rigid body, Picos is expected to be always faster than Pardiso, so the fastest one of all tested cases should be Picos solver using rigid bodies.

The expected results of Pardiso and Picos solvers are summarized in following Table 1:

Table 1: Summary of expected results.

	Pardiso – direct solver	Picos – iterative solver
Stiff structural element	<ul style="list-style-type: none"> - Large amount of memory used - Robust - Slowest 	<ul style="list-style-type: none"> - Less memory than Pardiso - Not so robust as Pardiso - Large number of iterations needed due to large stiffness difference between stiff elements and soil elements - Might still be faster than Pardiso
Rigid body	<ul style="list-style-type: none"> - Large amount of memory used (less than with stiff elements though) - Robust (more than stiff elements) - Not as slow as stiff elements 	<ul style="list-style-type: none"> - Much less memory used - More robust than Picos with structural elements, but less than Pardiso - Fastest one

3.2 PERFORMED CALCULATIONS

For the comparison of calculation times of Picos and Pardiso solvers the model used for verification of rigid bodies in Chapter 7.2 was used. The calculations performed are:

- Model with soil volume rigid body – Picos iterative solver
- Model with soil volume rigid body – Pardiso direct solver
- Model with very stiff soil body – Picos iterative solver
- Model with very stiff soil body – Pardiso direct solver

In the model suction pile is made of very stiff soil body, while two basic calculations are used – Vertical loading and Horizontal loading applied to the pad-eye on the wall of the pile. The loading is modelled by prescribing a displacement to the pad eye. In case of rigid body, suction pile was modelled using soil volume rigid body with the reference point at the position of the hypothetical pad-eye, in this case the displacement was prescribed to the reference point. The detailed description of the model is provided in Chapter 7.2.1 and 7.2.2.

The small model was comprised of 12 324 nodes and 7899 elements. This means that the calculations of all models are relevant to each other, as the size of the models are the same, the calculation results within the models can be compared to each other.

It is important to point out, that there are three options in Plaxis how to create a rigid body – soil volume rigid body, plate rigid body and surface rigid body. In this chapter only one option

was selected, as the purpose was to determine difference between calculation times of rigid body model and stiff structural element model, not to determine differences between single rigid body types. On the other hand, it can be easily concluded, that the slowest option will be plate rigid body, as the model is more complicated than soil volume rigid body or surface rigid body – in comparison to surface rigid body, the model is exactly the same, but it has plates modelled in addition to surfaces. The calculation results for soil volume rigid body and surface rigid body were observed to be very similar.

3.3 RESULTS

Eight calculation were performed in order to compare calculation times. For every model described above horizontal and vertical loading were used to make certain there are no any mistakes in single calculations. All the calculation times are shown in following Table 2:

Table 2: Calculation times of Picos and Pardiso solvers (in seconds).

Pardiso direct solver	Stiff soil volume - structural	Soil volume rigid body
Vertical loading	177.65	141.08
Horizontal loading	218.16	199.69
Picos iterative solver		
Vertical loading	225.77	127.19
Horizontal loading	311.34	155.42

Then, we can list the results (doesn't matter if horizontal or vertical loading – the results will be the same) from the fastest one to the slowest one:

1. Picos soil volume rigid body
2. Pardiso soil volume rigid body
3. Pardiso stiff soil volume
4. Picos stiff soil volume

As expected, rigid body using Picos solver showed the fastest calculation times, while Pardiso rigid body ended up second, followed by Pardiso using structural elements. The slowest calculation times showed Picos using stiff soil volume.

3.4 CONCLUSION

It was proven, that change of the model from structural element to rigid body will make the calculation faster in any case – no matter, if using Picos or Pardiso solvers. In addition, it can be seen, that while using Picos solver, the computation time can be twice faster for a rigid body than for soil structural element and that Picos solver is gaining the most from use of

rigid body. On the other hand Pardiso is faster with rigid body, but the difference is not very significant at the end – only between 10 and 20%.

While comparing Pardiso and Picos for stiff soil volume, we can see, that the influence of the large number of iterations needed due to contact of very stiff elements and soil is very significant and makes Picos solver the slowest one. It should be pointed out, that with different (smaller) stiffness of the structure, Picos will probably perform faster, but in this case of offshore structure vs. soil interaction we can clearly see Pardiso showing better computational times.

It can be concluded that for modeling of offshore structures and their interaction with soil, the best solution is to use model with rigid body. At first, it is shown in Chapter 7 that the results of rigid body model are showing very satisfactory result. Plus, the calculation times are significantly better for rigid body model and the difference can be expected to be much higher for bigger models up to 100 000 elements, which are used very often in practice.

4 CASE STUDY – SUCTION ANCHOR

This section describes the case study obtained from the company SPT Offshore designing and manufacturing suction piles. The model used by SPT Offshore of a suction anchor is described, then the results are reproduced using rigid bodies by comparing the results of SPT Offshore with the Plaxis rigid body model. Then, soil response stiffness and compliance matrices in different loading conditions are evaluated with the aim to provide the data to structural engineers designing the offshore superstructure.

Suction piles are one of the most effective and mostly used foundations of the offshore structures. The basic structure of a suction pile is a cylindrical unit. The bottom part of the cylinder is open and the top portion is covered. It is partly penetrating to the ground due to its own weight and partly due to suction developed inside the caisson by pumping the water out of the pile. The suction pile has to be designed to withstand two typical types of loading applied to the pile - the static load applied by the structure plus the environmental cyclic loading from waves, wind and currents. The main advantage of a suction caisson is that it can provide sufficient resistance to uplift loading (Samui et al, 2011). A more detailed description of suction piles and their behavior is given in Chapter 2.1.2.

4.1 PROBLEM DESCRIPTION

The model properties were obtained from the company SPT Offshore and the model corresponds to a real suction pile used as a foundation for a jack-up structure in the North Sea, the whole structure with the suction piles at the bottom is shown in Figure 19 and Figure 20.

Figure 19: Suction pile (courtesy of E. Alderlieste).



The buckets are 7.0 m in diameter, and have a total length of 7.4 m. The embedded depth is less than the shell length, this is to account for loosening of the soil inside the bucket. After installation a grout mixture was inserted to fill the space between soil and top plate inside the bucket. The structure was installed in water with a depth of about 20 m. At the location

of the project the seabed consists of sand. Accurate displacements were not the aim of the calculation, the attention was paid to the resultant bearing capacity.

Figure 20: Design of the suction pile and the jack-up structure (courtesy of E. Alderlieste).



4.2 PLAXIS MODEL

The geometry of the model, soil and pile itself together with soil and plate properties were obtained from company SPT offshore, so the basic model is a reproduction of the calculations performed by SPT offshore engineers.

4.2.1 Model properties

At first the suction pile was modelled in Plaxis by conventional structural elements with properties obtained from SPT Offshore. The size of the model is $-18 \leq x \leq 18$, $-18 \leq y \leq 18$, $-40 \leq z \leq 0$ and the water head was set to 20 m. The Hardening soil model is used to model the soil behavior. The soil properties are summarized in Table 3. It should be pointed out, that the properties of single soil layers only differ by their stiffness properties.

Table 3: Soil properties.

Parameter	Symbol	Sand 1	Sand 2	Sand 3	Sand 4	
Material model	Model	Hardening soil	Hardening soil	Hardening soil	Hardening soil	-
Behavior type	Type	Drained	Drained	Drained	Drained	-
Depth	d	[0, -2]	[-2, -5.5]	[-5.5, -8]	[-8, -20]	m
Weight sat	γ_{sat}	20.5	20.5	20.5	20.5	kN/m ³
Weight unsat	γ_{unsat}	20.5	20.5	20.5	20.5	kN/m ³
Secant stiffness in standard drained triaxial test	E_{50}^{ref}	80.10 ³	70.10 ³	90.10 ³	55.10 ³	kN/m ²
Tangent stiffness for primary oedometer loading	$E_{\text{oed}}^{\text{ref}}$	80.10 ³	70.10 ³	90.10 ³	55.10 ³	kN/m ²
Unloading/reloading stiffness	$E_{\text{ur}}^{\text{ref}}$	160.10 ³	140.10 ³	180.10 ³	110.10 ³	kN/m ²
Power for stress-level dependency of stiffness	m	0.5	0.5	0.5	0.5	-
Initial void ratio	e_{init}	0.5	0.5	0.5	0.5	-
Cohesion	c	0.5	0.5	0.5	0.5	kN/m ²
Friction angle	ϕ	35	35	35	35	°
Dilatancy angle	ψ	5	5	5	5	°
Poisson ratio for unloading/reloading	ν_{ur}	0.2	0.2	0.2	0.2	
Reference stress for stiffness	P_{ref}	100	100	100	100	kN/m ²
K_0 for normal consolidation	$K_{0, \text{nc}}$	0.43	0.43	0.43	0.43	
Initial cohesion	c_{inc}	0.0	0.0	0.0	0.0	kN/m ² /m
Reference depth	Z_{ref}	0.0	0.0	0.0	0.0	m
Failure ratio	R_f	0.9	0.9	0.9	0.9	-

Tension cut-off	-	No	No	No	No	-
Strength reduction factor	R_{inter}	0.8	0.8	0.8	0.8	
Consider gap closure		Yes	Yes	Yes	Yes	
K_0 determination		Automatic	Automatic	Automatic	Automatic	
Over-consolidation ration	OCR	1.0	1.0	1.0	1.0	
Pre-overburden pressure	POP	0.0	0.0	0.0	0.0	kN/m ²

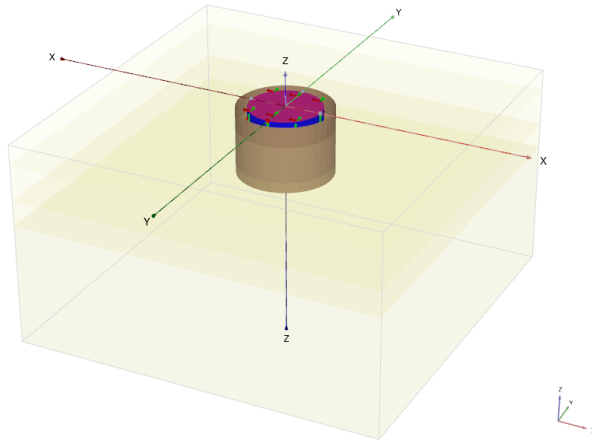
The suction pile is 6.5 m long and is fully incorporated into seabed, the radius of the pile is 3.5 m – it is closed at the top and open at the bottom. The plate properties are described in Table 4:

Table 4: Plate properties.

Parameter	Symbol	Wall	Top Plate	
Thickness	d	0.03	0.25	m
Unit weight	γ	67.15	67.15	kN/m ³
Young's modulus	E	210E6	210E6	kN/m ³
Poisson's ratio	ν	0.3	0.3	-

Inner and outer (positive and negative) interfaces are used around the caisson's walls. The interface strength is 0.8 times the strength in the surrounding soil. The suction pile as generated in Plaxis Structure mode is shown in Figure 21. Since the applied loads to the anchor are not symmetrical, it was necessary to use a full model instead of computationally more efficient symmetrical one.

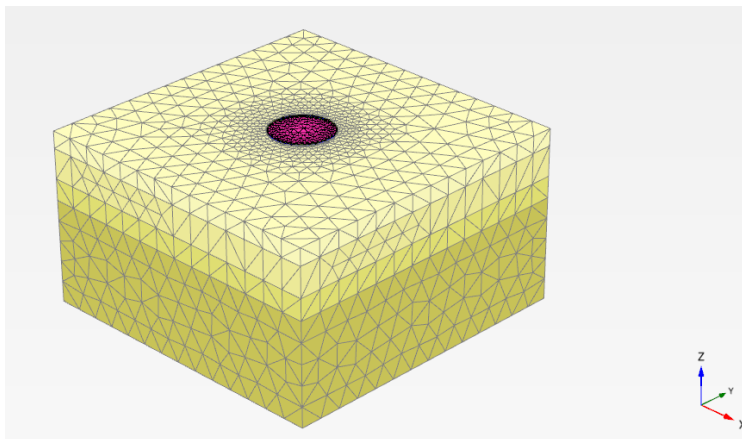
Figure 21: Suction pile as modelled in Plaxis.



Four point loads are defined on the top periphery of the pile in following positions: $[3.5, 0, 0]$, $[-3.5, 0, 0]$, $[0, 3.5, 0]$ and $[0, -3.5, 0]$ simulating the loads applied by the jack-up structure and its legs to the foundation.

For the mesh generation, *Expert* setting is used with Relative element size 0.95, Polyline angle tolerance 30.0, Surface angle tolerance 15.0 and Max cores to use 256. The final mesh is comprised of 41 273 nodes and 27 073 elements with average element size 0.9785 m. The mesh is refined around the suction pile – for the pile a Coarseness factor 0.3 is used. The mesh is depicted in Figure 22.

Figure 22: Final mesh of the model.



4.2.2 Calculations

The calculations in Plaxis are performed in Staged construction phase, in which the initial phase is simulated without any structures, then the construction of the suction pile and then loading by the jack-up structure is applied to the foundation. The aim of the calculations is to evaluate the bearing capacity of the suction pile under combined horizontal, vertical and moment (VHM) loading.

Phase 0: Initial conditions

The initial conditions are modelled using K_0 procedure with all soil clusters activated.

Phase 1: Suction pile installation

The suction pile is simulated in this phase by structural elements – plates, thus, the plates and interfaces are activated to simulate interaction between soil and plates. No loads are applied to the pile.

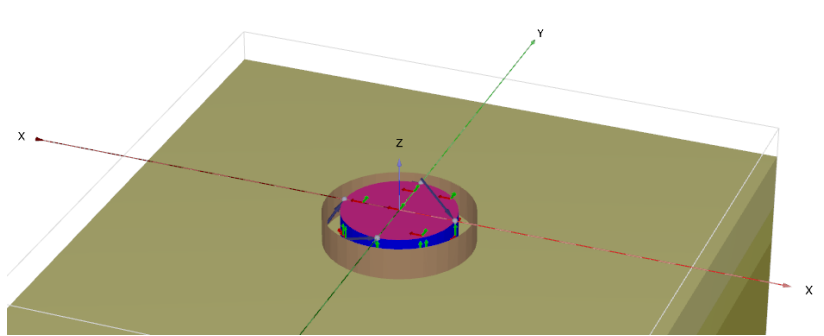
Phase 2: Loading phase

The point loads are activated:

- [3.5, 0, 0] – $F_x = 2190$ kN, $F_y = 0$ kN, $F_z = -2475$ kN
- [-3.5, 0, 0] – $F_x = 2190$ kN, $F_y = 0$ kN, $F_z = 3584$ kN
- [0, 3.5, 0] – $F_x = 2190$ kN, $F_y = 0$ kN, $F_z = 554.3$ kN
- [0, -3.5, 0] – $F_x = 2190$ kN, $F_y = 0$ kN, $F_z = 554.3$ kN

Thus, vertical, horizontal and moment loads are applied to the caisson. The situation is depicted in Figure 23. The upper soil layer is made invisible for better visualization of applied loads.

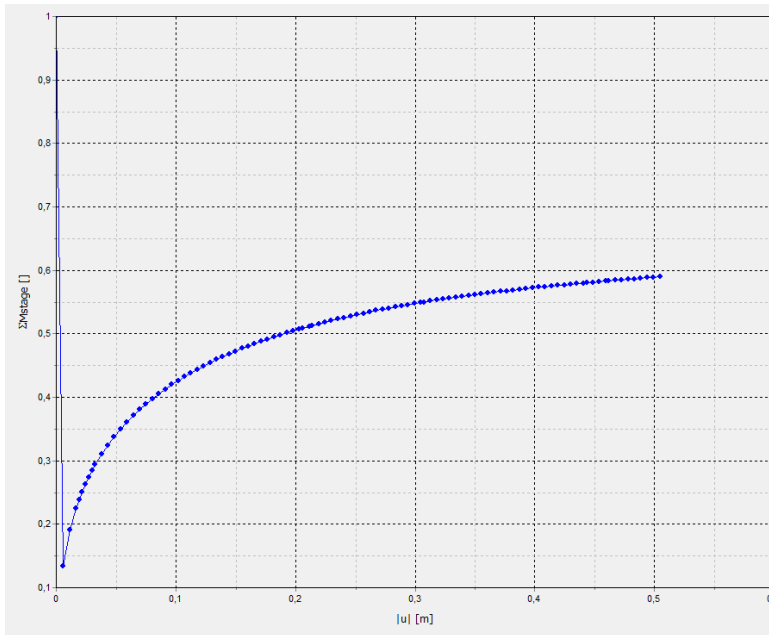
Figure 23: Loading applied to the suction pile.



4.2.3 Results

In the output part of the program, the deformed position of the suction pile can be visualized. The bearing capacity can be evaluated from the load – displacement in Figure 24.

Figure 24: Resultant bearing capacity of the suction pile.



The ΣM_{stage} parameter shown on the y-axis is calculated in following way:

$$\text{Applied load} = \Sigma M_{stage} \cdot \text{Total load applied in current phase} \quad (13)$$

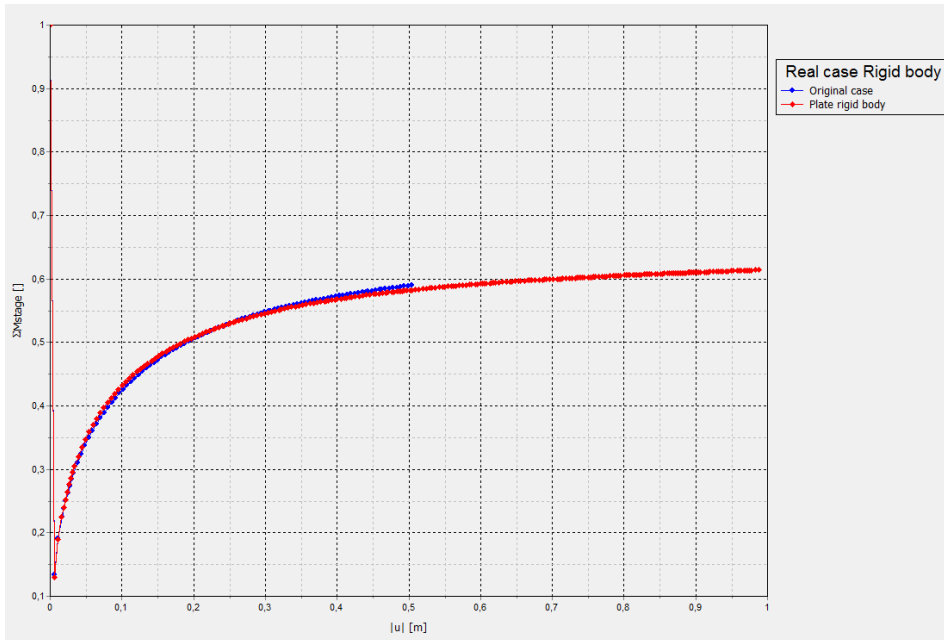
From Equation (13) we can deduce the bearing capacity of the pile, which is equal approximately to 0.6 of the applied load. It should be pointed out, that in this chapter, the interest is not in absolute values, but in comparison of the bearing capacities of a suction pile modelled by a rigid body and a suction pile modelled by structural elements. This comparison is elaborated in the following Chapter 4.3.

4.3 MODEL WITH RIGID BODY

In the next stage, the whole calculation process was reproduced for the model, where plates were replaced by a rigid body created from surface elements.

In the Structures mode of the program, plates were deleted and from the surfaces representing wall and top plate of the pile a single rigid body was created with reference point at [0, 0, 0]. Interfaces around the rigid body are exactly the same as the interfaces around the former plate structure. The mesh and calculations were carried out with exactly the same setting as for the plate suction pile – in *Phase 1* instead of activating plates, the rigid body was activated with reference point at [0, 0, 0] and all forces and moments applied were set to 0. In *Loading phase* point loads were activated and kept the same as in previous model, the rigid body was activated without any change from *Phase 1*. After this procedure, the same results for the rigid body suction pile were expected, the comparison of results is shown in Figure 25.

Figure 25: Comparison of rigid body and plate suction pile bearing capacity.



The biggest difference between the bearing capacities of the two cases is 1.2% with mostly values smaller than 1%. In addition, some differences are expected as the behavior of rigid body should be different to the behavior of very stiff plate elements. The plates in original case are allowed to deform, but the rigid body can just move and rotate without any deformation of the structure.

4.4 STIFFNESS MATRIX DETERMINATION

After reproducing the real case of suction pile installation with the rigid body model, the model itself was slightly changed for easier conditions while obtaining the soil response stiffness matrix from Plaxis. The data from Plaxis to determine the stiffness matrix can be obtained only for the model with rigid body, since from the definition of rigid body in Chapter 2.2.1 we can deduce, that it is the only option, how 6 exact values of displacements can be obtained from applied forces. In this case of a rigid body suction pile, the foundations described in Chapter 4.3 can be represented by a soil response stiffness matrix.

The geometry of the model remained the same, but point loads were deleted and all the loads and displacements were applied/prescribed to the rigid body reference point at $[0, 0, 0]$. This was the only option how to obtain displacements and rotations of a rigid body from current version of Plaxis. Soil layers, geometry of the model, geometry of the pile and interfaces remained the same, in all the following calculations, suction pile is modelled by surface-created rigid body with deactivated plates and reference point (point where the load/displacement is applied) at $[0, 0, 0]$.

4.4.1 Description of the procedure

In this chapter the procedure how the stiffness matrix or compliance matrix was built will be described. At the beginning it is necessary to describe calculation phases in staged construction mode performed in Plaxis:

Phase 0: Initial conditions

The initial conditions are modelled using K_0 procedure with all soil clusters activated.

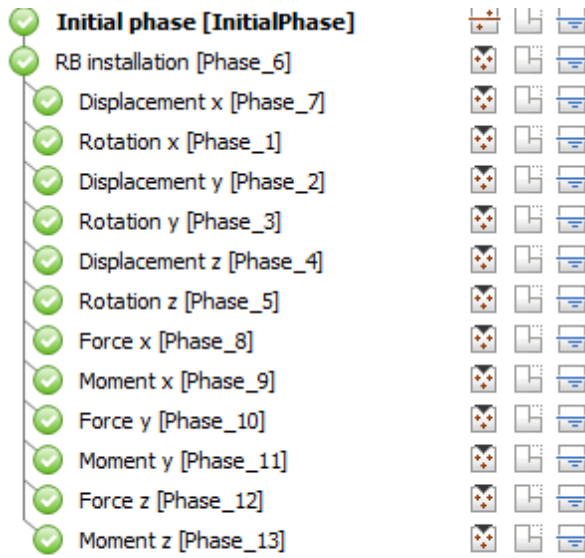
Phase 1: Suction pile installation

The suction pile is modelled in this phase by the rigid body with all the interfaces around active. No loads or displacements are applied to rigid body. The reference point is set to $[0, 0, 0]$.

Phase 2: Loading phases

In this part 12 individual calculation phases were performed – 6 with prescribed displacements and rotations for determination of the stiffness matrix and 6 with applied forces and moments for determination of the compliance matrix. The calculation process in Plaxis is shown in Figure 26.

Figure 26: Performed calculations as shown in Plaxis Input program.



Stiffness matrix

To obtain the stiffness matrix in every calculation one single displacement/rotation was prescribed to a non-zero value, while other values were set to zero. This was repeated for every displacement and rotation component (u_x , u_y , u_z , ϕ_x , ϕ_y and ϕ_z). From every calculation were obtained 6 reactions (F_x , F_y , F_z , M_x , M_y and M_z), then, using the equation (14):

$$\bar{f} = \bar{K} \bar{u} \quad (14)$$

single terms of stiffness matrix could be determined:

In the case of prescribing u_x and setting other values to zero, equation (14) takes a form:

$$\begin{Bmatrix} F_x \\ F_y \\ F_z \\ M_x \\ M_y \\ M_z \end{Bmatrix} = \begin{bmatrix} F_x/u_x & 0 & 0 & 0 & 0 & 0 \\ F_y/u_x & 0 & 0 & 0 & 0 & 0 \\ F_z/u_x & 0 & 0 & 0 & 0 & 0 \\ M_x/u_x & 0 & 0 & 0 & 0 & 0 \\ M_y/u_x & 0 & 0 & 0 & 0 & 0 \\ M_z/u_x & 0 & 0 & 0 & 0 & 0 \end{bmatrix} \begin{Bmatrix} u_x \\ u_y = 0 \\ u_z = 0 \\ \phi_x = 0 \\ \phi_y = 0 \\ \phi_z = 0 \end{Bmatrix} \quad (15)$$

This procedure can be repeated for every displacement and rotation component, always giving non-zero terms in the equivalent column of the global stiffness matrix, while zeroes are obtained in all other columns, since the rotations and displacements relevant to these columns are zero, giving:

$$\frac{F_i}{u_i} = 0 \quad (16)$$

After performing all the calculations, the final stiffness matrix is built in following form (17):

$$\bar{\bar{K}} = \begin{bmatrix} F_x/u_x & F_x/u_y & F_x/u_z & F_x/\varphi_x & F_x/\varphi_y & F_x/\varphi_z \\ F_y/u_x & F_y/u_y & F_y/u_z & F_y/\varphi_x & F_y/\varphi_y & F_y/\varphi_z \\ F_z/u_x & F_z/u_y & F_z/u_z & F_z/\varphi_x & F_z/\varphi_y & F_z/\varphi_z \\ M_x/u_x & M_x/u_y & M_x/u_z & M_x/\varphi_x & M_x/\varphi_y & M_x/\varphi_z \\ M_y/u_x & M_y/u_y & M_y/u_z & M_y/\varphi_x & M_y/\varphi_y & M_y/\varphi_z \\ M_z/u_x & M_z/u_y & M_z/u_z & M_z/\varphi_x & M_z/\varphi_y & M_y/\varphi_z \end{bmatrix} \quad (17)$$

From this, coupling between applied rotations/displacements and obtained forces/moments can be easily seen.

Compliance matrix

To build the compliance matrix a similar procedure is carried out, but here with prescribed forces instead of prescribed displacements. The definition of compliance matrix is as is shown in equation (18):

$$\bar{f} = \bar{\bar{C}} \bar{u} \quad (18)$$

Then, after applying forces and moments in the same manner as with the displacements and rotations for the stiffness matrix, we obtain at the end compliance matrix:

$$\bar{\bar{C}} = \begin{bmatrix} u_x/F_x & u_x/F_y & u_x/F_z & u_x/M_x & u_x/M_y & u_x/M_z \\ u_y/F_x & u_y/F_y & u_y/F_z & u_y/M_x & u_y/M_y & u_y/M_z \\ u_z/F_x & u_z/F_y & u_z/F_z & u_z/M_x & u_z/M_y & u_z/M_z \\ \varphi_x/F_x & \varphi_x/F_y & \varphi_x/F_z & \varphi_x/M_x & \varphi_x/M_y & \varphi_x/M_z \\ \varphi_y/F_x & \varphi_y/F_y & \varphi_y/F_z & \varphi_y/M_x & \varphi_y/M_y & \varphi_y/M_z \\ \varphi_z/F_x & \varphi_z/F_y & \varphi_z/F_z & \varphi_z/M_x & \varphi_z/M_y & \varphi_z/M_z \end{bmatrix} \quad (19)$$

4.4.2 Validation of the procedure – environmental loading

To make the verification of the procedure, the material model of the soil was changed to linear elastic and in the installation of the suction pile the rigid body is activated with the reference point at [0, 0, 0] and with no forces and displacements applied. Then, in the loading phase displacements and forces are applied as in Figure 26.

The values used are shown in following Table 5:

Table 5: Applied forces and displacements.

Displacement/Rotation	Value	Force/Moment	Value
ux	0.00067556 m	Fx	1 000 kN
uy	0.00067576 m	Fy	1 000 kN
uz	0.00048460 m	Fz	1 000 kN
ϕ_x	0.000018455 rad	Mx	1 000 kN m
Φ_y	0.000018465 rad	My	1 000 kN m
Φ_z	0.000016954 rad	Mz	1 000 kN m

Stiffness matrix from prescribed displacements/rotations and compliance matrix from applied forces/moments were obtained according to the procedure described above, then value of \bar{C}^{-1} was determined and compared to the resultant stiffness matrix \bar{K} .

(20)

$$\bar{K} =$$

3.020	0.000	0.000	0.000	-13.021	0.000
0.000	3.019	0.000	13.031	0.000	-0.002
0.000	0.000	2.065	-0.004	0.002	0.000
0.000	13.041	-0.004	110.454	-0.002	-0.011
-13.042	0.000	0.002	-0.002	110.344	0.000
0.000	-0.002	0.000	-0.011	0.000	58.957

$$\bar{C}^{-1} =$$

3.019	0.000	0.000	0.000	-13.039	0.000
0.000	3.018	0.000	13.036	0.000	-0.002
0.000	0.000	2.064	-0.004	0.002	0.000
0.000	13.036	-0.004	110.499	-0.002	-0.011
-13.034	0.000	0.002	-0.002	110.448	0.000
0.000	-0.002	0.000	-0.011	0.000	58.983

Then, we subtract the \bar{C}^{-1} from \bar{K} :

$$K - C^{-1} =$$

0.001	0.000	0.000	0.000	0.018	0.000
0.000	0.001	0.000	-0.005	0.000	0.000
0.000	0.000	0.002	0.000	0.000	0.000
0.000	0.004	0.000	-0.045	0.000	0.000
-0.008	0.000	0.000	0.000	-0.104	0.000
0.000	0.000	0.000	0.000	0.000	-0.026

At first, it should be pointed out, that the matrices were divided by 1.10^6 for better representation and understanding of the coupling. From the matrices is clearly visible the coupling between the terms, but in this case the interest was in comparison between stiffness and compliance matrices and from the results we can see, that the differences are insignificant and in all cases are smaller than 0.1 %. Both procedures are giving us mostly the same result and more importantly the same coupling between the terms.

This procedure is just to demonstrate and verify the process of stiffness and compliance matrix determination, since the evolution of the loading is not realistic and does not correspond to the Plaxis model of a real suction pile described above, but the loads applied to the pile are of the same order as expected environmental loading as wind, waves and currents (Shehata, 2013) applied through legs of a jack-up structure. So the resultant stiffness matrix is demonstrating the environmental loading applied to the pile without any influence of the theoretical structure above.

To obtain corresponding values of the single terms of the stiffness matrix compared to the inverse of the compliance matrix, at first forces and moments are applied in six single calculations from which the compliance matrix is determined. Then the obtained displacements ($F_i \rightarrow u_i$) are prescribed in another six calculations, from which the stiffness matrix is obtained. This procedure ensures, that the stiffness matrix is determined from the same point in the force/displacements curve.

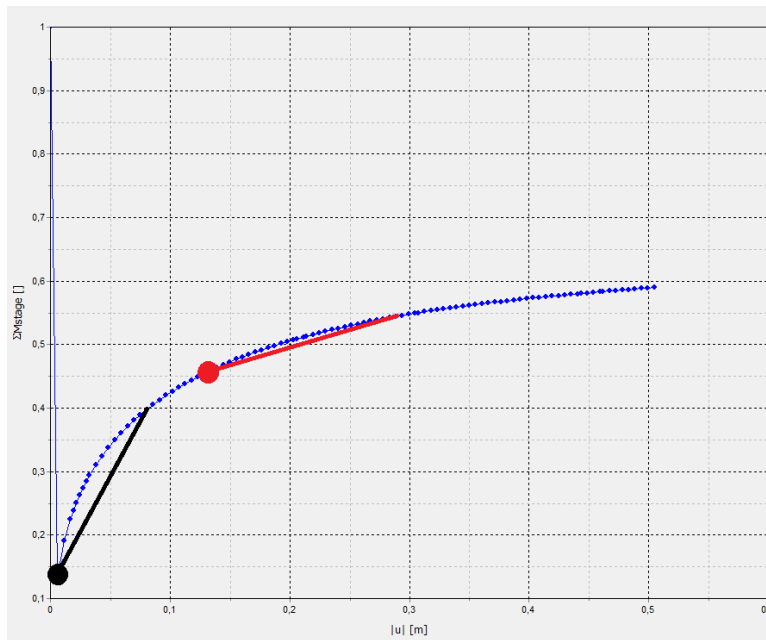
This validation procedure was performed for surface rigid body as shown above, then in addition for plate rigid body and soil rigid body. The resultant differences between the corresponding terms in stiffness and inverted compliance matrices are again within the range of 0.1% for plate and soil rigid body suction piles. In addition, the differences between values of corresponding terms in stiffness matrices of soil, plate and surface rigid bodies are smaller than 1%. All the following calculations were performed for surface rigid body. The reason for it is that calculations using surface rigid body are faster than with plate rigid body – the model with plate rigid body is bigger than the model with surface rigid body, as the models are identical, just the plate rigid body model has defined plate elements in addition to surface rigid body model. On the other hand, soil volume rigid body is less realistic compared to surface rigid body, especially in case of a model of suction pile – with surface rigid body just the walls and upper plate of suction pile are defined as rigid body, but with soil volume rigid body the whole volume of suction pile with the soil inside as well is defined as rigid body. Thus, soil rigid body will predict different bearing capacity especially for vertical uplift loading – the loading situation very typical for suction pile used for mooring of compliant structures. A more extensive comparison of soil volume rigid body suction pile and surface rigid body suction pile is described in Chapter 7.2.3.

4.4.3 Validation of the procedure – static loading

In this chapter a procedure will be shown to determine a stiffness matrix for a realistic case with static loading of the structure followed by environmental loading – surface rigid body with reference point at $[0, 0, 0]$ is used to model the suction pile. Then, the procedure is validated using the linear elastic model as in the previous Chapter 4.4.2. As all the model properties are the same as in the previous chapter and the behavior is linear elastic, exactly the same terms in the global stiffness matrix were expected.

On the load displacement curve created from the case study can be shown secant stiffness matrices corresponding to the procedures described in Chapter 4.4.2 and 4.4.3. The black line is representing a stiffness matrix for pure environmental loading without any static load. The red line is representing a stiffness matrix after application of a static load by the structure followed by environmental loading. The curve is shown in Figure 27. The purpose is to show evolution of the stiffness matrix with loading and the difference between the matrices for the real case.

Figure 27: Load-displacement curve with highlighted secant stiffness matrices. The case of environmental loading in black and the case of static loading + environmental loading in red.



The first two calculation phases used in the model are exactly the same as in previous case:

Phase 0: Initial conditions

The initial conditions are modelled using K_0 procedure with all soil clusters activated.

Phase 1: Suction pile installation

The suction pile is modelled in this phase by rigid body with all the interfaces around active. No loads or displacements are applied to rigid body. The reference point is set to $[0, 0, 0]$. The displacements are set to zero.

Phase 2: Static load

In this phase a static load of the jack-up structure is applied to the suction pile. The load is applied to the rigid body reference point at $[0, 0, 0]$. Forces, moments applied to the rigid body and the reference point are shown in Figure 28:

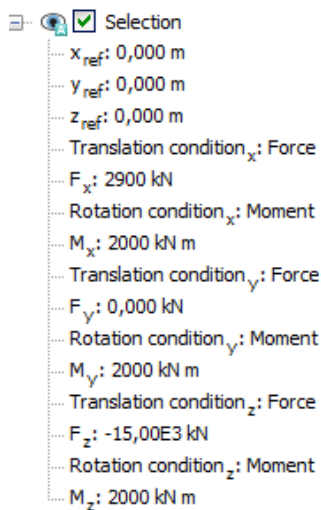


Figure 28: Reference point and forces and moments applied to the rigid body.

The forces and moments applied to the rigid body are of order of magnitude as the obtained values for real case suction pile. The option Reset displacements to zero is activated.

Phase 3: nil step

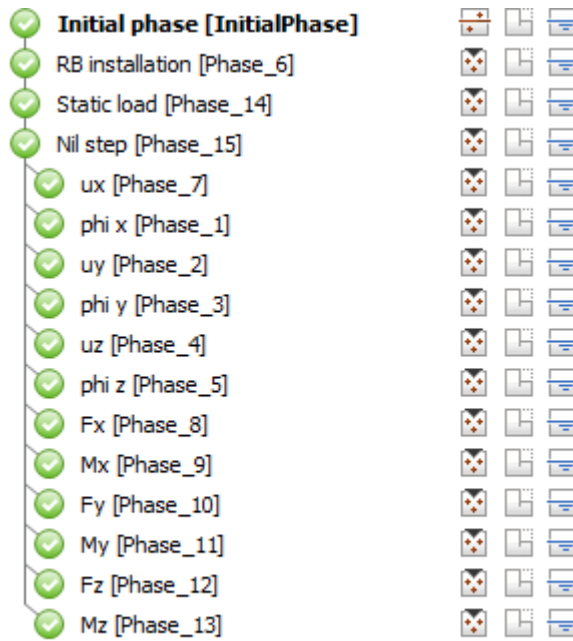
The so-called NIL step is adopted to ensure that the initial stress field is in equilibrium. It is a calculation step in which no additional load is applied. After completion of this step, the stress field is in equilibrium. To achieve, that displacements calculated during a nil-step do not affect later calculations, the Reset displacements to zero is adopted in later calculations.

Phase 4: Environmental loading

This part is exactly the same as environmental loading phase in previous validation: 6 single displacements/rotations and 6 single forces/moments are prescribed from which stiffness and compliance matrices are determined. In every phase option Reset displacements to zero is activated. The values of forces/moments and displacements/rotations are shown in Table 5 and are the same as in previous validation. The resultant secant stiffness matrix is represented by red line in the Figure 27.

The whole calculation procedure in Staged construction mode is shown in Figure 29:

Figure 29: All calculation phases carried out in Staged construction.



The resultant stiffness matrix is as following:

$$\bar{K} = \begin{bmatrix} 3.019 & 0.000 & 0.000 & 0.000 & -13.021 & 0.000 \\ 0.000 & 3.018 & 0.000 & 13.031 & 0.000 & -0.002 \\ 0.000 & 0.000 & 2.065 & -0.003 & 0.001 & 0.000 \\ 0.000 & 13.040 & -0.003 & 110.453 & -0.001 & -0.010 \\ -13.041 & -0.000 & 0.001 & -0.001 & 110.344 & 0.000 \\ 0.000 & -0.002 & 0.000 & -0.010 & 0.000 & 58.957 \end{bmatrix} \quad (23)$$

and the inverse of compliance matrix:

$$\overline{C}^{-1} = \begin{bmatrix} 3.018 & 0.000 & 0.000 & 0.000 & -13.038 & 0.000 \\ 0.000 & 3.017 & 0.000 & 13.036 & 0.000 & -0.002 \\ 0.000 & 0.000 & 2.063 & -0.003 & 0.001 & 0.000 \\ 0.000 & 13.036 & -0.003 & 110.498 & -0.001 & -0.010 \\ -13.033 & 0.000 & 0.001 & -0.001 & 110.447 & 0.000 \\ 0.000 & -0.002 & 0.000 & -0.010 & 0.000 & 58.983 \end{bmatrix} \quad (24)$$

Then, after subtracting the inverse of the compliance matrix to the stiffness matrix we obtain the difference between two procedures:

$$K - C^{-1} = \begin{array}{|c|c|c|c|c|c|} \hline 0.001 & 0.000 & 0.000 & 0.000 & 0.018 & 0.000 \\ \hline 0.000 & 0.001 & 0.000 & -0.005 & 0.000 & 0.000 \\ \hline 0.000 & 0.000 & 0.002 & 0.000 & 0.000 & 0.000 \\ \hline 0.000 & 0.004 & 0.000 & -0.045 & 0.000 & 0.000 \\ \hline -0.008 & 0.000 & 0.000 & 0.000 & -0.104 & 0.000 \\ \hline 0.000 & 0.000 & 0.000 & 0.000 & 0.000 & -0.026 \\ \hline \end{array} \quad (25)$$

From (49) we can conclude, that the maximum error between the two procedures is smaller than 0.1%. Then, as in both cases exactly the same model is used and the material model is linear elastic, all the stiffness matrices should be the same. For this purpose inverse of the compliance matrix from the first case (only environmental loading) and the second case will be compared (static load plus environmental loading). The reason why the inverse of compliance matrix is used instead of the stiffness matrix is, that the inverse of compliance matrix is more realistic, because it was built using applied forces to the structure instead of prescribed displacements. In realistic cases, the foundation is loaded by forces from the structure and from the environmental load, on the other hand prescribed displacements are not a type of loading seen in the application. In addition, the engineers projecting structures such as suction piles are used to work with applied load instead of applied displacements, since it is simulating the real loading much more precisely.

The resultant difference between both C^{-1} is shown in following equation (50):

$$C^{-1}(1) - C^{-1}(2) = \begin{array}{|c|c|c|c|c|c|} \hline 0.000 & 0.000 & 0.000 & 0.000 & 0.000 & 0.000 \\ \hline 0.000 & 0.000 & 0.000 & 0.000 & 0.000 & 0.000 \\ \hline 0.000 & 0.000 & 0.000 & 0.000 & 0.000 & 0.000 \\ \hline 0.000 & 0.000 & 0.000 & 0.000 & 0.000 & 0.000 \\ \hline 0.000 & 0.000 & 0.000 & 0.000 & 0.000 & 0.000 \\ \hline 0.000 & 0.000 & 0.000 & 0.000 & 0.000 & 0.000 \\ \hline \end{array} \quad (26)$$

As the matrices are exactly the same and the material model is linear elastic, we can conclude that the procedure is verified and we can build soil response stiffness matrices in this manner.

4.4.4 Stiffness matrix determination for the case study

In this chapter will be presented final soil response stiffness matrix of the real case suction pile presented in Chapter 4.2 and 4.3 – the real case with suction pile defined as rigid body with reference point at [0, 0, 0].

4.4.4.1 Linear elastic and Mohr-Coulomb model comparison

At first, results using linear elastic and Mohr – Coulomb material models are compared. For the comparison, the procedure used in Chapter 4.4.2 was used, thus, an environmental loading was applied to the rigid body and stiffness matrix was determined by applying single force components. The resultant soil response stiffness matrix for linear elastic model is:

$$\bar{\bar{K}}_{lin} = \begin{array}{c} \begin{array}{|c|c|c|c|c|c|} \hline 3.019 & 0.000 & 0.000 & 0.000 & -13.039 & 0.000 \\ \hline 0.000 & 3.018 & 0.000 & 13.036 & 0.000 & -0.002 \\ \hline 0.000 & 0.000 & 2.064 & -0.004 & 0.002 & 0.000 \\ \hline 0.000 & 13.036 & -0.004 & 110.499 & -0.002 & -0.011 \\ \hline -13.034 & 0.000 & 0.002 & -0.002 & 110.448 & 0.000 \\ \hline 0.000 & -0.002 & 0.000 & -0.011 & 0.000 & 58.983 \\ \hline \end{array} \end{array} \quad (27)$$

While the soil response stiffness matrix for Mohr – Coulomb model is:

$$\bar{\bar{K}}_{MC} = \begin{array}{c} \begin{array}{|c|c|c|c|c|c|} \hline 2.206 & 0.002 & 0.001 & 0.008 & -9.796 & 0.003 \\ \hline 0.001 & 2.199 & -0.001 & 9.773 & 0.000 & -0.006 \\ \hline -0.351 & -0.526 & 1.910 & -2.615 & 1.289 & -0.044 \\ \hline 0.006 & 15.528 & -0.004 & 118.917 & -0.047 & -0.022 \\ \hline -15.485 & 0.016 & 0.001 & 0.040 & 118.689 & 0.021 \\ \hline -0.019 & 0.017 & 0.003 & 0.059 & 0.033 & 56.486 \\ \hline \end{array} \end{array} \quad (28)$$

For better visualization of the results, both stiffness matrices are shown again with all the values smaller than $|0.1|$ (all the values smaller than 5% of the smallest value on the main diagonal) set to zero:

$$\bar{\bar{K}}_{lin0} = \begin{array}{c} \begin{array}{|c|c|c|c|c|c|} \hline 3.019 & 0 & 0 & 0 & -13.039 & 0 \\ \hline 0 & 3.018 & 0 & 13.036 & 0 & 0 \\ \hline 0 & 0 & 2.064 & 0 & 0 & 0 \\ \hline 0 & 13.036 & 0 & 110.499 & 0 & 0 \\ \hline -13.034 & 0 & 0 & 0 & 110.448 & 0 \\ \hline 0 & 0 & 0 & 0 & 0 & 58.983 \\ \hline \end{array} \end{array} \quad (29)$$

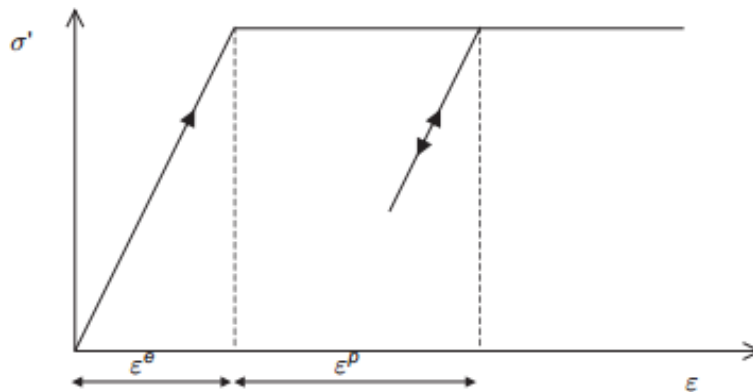
and

$$\bar{\bar{K}}_{MC0} = \begin{array}{|c|c|c|c|c|c|} \hline 2.206 & 0 & 0 & 0 & -9.796 & 0 \\ \hline 0 & 2.199 & 0 & 9.773 & 0 & 0 \\ \hline -0.351 & -0.526 & 1.910 & -2.615 & 1.289 & 0 \\ \hline 0 & 15.528 & 0 & 118.917 & 0 & 0 \\ \hline -15.485 & 0 & 0 & 0 & 118.689 & 0 \\ \hline 0 & 0 & 0 & 0 & 0 & 56.486 \\ \hline \end{array} \quad (30)$$

Since the linear elastic model is purely elastic (ε^e part of x-axis in the graph in Figure 30) and Mohr-Coulomb model is elastic – perfectly plastic (plastic behaviour is represented by ε^p part of x-axis in the same graph), we can conclude, that the differences between the two matrices has to be due to perfectly plastic behaviour of Mohr-Coulomb model. Thus, the coupling between the terms in $\bar{\bar{K}}_{lin0}$ (forming a cross-like shape of a non-zero terms in stiffness matrix) is caused by elastic properties of the material. On the other hand additional coupling with u_z is caused by perfectly plastic properties of Mohr-Coulomb model.

Linear elastic a Mohr-Coulomb (MC) models are shown in Figure 30, while MC is represented by the whole curve, but linear elastic only by ε^e part of the curve.

Figure 30: Mohr - Coulomb model.



Another interesting fact in comparison of the matrices is, that in $\bar{\bar{K}}_{lin0}$ terms $K_{15} = K_{51}$ and $K_{24} = K_{42}$ and the matrix is symmetric. In case of $\bar{\bar{K}}_{MC0}$ matrix is not symmetric and the terms $K_{15} \neq K_{51}$ and $K_{24} \neq K_{42}$.

4.4.4.2 Hardening soil model

Then, soil response stiffness matrix was determined for Hardening soil model – the original way, how was the model of suction pile used by the SPT offshore company.

Environmental loading

Firstly, only environmental loading was applied to the suction pile, the obtained stiffness matrix is:

$$\bar{\bar{K}}_{HS} = \begin{array}{|c|c|c|c|c|c|} \hline 0.830 & 0.000 & 0.001 & 0.002 & -3.935 & 0.000 \\ \hline 0.001 & 0.830 & 0.000 & 3.938 & -0.006 & -0.008 \\ \hline -0.190 & -0.167 & 0.995 & -0.477 & 1.229 & 0.457 \\ \hline -0.005 & 5.347 & -0.003 & 40.981 & 0.048 & -0.062 \\ \hline -5.334 & 0.001 & -0.001 & -0.002 & 40.891 & -0.008 \\ \hline -0.011 & 0.001 & 0.000 & 0.004 & 0.082 & 14.762 \\ \hline \end{array} \quad (31)$$

And with all the terms smaller than |0.1| set to zero:

$$\bar{\bar{K}}_{HS0} = \begin{array}{|c|c|c|c|c|c|} \hline 0.830 & 0 & 0 & 0 & -3.935 & 0 \\ \hline 0 & 0.830 & 0 & 3.938 & 0 & 0 \\ \hline -0.190 & -0.167 & 0.995 & -0.477 & 1.229 & 0.457 \\ \hline 0 & 5.347 & 0 & 40.981 & 0 & 0 \\ \hline -5.334 & 0 & 0 & 0 & 40.891 & 0 \\ \hline 0 & 0 & 0 & 0 & 0 & 14.762 \\ \hline \end{array} \quad (32)$$

In the result of Hardening soil model, we can see coupling of all the force/moment terms with displacement in z direction, in one case (M_y versus u_z) the value of the term is even bigger than in some terms on the main diagonal. In contrast to elastic perfectly-plastic Mohr-Coulomb model, the yield surface of a Hardening soil model is not fixed, but can expand due to plastic straining, thus, we can deduce that the coupling shown in $\bar{\bar{K}}_{HS0}$ is due to additional plastic straining compared to Mohr-Coulomb model. Although the comparison of the models was carried out in order to determine the coupling between the terms and their change with the change of the model, we can see that on main diagonal Hardening soil model is showing smaller values of secant stiffness than linear elastic and Mohr Coulomb model, this results are in agreement with the theory of the models.

Loading by structure followed by environmental loading

Then, in the last calculations, an exactly same model as in Chapter 4.2.2 was used – After installation of the suction pile, the pile is loaded by the jack-up structure above, then the procedure created in Chapter 4.4.3 is carried out – Nil step is carried out ensure that the initial stress field is in equilibrium and then, environmental loading is simulated by applying the individual force components.

The resultant stiffness matrix is:

$$\bar{\bar{K}}_{HSLarge} = \begin{array}{|c|c|c|c|c|c|} \hline 1.245 & 0.093 & 0.021 & 0.541 & -6.206 & 0.017 \\ \hline 0.006 & 1.321 & -0.001 & 6.681 & -0.065 & 0.022 \\ \hline -0.225 & -1.417 & 0.595 & -8.039 & 0.271 & 0.262 \\ \hline 0.023 & 8.877 & 0.002 & 57.61 & -0.024 & 0.497 \\ \hline -8.718 & 0.003 & -0.054 & 0.065 & 56.953 & -0.056 \\ \hline -0.077 & 0.024 & 0.090 & 0.623 & 0.594 & 20.279 \\ \hline \end{array} \quad (33)$$

And, after setting all the terms smaller than $|0.1|$ set to zero again we obtain:

$$\bar{\bar{K}}_{HSLarge0} = \begin{array}{|c|c|c|c|c|c|} \hline 1.245 & 0 & 0 & 0.541 & -6.206 & 0 \\ \hline 0 & 1.321 & 0 & 6.681 & 0 & 0 \\ \hline -0.225 & -1.417 & 0.595517 & -8.039 & 0.271 & 0.262 \\ \hline 0 & 8.877 & 0 & 57.613 & 0 & 0.497 \\ \hline -8.718 & 0 & 0 & 0.165 & 56.953 & 0 \\ \hline 0 & 0 & 0 & 0.623 & 0.594 & 20.279 \\ \hline \end{array} \quad (34)$$

In this case we can see much stronger coupling, or more precisely said, coupling between the terms is much more common. We can see, that the pattern firstly observed in stiffness matrix determined from model using Mohr-Coulomb material still form basic structure of non-zero terms of the matrix. On the other hand, we can see additional coupling for all the terms containing M_x .

Interestingly, applying force in z direction is still affecting only displacement in z direction, other applied forces or moments are affecting at least 3 displacements or rotations.

4.5 CONCLUSION

In this chapter was used the model obtained by company SPT offshore – more particularly results of a full scale field test of a suction pile supporting jack-up structure. At first the model using stiff structural elements was used, all the data in the model were obtained from the company SPT offshore. Then, the results were reproduced with the model using rigid bodies (particularly surface rigid bodies) yielding the resultant bearing capacity with difference smaller than 1%.

Then the procedure to determine soil response stiffness matrix was described and validated using a model with soil described by linear elastic material model. At the end this procedure was used to determine soil response stiffness matrix of the case study – three material models were used: linear elastic, Mohr-Coulomb and at then original Hardening soil model. Use of Hardening soil model was recommended by SPT offshore.

Unfortunately, it was impossible to determine tangent stiffness matrix by applying very small forces or displacements, because the unbalance forces in the model became significant after applying forces smaller than 10kN, so the resultant stiffness matrix was showing unrealistic results. After finding out this issue, it was decided to build soil response stiffness matrices for the load values corresponding of order of typical environmental loading. The coupling was observed in all the models with more coupling in more sophisticated models (linear elastic -> Mohr-Coulomb -> Hardening soil).

Typical coupling pattern occurring due to elastic response was a cross shape pattern with zeroes in other terms, the patterns is shown in following Equation (35):

$$\bar{K} = \begin{array}{c} \begin{array}{|c|c|c|c|c|c|} \hline K_{11} & 0 & 0 & 0 & -K_{15} & 0 \\ \hline 0 & K_{22} & 0 & K_{24} & 0 & 0 \\ \hline 0 & 0 & K_{33} & 0 & 0 & 0 \\ \hline 0 & K_{42} & 0 & K_{44} & 0 & 0 \\ \hline -K_{51} & 0 & 0 & 0 & K_{55} & 0 \\ \hline 0 & 0 & 0 & 0 & 0 & K_{66} \\ \hline \end{array} \end{array} \quad (35)$$

Then, using perfect plasticity (Mohr-Coulomb model), it was observed, that coupling of force components with displacement in z direction became significant as well.

Then, with the real case using Hardening soil model, two secant stiffness matrices were determined:

1. Stiffness matrix for environmental loading applied to the suction pile prior to construction of the jack-up structure
2. Stiffness matrix after application of static load by the structure followed by environmental loading.

This two matrices were compared to investigate an evolution of the stiffness matrix with loading (with the change of its position in load-displacement curve show for example in Figure 27). In the first case, a typical 'cross-like shape coupling' of the terms in stiffness matrix is visible, in addition for every force applied we can see coupling with displacement in z direction. For the second case with the larger displacement, we can observe coupling between more terms - for every force or moment applied at least three non-zero terms in stiffness matrix were obtained, the only exception was F_z , which contributed only in displacement in z direction.

It is important to point out, that the coupling described in Equation (35) is typically observed by engineers in SPT offshore company (personal communication, April, 2010).

5 CONCLUSIONS AND RECOMMENDATIONS

This chapter contains the conclusions and recommendations rising from these objectives:

1. Gain insight into offshore geotechnics, rigid bodies and their implementation into Plaxis.
2. Validation of rigid body elements in Plaxis.
3. Creating a procedure to determine a soil response stiffness matrix from Plaxis computational results.
4. Compare computational times of models with rigid bodies with models with structural elements, following this to give recommendations for use of rigid bodies in Plaxis computational software.

Conclusion – objective 1

The first objective was to gain insight into offshore geotechnics rigid bodies and their implementation into Plaxis. At first, description of offshore geotechnics was performed and the differences between typical offshore and onshore practice were drawn. All the most typical types of offshore foundations and their typical loading conditions were described with special attention to suction piles. The most significant difference to onshore practice lies in environmental loading by wind, waves and currents applied to the structures in many (up to 10^9) cycles in the life of the foundation.

Then, the possibility to describe offshore foundations as rigid body was concluded from the fact that the stiffness differences between the surrounding soil on the seabed and the foundation can be very significant, leading to rigid-like behavior of the foundation.

After this, description of the implementation of rigid body in Plaxis kernel followed and types of solvers in Plaxis were described, as it was expected, that with implementation of rigid body, the calculation times with rigid bodies will become faster and it will influence different solver types in different manner.

Conclusion – objective 2

The validation of implementation of rigid body was the first objective of the thesis. The basic validations were performed – for testing of interaction of interface elements with rigid body a model of sliding block using Mohr-Coulomb criterion was used and the results were verified by calculation “by hand”, in the next step the same model only with different geometry was used to validate behavior of the whole model with symmetrical rigid objects and surface, soil volume and plate rigid bodies. Moreover, the model with more than one rigid body and the model with more interconnected rigid bodies with the same translation condition (or applied force) and reference point were tested.

In the next part models using all the basic calculation types (plastic calculation, safety factor, consolidation and dynamics) were tested. In every verification case two similar models were created – one with rigid body and one with very stiff soil element, then the results were compared to each other. For all the calculation types, same results were obtained.

In the last part of the validation, more complicated model of a suction pile was used. Because of the topic of the thesis and because in the case study suction pile was used, it was decided to use a model of a suction pile. The model was obtained from detailed study of suction pile behavior from Andersen et al (2004) – the resultant bearing capacities of different suction pile geometries and soil conditions were compared to the results obtained from the literature. Andersen et al (2004) used different models to find bearing capacity, so the interval of expected bearing capacities were provided – all the models with rigid body fit into the interval. In addition, every calculation was performed for soil volume and surface rigid body, plus all the results were validated by using corresponding very stiff structural elements. It can be concluded that the rigid element was properly implemented Plaxis 3D.

Conclusion – objective 3

The third objective was to create a procedure, how to determine single terms of soil response stiffness matrix from Plaxis computational results after applying the individual force components and then to use the procedure to determine a stiffness matrix for full scale field test.

For this purpose, a model was created from the data obtained from company SPT offshore manufacturing and designing suction pile. The particular pile was used as foundation beneath the jack-up structure in the North Sea. To create a benchmark for further calculation, a model recommended by SPT offshore was used – the sand was modelled by Hardening soil model and the whole geometry was made according to SPT offshore. At first, the suction pile was modelled using stiff plate elements. After that the results from SPT offshore were reproduced, plates in the model were changed to rigid bodies and the results were compared leading to difference in bearing capacity in maximum of 1%. This difference can be accounted to the fact that very stiff plate are still able to deform a little bit. On the other hand, rigid body can be only displaced or rotated.

Following the construction of the model with rigid body, the process of building of the stiffness matrix could be created. Two types of loading were taken into account:

1. Environmental loading applied to the suction pile prior to construction of the jack-up structure
2. Static loading by the structure followed by environmental loading,

giving two different secant stiffness matrices. Using these two steps, it was possible to determine a typical coupling pattern of the terms in the stiffness matrix, the evolution of the matrix with loading and the evolution of coupling of the terms with loading.

To validate the procedure, a model with soil using linear elastic model was used. In the first case individual force components were applied and the compliance matrix was determined, then corresponding values of individual displacements were applied and stiffness matrix was obtained. Then, the matrices were compared showing no differences, the same procedure was applied for the point 2, but with application of static loading prior to application of individual forces/displacements simulating and environmental loading.

It should be pointed out, that unfortunately it was impossible to determine tangent stiffness matrix by applying very small forces or displacements, because the unbalance forces in the

model became significant after applying forces smaller than 10kN, so the resultant stiffness matrix was showing unrealistic results. After this finding, it was decided to apply load values of order of typical environmental loading.

Typical coupling pattern occurring due to elastic response was a cross shape pattern with zeroes in other terms, the patterns is shown in following

$$\bar{\bar{K}} = \begin{array}{c} \begin{array}{|c|c|c|c|c|c|} \hline K_{11} & 0 & 0 & 0 & -K_{15} & 0 \\ \hline 0 & K_{22} & 0 & K_{24} & 0 & 0 \\ \hline 0 & 0 & K_{33} & 0 & 0 & 0 \\ \hline 0 & K_{42} & 0 & K_{44} & 0 & 0 \\ \hline -K_{51} & 0 & 0 & 0 & K_{55} & 0 \\ \hline 0 & 0 & 0 & 0 & 0 & K_{66} \\ \hline \end{array} \end{array} \quad (36)$$

Then, using perfect plasticity (Mohr-Coulomb model), it was observed, that coupling of force components with displacement in z direction became significant as well.

Then, the soil response secant stiffness matrices were built for the case of full scale field test modelled at the beginning of this chapter. First one representing only environmental loading and second one representing load of the jack-up structure followed by application of environmental loading.

Conclusion – objective 4

Since prior to implementation of rigid bodies it was expected that the models with rigid bodies should perform faster, the validation of this assumption was depicted as one of the objectives of the thesis.

It was observed, that the models with rigid bodies perform better – are faster – than models using stiff structural elements. This was proved for both types of solvers in Plaxis – Picos and Pardiso. In addition, the models with rigid bodies using Picos solver perform twice as fast as the same models using structural elements. Picos solver is more impacted by the use of rigid body, the reason for it is that Picos is an iterative solver, thus it assembles the full global stiffness matrix and calculates the degrees of freedom in every step while converging to the final solution and by use of rigid body, the total number of degrees of freedom in the model is significantly lower than for the model with structural elements. On the other hand, use of rigid body makes Pardiso (direct solver) faster only by 10 to 20%.

It can be concluded that for modeling of offshore structures and their interaction with soil, the best solution is to use model with rigid body. At first, it is shown in Chapter 7 that the results of rigid body model shows very satisfactory results. Plus, the calculation times are significantly better for rigid body model and the difference can be expected to be much higher for bigger models up to 100 000 elements, which are used very often in practice.

6 BIBLIOGRAPHY

Acosta-Martinez, Hugo E., Susan M. Gourvenec, and Mark F. Randolph. "An experimental investigation of a shallow skirted foundation under compression and tension." *Soils and Foundations* 48.2 (2008): 247-254.

Achmus, Martin, Yu-Shu Kuo, and Khalid Abdel-Rahman. "Behavior of monopile foundations under cyclic lateral load." *Computers and Geotechnics* 36.5 (2009): 725-735.

Advanced Geomechanics: Services. *Advanced Geomechanics*, 24 June 2012, Web. 28 May (2014). <http://www.ag.com.au/services/default.aspx>

Andersen, K. H., et al. "Suction anchors for deepwater applications." *Proc. Int. Symp. on Frontiers in Offshore Geotechnics (ISFOG)*. (2005)

Andresen, L., et al. "Finite element analyses in offshore foundation design." The 12th International Conference of International Association for Computer Methods and Advances in Geomechanics. Goa. (2008)

Brinkgreve, R. B. J., Engin, E., Swolfs, W. M., Waterman, D., Chesaru, A., Bonnier, P. G., & Galavi, V. (2011). PLAXIS 3D 2011.

Chen, R., C. Gaudin, and M. J. Cassidy. "Investigation of the vertical uplift capacity of deep water mudmats in clay." *Canadian Geotechnical Journal* 49.7 (2012): 853-865.

De Vries, W. Assessment of bottom-mounted support structure types with conventional design stiffness and installation techniques for typical deep water sites. Delft, Netherlands, (2007). Delft University of Technology.

Gazis, Nikolaos. "A Probabilistic Approach for Mud Mat Stability Analysis." *The Twenty-third International Offshore and Polar Engineering Conference*. International Society of Offshore and Polar Engineers. (2013)

Gould, Nicholas IM, Jennifer A. Scott, and Yifan Hu. "A numerical evaluation of sparse direct solvers for the solution of large sparse symmetric linear systems of equations." *ACM Transactions on Mathematical Software (TOMS)* 33.2 (2007): 10.

Haas, Mark E. "Mudmats for offshore platform support." U.S. Patent No. 6,004,075. 21 Dec. 1999.

Hackl, Klaus, and Mehdi Goodarzi. "An Introduction to Linear Continuum Mechanics." (2010)

Huang, Jun, Jianchun Cao, and Jean ME Audibert. "Geotechnical design of suction caisson in clay." *The Thirteenth International Offshore and Polar Engineering Conference*. International Society of Offshore and Polar Engineers, (2003)

Jamil, Noreen. "A Comparison of Direct and Indirect Solvers for Linear Systems of Equations." *Int. J. Emerg. Sci* 2.2 (2012): 310-321.

Li, Miao, Hong Zhang, and Hong Guan. "Study of offshore monopile behaviour due to ocean waves." *Ocean Engineering* 38.17(2011): 1946-1956.

- Lee, Junhwan, and Mark Randolph. "Penetrometer-based assessment of spudcan penetration resistance." *Journal of Geotechnical and Geoenvironmental Engineering* 137.6 (2010): 587-596.
- Mana, Divya SK, Susan Gourvenec, and Mark F. Randolph. "Experimental investigation of reverse end bearing of offshore shallow foundations." *Canadian Geotechnical Journal* 50.10 (2013): 1022-1033.
- Martin, C. M., and G. T. Houlsby. "Combined loading of spudcan foundations on clay: numerical modelling." *Géotechnique* 51.8 (2001): 687-699.
- Mase, G. Thomas, and George E. Mase. *Continuum mechanics for engineers*. CRC press. (2010)
- Monajemi, H., and H. Abdul Razak. "Finite element modeling of suction anchors under combined loading." *Marine Structures* 22.4 (2009): 660-669.
- Narasimha Rao, S., et al. "Studies on pullout capacity of anchors in marine clays for mooring systems." *Applied Ocean Research* 28.2 (2006): 103-111.
- Oksuzler, Yalcin. "Method and apparatus for positioning an offshore platform jacket." U.S. Patent No. 4,690,586. 1 Sep. 1987.
- Raheem, Shehata E. Abdel. "Nonlinear response of fixed jacket offshore platform under structural and wave loads." *Coupled Sys tems Mechanics* 2.1 (2013): 111-126.
- Rahman, M. S., et al. "A neural network model for the uplift capacity of suction caissons." *Computers and Geotechnics* 28.4 (2001): 269-287.
- Randolph, Mark, et al. "Challenges of offshore geotechnical engineering." *PROCEEDINGS OF THE INTERNATIONAL CONFERENCE ON SOIL MECHANICS AND GEOTECHNICAL ENGINEERING*. Vol. 16. No. 1. AA BALKEMA PUBLISHERS. (2005)
- Randolph, Mark F., et al. "Recent advances in offshore geotechnics for deep water oil and gas developments." *Ocean Engineering* 38.7(2010): 818-834.
- Saito, Takashi, et al. "Skirt suction foundation-application to strait crossings." (2004)
- Samui, Pijush, Sarat Das, and Dookie Kim. "Uplift capacity of suction caisson in clay using multivariate adaptive regression spline." *Ocean Engineering* 38.17 (2011): 2123-2127.
- Schenk, Olaf, et al. "PARDISO: a high-performance serial and parallel sparse linear solver in semiconductor device simulation." *Future Generation Computer Systems* 18.1 (2001): 69-78.
- Qiu, Gang, and Sascha Henke. "Controlled installation of spudcan foundations on loose sand overlying weak clay." *Marine structures* 24.4 (2011): 528-550.
- Taiebat, H. A., and J. P. Carter. "A failure surface for circular footings on cohesive soils." *Géotechnique* 60.4 (2010): 265-273.
- Tjelta, Tor Inge. "Suction piles: Their position and application today." *Proceedings of the 11th International Offshore and Polar Engineering Conference*. Cupertino: International Society of Offshore and Polar Engineers. Vol. 2. (2001)

Zhang, Jianhua, et al. "Static and Dynamic Analysis of Monopile Foundation for Offshore Wind Farm." *Proceedings of the Twentieth (2010) International Offshore and Polar Engineering Conference, Beijing, China, June 20*. Vol. 25. 2010.

7 APPENDIX A: VALIDATION OF A RIGID BODY IN PLAXIS 3D

The validation of implementation of rigid body is the first objective of the thesis. A *Rigid body* is an object without any change in shape during motion. Thus, the distance between every two point in the body remains constant and kinematics of rigid body motion is expressed in terms of translation and rotation. A detailed description of rigid body and its implementation in Plaxis kernel is described in Chapter 2.2. At the beginning basic validations will be performed – from the simplest ones as a model of a sliding block to validate interaction between interfaces and rigid bodies to more complex models validating basic calculation types in Plaxis (plastic calculation, safety factor, consolidation and dynamics). Then, more sophisticated model of suction pile will be modelled and the results of Plaxis model using rigid bodies will be compared to results of a model using very stiff structural elements and to results for the case obtained from literature.

7.1 BASIC RIGID BODY VALIDATIONS

In order to validate the implementation of rigid bodies in Plaxis 3D verifications of basic rigid body properties and behavior were performed.

7.1.1 Interfaces

One of the basic and important features in Plaxis are interfaces – joint elements, which can be added to plates, surfaces or geogrids for a proper modelling of soil – structure interaction. They can be used for example for simulation of zone of intense shearing between a plate and the surrounding soil (Plaxis, 2014). To validate this feature in Plaxis 3D for rigid bodies, a model of a sliding block was used.

Input

The model design is showed in Figure 31 - the model consists of two blocks, one on the top of another. The block on the bottom is in the position $0 \leq x \leq 12$, $0 \leq y \leq 8$ and $0 \leq z \leq 1$. Upper block lies in position $1 \leq x \leq 11$, $1 \leq y \leq 7$ and $1 \leq z \leq 2$. Defined values of other model properties are used, as 10 - noded elements and Earth gravity.

Interface is then used to model the sliding of the upper block on the bottom block. To compare the results for rigid bodies with the common solution in Plaxis 3D, two types of input are used:

- 1) Surface prescribed displacement of left part of the upper block ($x=1$). The displacement is prescribed in horizontal x direction with value of 0.002 m, displacement in y direction is fixed and in z direction the surface is free to move.
- 2) Upper block is defined as rigid body with reference point in the center of the upper block ($x=6$, $y=4$, $z=1.5$). Displacement in x direction is prescribed to the whole body with value of 0.002 m, the body is fixed in y direction and free to move in z direction, all rotations are free as well.

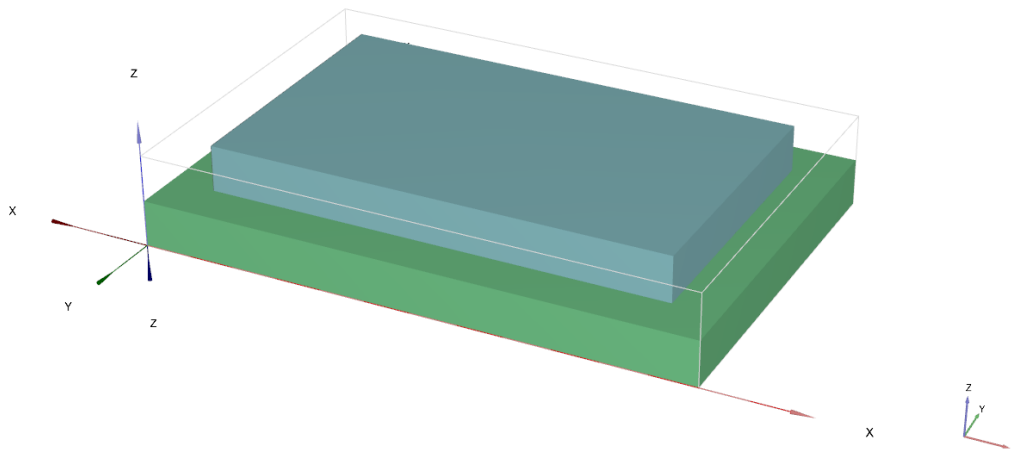


Figure 31: Model definition in Plaxis 3D.

Materials

All material datasets are described in Table 6. Both blocks are defined as very stiff linear elastic materials, bottom soil is defined as zero – weight. Interface between top and bottom block of soil is defined as separate interface material with different properties to the blocks: Mohr-Coulomb with cohesion equal to 1 and friction angle equal to 0°, respectively 30°. K_0 settings are defined manually to zero.

Table 6: Material properties

Parameter	Name	Top soil	Bottom soil	Interface 0(30)	Unit
Material model	Model	Linear elastic	Linear elastic	Mohr-Coulomb	-
Behavior	Type	Non - porous	Non - porous	Drained	-
Unit weight	γ	20	0	0	kN/m ³
Young's modulus	E	$1 \cdot 10^6$	$5 \cdot 10^4$	$1 \cdot 10^6$	kN/m ²
Poisson's ratio	ν	0	0	0	
Internal friction angle	ϕ	-	-	0(30)	°
Cohesion	c	-	-	1	kN/m ²
Dilatancy angle	ψ	-	-	0	°
Tension cut-off		-	-	yes	

Meshing

An overall very coarse global coarseness is used.

Calculations

Initial stresses in the model are calculated using *Gravity loading* calculation. After this phase two different phases, both using *Plastic analysis* calculation type and *Reset displacements to zero* option, are defined according to Figure 32:

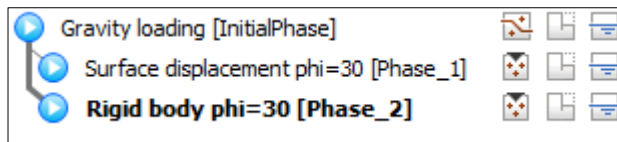


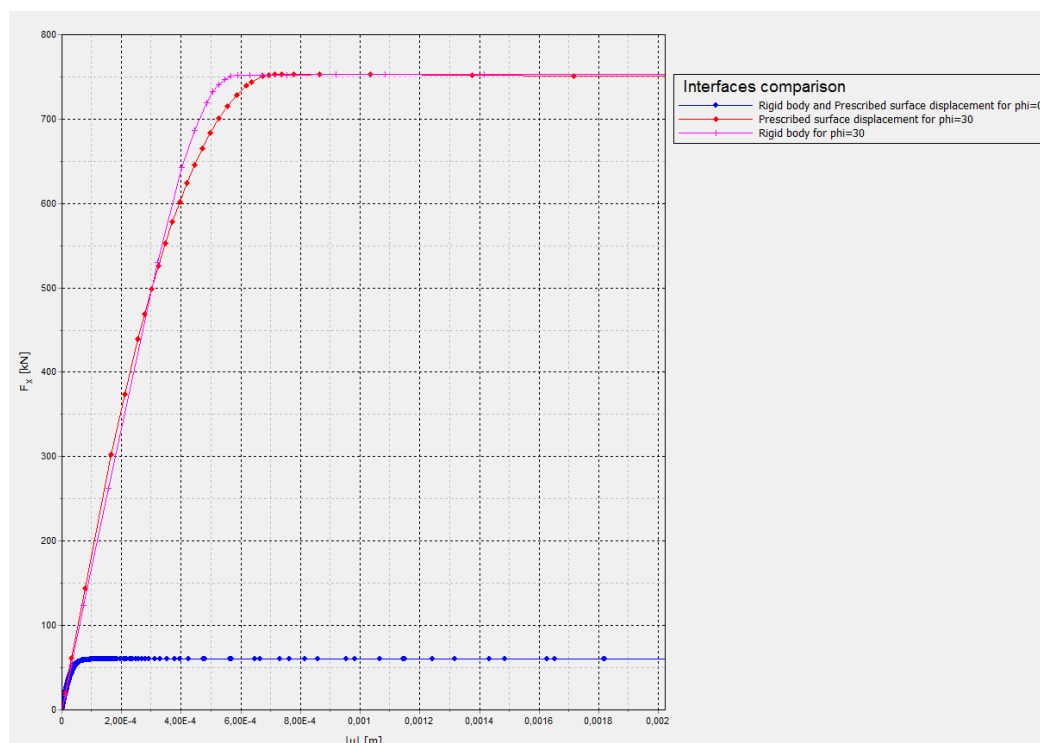
Figure 32: Calculation phases.

- 1) Phase with activation of surface displacement and interface with internal friction angle equal to 0° , respectively 30° .
- 2) Phase with activation of rigid body and interface with internal friction equal to 0° , respectively 30° .

Output

As the upper block is pushed the left, the force in x direction increases up to failure, where the value of shear force in failure is reached. The evolution of shear force applied on the interface against total displacement of the point lying exactly in the middle of upper block ($x=6$, $y=4$, $z=1.5$) is shown in Figure 33. The prescribed surface displacement for internal friction angle 30° is represented by red curve, rigid body for the same friction by pink curve and both rigid body and prescribed surface displacement for internal friction angle 0° by blue curves. The curves for only cohesion interface coincide in this scale, so they are represented by the same color for easier interpretation.

Figure 33: Comparison of evolution of force/displacement curve for prescribed surface displacement (red) and rigid body (pink) for internal friction angle of interface 30° . In red are shown the same curves for internal friction angle 0° for both rigid body and prescribed surface displacement.



Verification

The interface is modelled by Mohr-Coulomb material model. Due to high stiffness of the upper block it hardly deforms for surface prescribed displacement and doesn't deform at all

for rigid body, the solution should be possible to find using Mohr-Coulomb failure criterion for maximum shear stress on the interface:

$$\tau_{\max} = c + \sigma \cdot \tan\varphi \quad (37)$$

Analytical solution to this equation is, for described model, shown in following Table 7:

Table 7: Maximum shear force applied to upper block

	Analytical solution	Surface prescribed displacement	Rigid body	
Internal friction angle 30°	752.82	753.20	752.82	kN/m ²
Internal friction angle 0°	60.00	60.19	60.00	kN/m ²

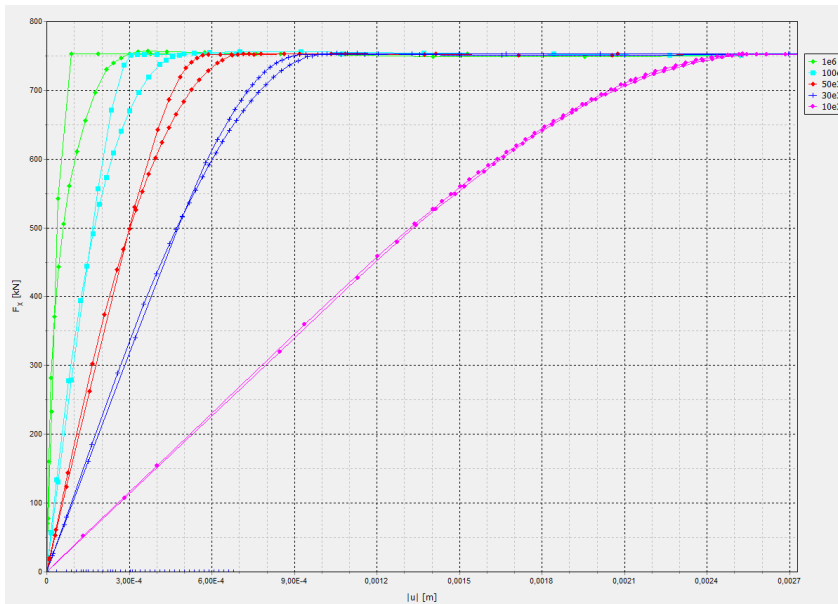
As seen in Figure 33 a difference in the interface stiffness is visible from the curve. Better illustration of it is in Figure 34, where evolutions of curves for different values of upper and lower block Young's modulus are shown. The value for upper block is always set to $1 \cdot 10^6$ and for lower block it varies for every calculation.

The values of Young's modulus of the upper block were following (from left to right at the picture):

- $1 \cdot 10^6$ – green curves, equal to Young's modulus of lower block
- $1 \cdot 10^5$ – light blue curves
- $5 \cdot 10^4$ – red curves
- $3 \cdot 10^4$ – blue curves
- $1 \cdot 10^4$ – pink curves

The convergence of both curves as the stiffness difference is higher is clearly visible. The slope difference of both curves is changing from around 10% for same stiffnesses to around 1% for the pink curve, where the stiffness difference is of two orders.

Figure 34: Convergence of interface stiffness for rigid body a prescribed surface displacement.



For the surface prescribed displacement maximum shear force at failure converges in the same manner as in previous case, values of maximum shear force are shown at Table 8.

Table 8: Evolution of maximum shear force with stiffness difference of the two blocks

Young's modulus of upper block (kN/m ²)	$1 \cdot 10^6$	$1 \cdot 10^5$	$5 \cdot 10^4$	$3 \cdot 10^4$	$1 \cdot 10^4$
Maximum shear force (kN/m ²)	756.585	756.385	753.200	753.013	752.786

From both previous examples is clearly visible, that the behaviour of the interface of the block with prescribed surface displacement is getting closer to the behavior of the rigid body, as the stiffness difference of the blocks is increasing.

7.1.2 Model behavior with rigid bodies

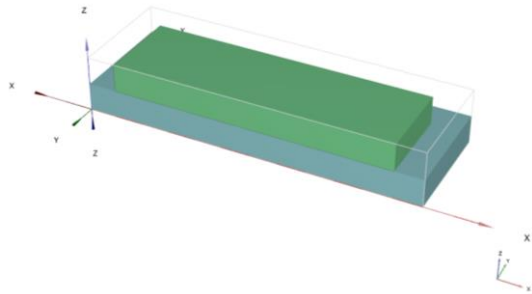
The following validation of interface behavior model reaction to different types and combinations of rigid bodies was studied. In this procedure were used exactly the same steps as in section 7.1.1 and failure shear forces were compared at the end in the same manner as in Table 7.

7.1.2.1 Symmetrical model

The exactly same procedure as in section 7.1.1 was used for the whole computation process, but in the middle of the model along x axis was put axis of symmetry as shown in Figure 35. Then failure shear force in the model was compared to the analytical solution – exactly same

results were obtained, in addition the force in x direction was exactly half of force obtained in Interface verification.

Figure 35: Model to test symmetry



7.1.2.2 More than one rigid body in a model

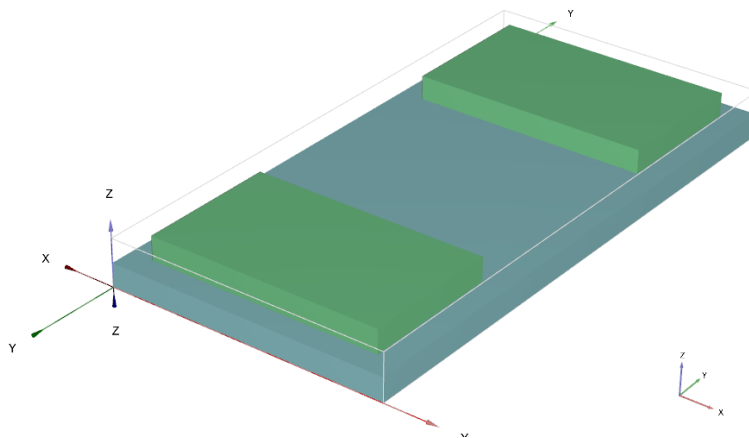


Figure 36: Two rigid bodies in model.

Two rigid bodies next to each other were used to test model behavior. First upper block has same dimensions as in section 7.1.1: $1 \leq x \leq 11$, $1 \leq y \leq 7$, $1 \leq z \leq 2$ and second one is positioned as following: $1 \leq x \leq 11$, $16 \leq y \leq 23$ and $1 \leq z \leq 2$. The reference point of both rigid bodies is defined exactly in their middle.

The same procedure and datasets were used for materials, meshing and calculation as in interface validation.

The resulting shear failure force applied to two rigid bodies is exactly two times higher than for single rigid body and is exactly equal to analytical solution.

7.1.2.3 Plate element and soil element rigid body

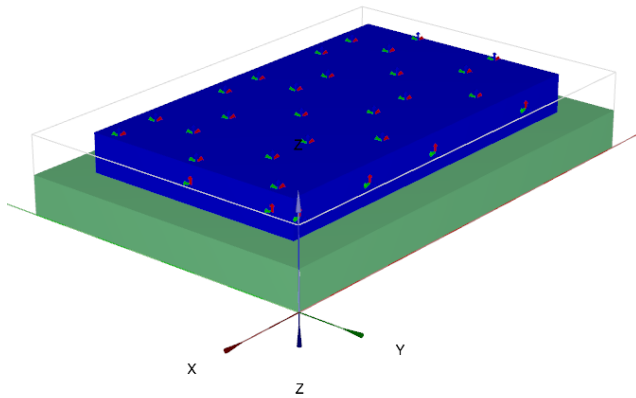
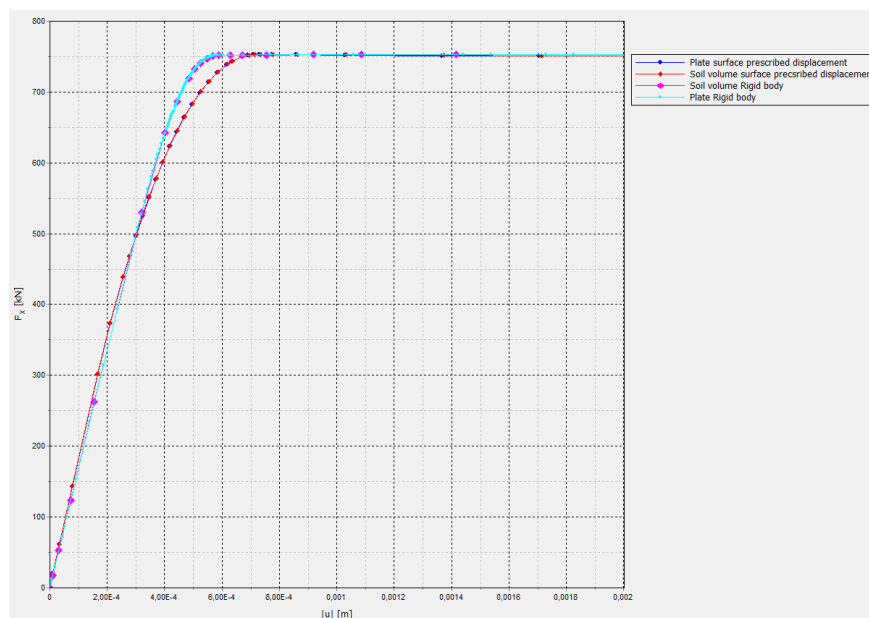


Figure 37: Plate elements rigid body.

The study performed in section 7.1.1 to validate interfaces was performed for soil volume rigid body and for plate rigid body. The comparison of results is shown below in Figure 38, from curves it is clearly visible there is no difference in behavior of soil volume rigid body and plate rigid body. Furthermore, the results for both of them are exactly equal to analytical solution as shown in Table 7, where column “Rigid body” corresponds to both rigid body models.

Using this model was also validated behavior of more interconnected rigid bodies with similar properties – reference point and all the degrees of freedom are the same for all six plate rigid bodies. The model itself is shown in Figure 37. From the results is evident, that the upper block made out of 6 rigid bodies behaves like one big rigid body.

Figure 38: Comparison of soil volume rigid body and plate rigid body



7.1.3 Construction of an embankment – safety analysis

The Safety calculation type is an option available in Plaxis to compute global safety factors. In this approach, the shear strength parameters $\tan \phi$ and c of the soil as well as tensile strength are successively reduced until failure of the structure occurs (Plaxis, 2014).

For validation of drained and undrained plastic calculations followed by safety analysis was used example from Plaxis 3D Tutorial manual 2014 called “Construction of a road embankment” (Plaxis, 2014). In addition to the manual footing was modelled on the top of the embankment – once in conventional way using very stiff soil body and in second case using rigid body, then the results were compared.

Input of the basic model

For the basic model construction the Tutorial example called “Construction of a road embankment” was used (Plaxis, 2014). In the initial phase the model is 80 *m* long, 2 *m* wide and 10 *m* deep and consist of three soil layers, which parameters are described in [Table 9](#). Peat lies in upper 3 meters, in interval 3 to 7 *m* is Clay and beneath is Sand. The phreatic surface is 1 *m* beneath original ground surface.

Table 9: Soil properties of embankment and subsoil (Plaxis, 2014)

Parameter	Name	Embankment	Sand	Peat	Clay	Unit
General						
Material model	<i>Model</i>	Hardening soil	Hardening soil	Soft soil	Soft soil	-
Drainage type	<i>Type</i>	Drained	Drained	Undr. (A)	Undr. (A)	-
Soil unit weight above phreatic level	γ_{unsat}	16	17	8	15	kN/m ³
Soil unit weight below phreatic level	γ_{sat}	19	20	12	18	kN/m ³
Initial void ratio	e_{init}	0.5	0.5	2.0	1.0	-
Parameters						
Secant stiffness in standard drained triaxial test	E_{50}^{ref}	2.5 · 10 ⁴	3.5 · 10 ⁴	-	-	kN/m ²
Tangent stiffness for primary oedometer loading	E_{oed}^{ref}	2.5 · 10 ⁴	3.5 · 10 ⁴	-	-	kN/m ²
Unloading / reloading stiffness	E_{ur}^{ref}	7.5 · 10 ⁴	1.05 · 10 ⁵	-	-	kN/m ²
Power for stress-level dependency of stiffness	m	0.5	0.5	-	-	-
Modified compression index	λ^*	-	-	0.15	0.05	-
Modified swelling index	κ^*	-	-	0.03	0.01	-
Cohesion	c_{ref}	1.0	0.0	2.0	1.0	kN/m ²
Friction angle	φ^*	30.0	33.0	23.0	25.0	°
Dilatancy angle	ψ	0.0	3.0	0.0	0.0	°
Advanced: Set to default	-	Yes	Yes	Yes	Yes	-
Flow parameters						
Data set	-	USDA	USDA	USDA	USDA	-
Model	-	Van Genuchten	Van Genuchten	Van Genuchten	Van Genuchten	-
Soil type	-	Loamy sand	Sand	Clay	Clay	-
< 2 μ m	-	6.0	4.0	70.0	70.0	%
2 μ m – 50 μ m	-	11.0	4.0	13.0	13.0	%
50 μ m – 2mm	-	83.0	92.0	17.0	17.0	%
Set to default	-	Yes	Yes	No	Yes	-
Horizontal permeability (x-direction)	k_x	3.499	7.128	0.1	0.04752	m/day
Horizontal permeability (y-direction)	k_y	3.499	7.128	0.1	0.04752	m/day
Vertical permeability	k_z	3.499	7.128	0.05	0.04752	m/day
Change in permeability	c_k	1 · 10 ¹⁵	1 · 10 ¹⁵	1.0	0.2	-
Interfaces						
Interface strength	-	Rigid	Rigid	Rigid	Rigid	-
Strength reduction factor	R_{inter}	1.0	1.0	1.0	1.0	-
Initial						
K_0 determination	-	Automatic	Automatic	Automatic	Automatic	-
Over-consolidation ratio	<i>OCR</i>	1.0	1.0	1.0	1.0	-
Pre-overburden pressure	<i>POP</i>	0.0	0.0	5.0	0.0	kN/m ²

After initial phase using K_0 procedure as calculation type the embankment is constructed on the subsoil in following steps:

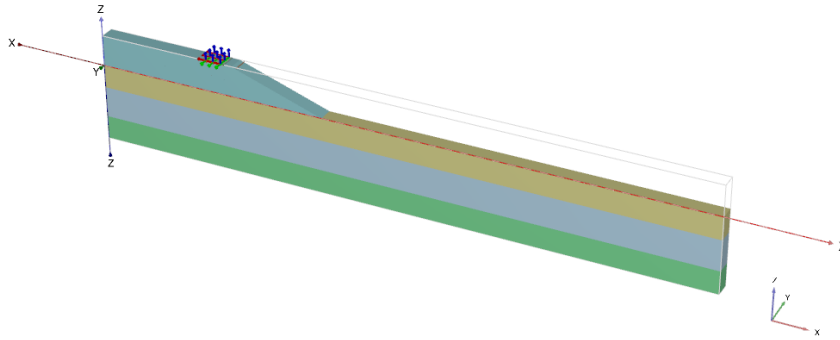
- Construction of 2 meters high bottom part of the embankment in 2 days
- 30 day period of consolidation
- Construction of second part of the embankment, 2 meters high again, in 2 days
- Consolidation until minimum excess pore pressure of 1 kPa is reached

All the procedures described so far can be found in Plaxis 3D Tutorial manual 2014 (Brinkgreve, 2013) for more detailed description of the procedure.

Input for safety analysis

After modelling basic geometry and construction of an embankment shown in Figure 39 the footing with applied load is modelled in *Structures* mode.

Figure 39: Model geometry definition



The footing is 0.2 m deep and is situated in position: $14 \leq x \leq 17$ and $0 \leq y \leq 2$ and lies on top of an embankment with geometry – bottom: $0 \leq x \leq 30$ and top: $0 \leq x \leq 18$. From this is clear, that the slope inclination is 1:3 as the embankment is 4 m high and the footing lies 1 m from the edge.

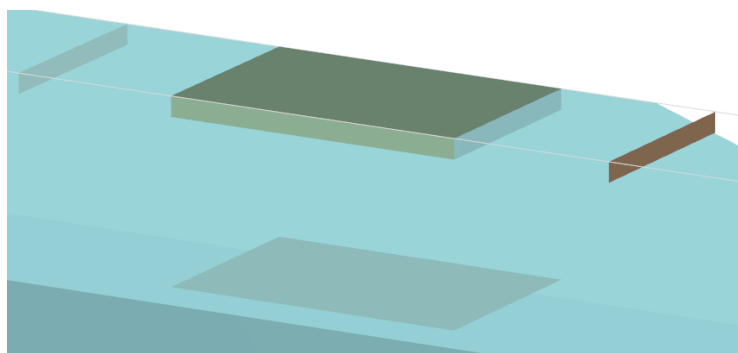
To make verification of rigid bodies and safety analysis two ways of modelling of the footing were carried out:

1. Very stiff soil body with uniformly distributed surface load applied on the top surface with value -10 kN/m^2 in z direction.
2. Rigid body with applied force of -60 kN in z direction as the surface area of the footing is 6 m^2 . The rigid body is movement-fixed in y direction and rotation-fixed around z axis, other movements and rotations are free. The reference point for the rigid body is in position [15.5, 1, and 3.9] – in the middle of footing.

For both cases interfaces were defined around the footing with material mode selected to "From adjacent soil", what in this case meant properties of an *Embankment* soil type from Table 9.

The position and geometry of the footing is shown in Figure 40, where soil around the footing is shown 70% opaque to make all the interfaces around visible.

Figure 40: Position and geometry of the footing with interfaces



Materials

The properties of subsoil and embankment are described in Table 9 and the properties of the footing material are in following Table 15.

Table 10: Footing material properties

Material model	Drainage type	Unit weight (γ)	Young's modulus (E)	Poisson's ratio (ν)
Linear elastic	Non-porous	25 kN/m ³	1·10 ⁶ kN/m ²	0.3

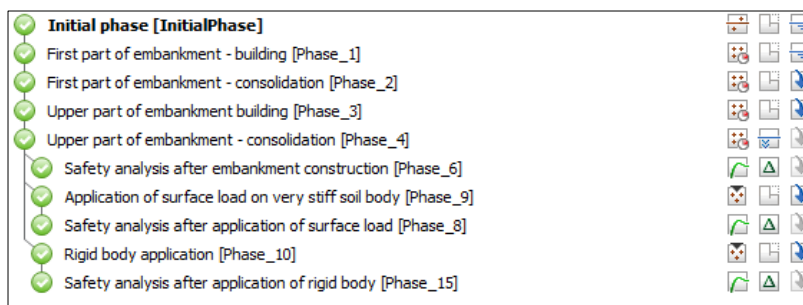
Meshing

An overall *Medium* global coarseness is used with total number of 2257 nodes.

Calculations

All calculation phases of the project are shown in Figure 41. After constructing an embankment *Safety* calculation type is carried out (“*Safety analysis after embankment construction*”) with option *reset displacements to zero* in order to exclude previous deformations from resulting failure mechanism. Then, footing installation is modelled by *Plastic* calculation type and loading type *Staged construction* with surface load in the first case and as a rigid body is the second case, both of them followed by safety analysis in the same manner as after embankment construction.

Figure 41: Calculation phases of the whole project



Output

At the beginning it is necessary to describe, how Plaxis program is defining and calculating safety factor. The shear strength parameters $\tan \varphi$ and c of the soil as well as tensile strength are successively reduced until failure occurs – the so called *phi/c reduction* method. The total multiplier ΣMsf is used to define the value of the soil parameters at a given stage:

$$\Sigma Msf = \frac{\tan \varphi_{input}}{\tan \varphi_{reduced}} = \frac{C_{input}}{C_{reduced}} = \frac{S_{u,input}}{S_{u,reduced}} = \frac{Tensile\ strength_{input}}{Tensile\ strength_{reduced}}$$

Where the parameters with subscript *input* mean values of parameters defined at the beginning in material sets and parameters with subscript *reduced* mean the reduced values used in the analysis. Using *Incremental multipliers* loading option ΣMsf is set to 1.0 at the beginning of the safety calculation with increment 0.1. The strength parameters are

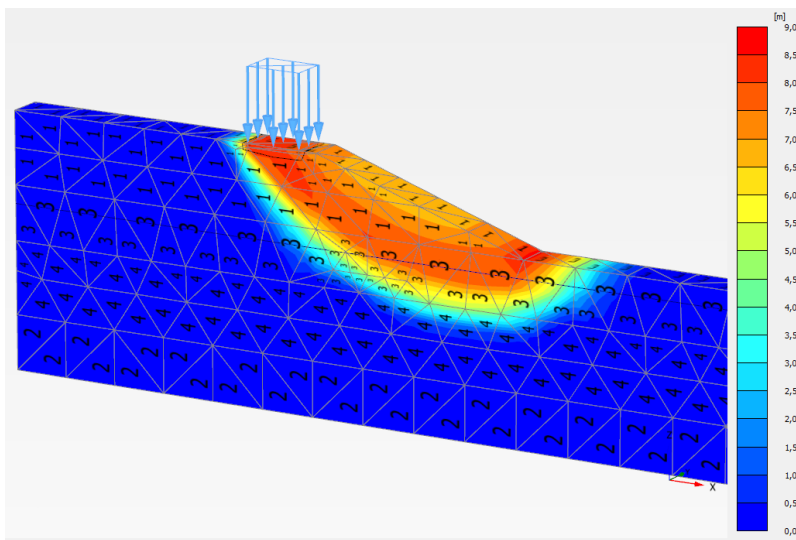
successively reduced until the failure occurs. The safety factor is then obtained from value of $\sum Msf$ at failure:

$$SF = \frac{\text{available strength}}{\text{strength at failure}} = \text{value of } \sum Msf \text{ at failure}$$

Large displacements are generated during safety analysis, these results don't have exact physical meaning, but from *Incremental displacements* at failure can be seen the type of failure mechanism.

In the following Figure 42 failure mechanism is shown. The exactly same results were obtained for surface loading as for rigid body.

Figure 42: Failure mechanism evolution after footing installation

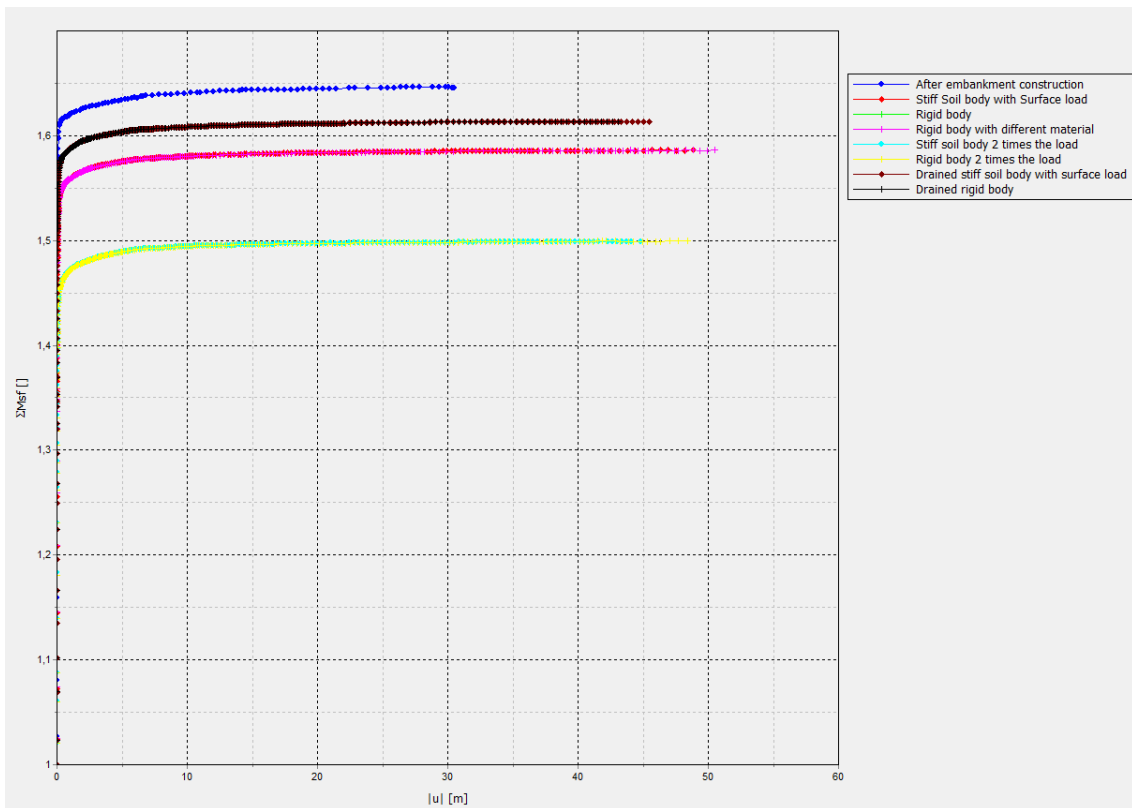


For the representation of safety factor, the best way is to show evolution of $\sum Msf$ with deformation, even though the deformations are not relevant in that case, from this plot can be seen, that the failure mechanism is fully developed, if value of $\sum Msf$ is constant with successive increment of deformation.

For the purpose of validation of rigid body behaviour, following loading options were performed and then summarized in Figure 43:

1. Basic undrained analysis described in Tutorial manual with loading conditions mentioned before in "Input for safety analysis".
2. The same analysis, but for load twice the value in the first case
3. The same analysis as in second case, but the material properties of the footing were changed for model using rigid body in following manner: material properties were changed to *Embankment*, but the unit weight was let 25 kN/m^3 to show, that the only property influencing behaviour of rigid body is its weight in this model.
4. Drained analysis – performed by changing drainage type of *Peat* and *Clay* material from Undrained(A) to Drained

Figure 43: Evolution of ΣMsf with deformation, the reference point for the deformation is at the tip of an embankment.



All curves with same loading conditions for surface loading and rigid body exactly coincide – namely red and green curve for Undrained analysis with basic load (1), light blue and yellow curves for Undrained analysis with 2 times bigger load (2) and brown and black curves for drained analysis (4).

The curve representing case (3) is shown in pink and exactly coincide with curves from model (1).

To sum up the results, values of factor of safety from all the models are:

- $\Sigma Msf = 1.646$, After construction of embankment
- $\Sigma Msf = 1.614$, Drained analysis with load -10 kN/m^2
- $\Sigma Msf = 1.586$, Undrained analysis with load -10 kN/m^2
- $\Sigma Msf = 1.499$, Undrained analysis with load -20 kN/m^2

As expected, factor of safety is higher for drained analysis than for undrained.

7.1.4 Consolidation

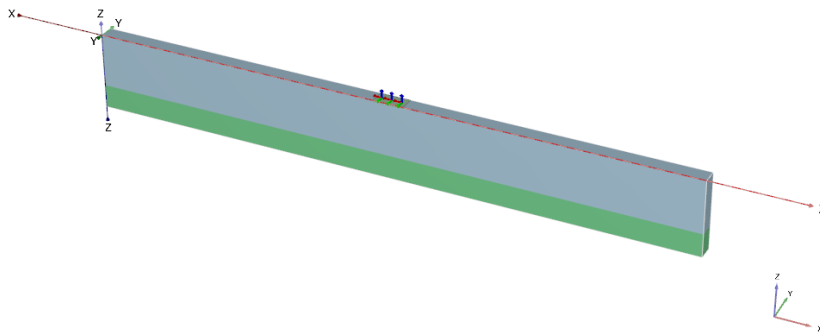
One of the important features in Plaxis 3D is *Consolidation* calculation type. To verify its proper working with rigid bodies, simple model of footing installation on clay was used.

Input and material properties

The model used in this project is shown in Figure 44. The dimensions of subsoil are $0 \leq x \leq 80$, $0 \leq y \leq 2$ and $-10 \leq z \leq 0$. The material of upper soil is *Clay* and the material of lower soil is *Sand*, both described in Table 9. The phreatic surface is 0.5 m below the ground level.

The footing occupies volume $38 \leq x \leq 42$, $0 \leq y \leq 2$ and $-0.2 \leq z \leq 0$ and is surrounded by interfaces on its contact with soil. Interface material mode is set to *From adjacent soil* and *Permeable* option set to *No*.

Figure 44: Model definition



The footing is modelled in three ways:

1. Very stiff soil body with application of surface load -10 kN/m^2 in z direction.
2. Rigid body with the same properties as in (1) with reference point in $[40, 1, -0.1]$, so in the geometrical middle of the footing. The force prescribed to the rigid body is -80 kN in z direction, as the area of the footing is 8 m^2 . The displacement in y direction is fixed as well as rotation around z axis.
3. Exactly the same model as in (2), but the soil inside rigid body has properties of *Clay* (Table 9) surrounding the footing, only with changed unit weight to 25 kN/m^3 .

Footing properties are summarized in following Table 11:

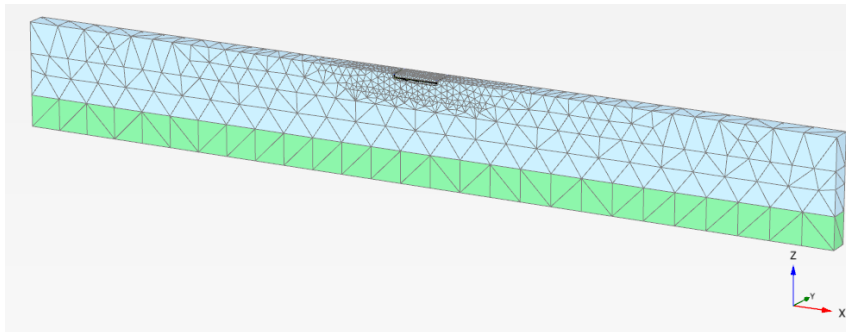
Table 11: Footing material description

Model	Drainage type	Unit weight (γ)	Young's modulus (E)	Poisson's ratio (ν)
1	Non-porous	25 kN/m^3	$1 \cdot 10^6 \text{ kN/m}^2$	0.3
2	Rigid body $[40, 1, -0.1]$ with soil properties of (1)			
3	Rigid body $[40, 1, -0.1]$ with soil properties like <i>Clay</i> (Table 9), but Unit weight = 25 kN/m^3			

Meshing

The global coarseness is set to *Medium*. For more accurate results, under the footing is modelled a surface with dimensions $33 \leq x \leq 47$, $0 \leq y \leq 2$ with *Coarseness factor* set to 0.1 and footing itself has coarseness factor 0.1 as well. Resulting mesh is shown in Figure 45.

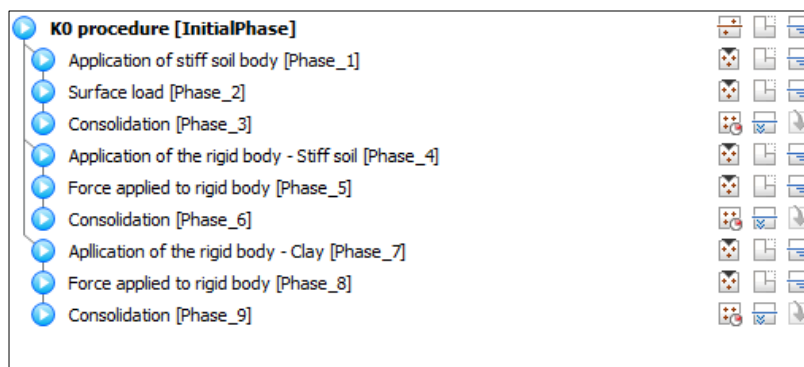
Figure 45: Generated mesh



Calculations

All calculation carried out are shown in Figure 46:

Figure 46: Calculation phases



Initial stress distribution is calculated using K_0 procedure. Then, stiff soil body (phase 1) or rigid body (phase 4 and 7) is applied to the footing location using *Plastic* Calculation type and *Staged construction* Loading type. Next phase is application of surface load to the upper surface of stiff soil body (phase 2) or application of force to the rigid body (phase 5 and 8).

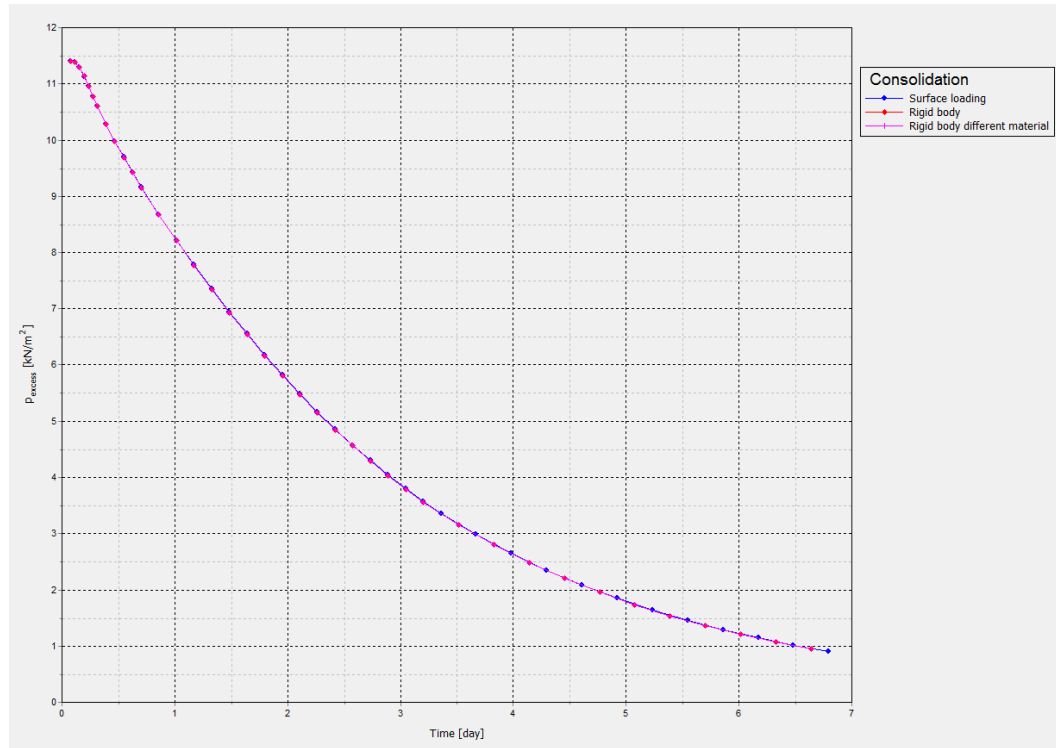
At the end, *Consolidation* calculations are performed with Loading type *Minimum excess pore pressure* set to 1 kN/m².

Output

For verification of results using rigid body point for measuring of excess pore pressure was selected beneath the footing at the position: [x=39.92, y=0.88, z=-1.29]. Evolution of excess pore pressure with time is shown in Figure 47.

From the graph it is clearly visible, that all the curves – for surface loading, rigid body and rigid body with different material - are exactly the same.

Figure 47: Consolidation beneath the footing



7.1.5 Dynamic calculations

One of the newest features in Plaxis 3D are Dynamic calculations. This module can be used for analysis of wave propagation through the soil – from seismic loading to vibration due to construction activities. For verification of rigid body behavior with Dynamic calculation, simple model with 2 soil layers was used. Particularly *Free vibration analysis* is carried out, in which can be shown possible free vibration of a system after the release of an existing static load. In our case the static surface load is applied at the beginning and then deactivated in the following Dynamic steps.

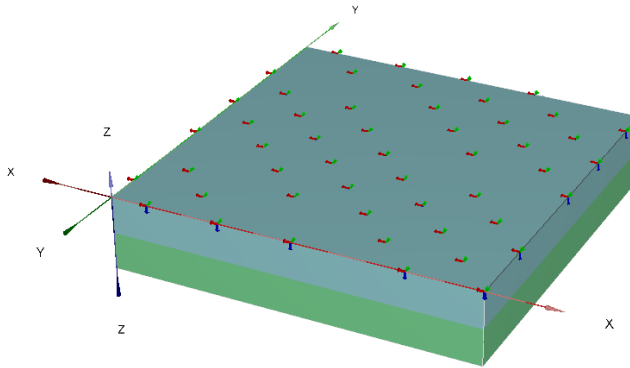
Input

The model is shown in Figure 48. It consists of two soil layers with the same size. The position of the layers is as following:

- Upper layer: $0 \leq x \leq 10, 0 \leq y \leq 10, 0 \leq z \leq -1$
- Lower layer: $0 \leq x \leq 10, 0 \leq y \leq 10, -1 \leq z \leq -2$

The water head is set to -2 m (thus the water is excluded from the model) and defined values of other model properties are used.

Figure 48: Model definition



Two cases are modelled, in the first one, common Plaxis structural elements are used and in the second one is used rigid body. The bottom layer is defined as zero – weight with very small stiffness $E = 10 \text{ kN/m}^2$.

1. Surface load of -1 kN/m^2 is applied on the top of the upper soil layer in z direction, while the layer itself is modelled as very stiff linear elastic material.
2. Surface load of -1 kN/m^2 is applied on the top of the upper soil layer in z direction, but the layer itself is modelled as rigid body with the reference point at $(x = 5, y = 5, z = -0.5)$. The rigid body has fixed movement in x and y direction and the rotation is fixed around all axes (x, y and z).

The material properties of both layers are shown in following Table 12. For all other properties are used defined values.

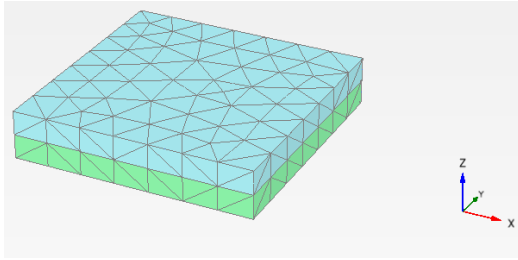
Table 12: Material properties

Parameter	Name	Top soil	Bottom soil	Unit
Material model	Model	Linear elastic	Linear elastic	-
Behavior	Type	Non - porous	Non - porous	-
Unit weight	γ	10	0	kN/m^3
Young's modulus	E	$1 \cdot 10^9$	10	kN/m^2
Poisson's ratio	ν	0	0	
Internal friction angle	ϕ	-	-	$^\circ$
Cohesion	c	-	-	kN/m^2
Dilatancy angle	ψ	-	-	$^\circ$
Tension cut-off		-	-	

Meshing

An overall very coarse mesh setting is used with coarseness factors = 1.0 for all the structures in the model. Final mesh is shown in the following Figure 49.

Figure 49: Generated mesh

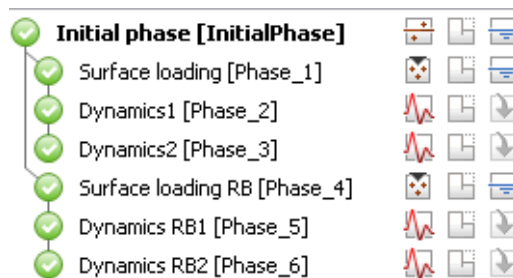


Calculations

Initial stresses in the model are calculated using K_0 procedure. Then, two “branches” of calculations were created. In the first one, very stiff soil body is used with properties described before. In the second one, rigid body is used. The procedures in both branches are exactly the same, the difference is only in definition of the upper block.

The next step after initial phase is application of a surface load -1 kN/m^2 on the upper surface of the upper block in z direction. In this phase the rigid body is activated in the second branch. The properties of rigid body are set to: the reference point has position $x = 5$, $y = 5$, $z = -0.5$ and the body displacement is fixed in x and y direction and the rotation is fixed around all the axes.

Figure 50: All carried out calculation phases



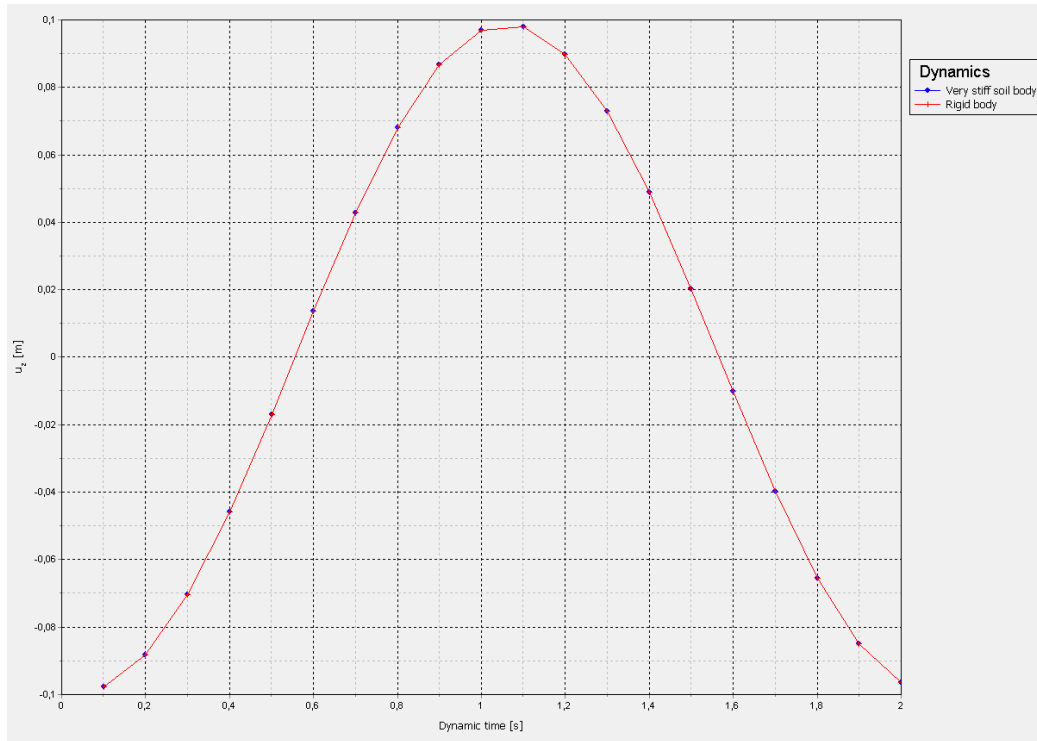
Then, as the free vibration analysis is used, surface load is deactivated and 2 phases of dynamic calculations are carried out. For all the dynamic calculations settings are exactly the same: *Dynamic time interval* is set to 1 s and Max number of steps is set to 10 and option *Dynamics* in *Model conditions* is deactivated, all other settings are used as defined.

Output

The free vibration of the upper very stiff soil after release of surface load can be shown in graph with Dynamic time at x axis and displacement in z direction on y axis. The graph is showing movement of the upper soil layer in the two dynamic phases of both branches as described in Calculations.

The blue curve characterize behaviour of very stiff soil body and the red curve characterize behaviour of rigid body. From the graph is easily visible, that the two curves coincide exactly. In the result it means the behaviour of a rigid body is exactly the same as behaviour of very stiff structure element in Plaxis, when dynamic load is applied.

Figure 51: Free vibration of the upper soil layer after release of a surface load



7.2 SUCTION ANCHOR BEARING CAPACITY

Suction anchor is an open ended circular shaped cylinder with closed top which is penetrated into the soil by its own weight and assisted with suction inside the enclosed compartment formed after initial penetration (Tjelta, 2001). The length to diameter ratio is typically six or less and mooring loads applied to the anchor are usually attached to the side of the caisson. The maximum holding capacity is obtained if the chain is attached at a depth where the anchor failure mode is large translational displacements with minimal rotation – optimum load attachment point (Andersen et al, 2005). Detailed description of suction pile is in Literature review.

The model results of this verification are compared with paper (Andersen et al, 2005), which summarizes the results of an industry sponsored study on the design and analyses of suction anchors in soft clays. The references on more than 200 suction anchors study cases were collected in this particular article, leaving very detailed study with consistent and well-documented results.

7.2.1 Basic model properties

Four hypothetical cases with two different depth/diameter ratios ($D/B = 5$ and $D/B = 1.5$) in two different soil profiles (one normally consolidated and one lightly overconsolidated) were defined. The properties of soil profiles are summarized in Table 13.

Table 13: Soil properties

Parameter	Symbol	Top clay	Bottom clay	Uniform clay	Plug	
Material model	Model	MC	MC	MC	Linear elastic	-
Behavior type	Type	Undrained C	Undrained C	Undrained C	Undrained C	-
Depth	d	[0, -5]	[-5, -40]	[0, -40]		m
Dry weight	γ	17.2	17.2	17.2	17.2	kN/m ³
Young's modulus	$E_{u, ref}$	5000	5000	5000	10E6	kN/m ²
Poisson's ratio	ν	0.49	0.49	0.49	0.49	-
Cohesion	c	10	10	10	-	kN/m ²
Friction angle	ϕ	0	0	0	-	°
Dilatancy angle	ψ	0	0	0	-	°
Young's modulus increment	$E_{u, inc}$	0	1000	0	-	kN/m ³
Reference position	y_{ref}	-	-5	0	-	m
Shear strength increment	$S_{u, inc}$	0	2	1.25	-	kN/m ³
Tension cut-off	-	No	No	No	-	-
Reduction factor	R_{inter}	0.65	0.65	0.65	1	-
Coefficient of lateral stress	K_0	1	0.65	0.55	1	-

Incompressible behavior is simulated by setting Poisson's ratio very close to 0.5.

For every study case, numerous models were created, as summarized here:

- In the first case, the anchor is modelled by very stiff soil body – material *Plug* in Table 13. Loading is simulated by *point prescribed displacement* in the center of the body and in depth corresponding to the depth of the pad-eye.
- The anchor is simulated by soil rigid body in the position of the whole *Plug* from the first case. The reference point of the rigid body is in the middle of circular horizontal surface of the anchor and in the depth of pad-eye.
- The anchor is formed by plates with the properties shown in Table 14. The inner part of the anchor is filled by soil of the same properties as the soil around the anchor. The *point prescribed displacement* lies on the plate in the exact position of the hypothetical pad-eye.

- d) The plates from the previous case are defined as rigid bodies. All of them are connected and has the same properties, reference point and degrees of freedom. The position of the reference point is the same as position of *point prescribed displacement* in previous case.
- e) For all the previous cases were carried out simulations with different ratio between horizontal and vertical loading – combined loading.

Table 14: Plate properties

Parameter	Symbol	Steel anchor	Upper part of the anchor	
Thickness	d	0.5	3	m
Unit weight	γ	0	0	kN/m ³
Young's modulus	E	200E6	200E6	kN/m ³
Poisson's ratio	ν	0.3	0.3	-

Due to symmetry conditions, only half of the suction pile can be modelled. Considerable part of the model is the same for all the cases, the differences are only in following points:

- Pile geometry: 7.5 or 25m long
- Surrounding soil properties: Top clay and bottom clay in the first case and Uniform clay in the second one
- Use of plate element rigid body or soil volume rigid body

All the models carried out are shown in following Table 15:

Table 15: Hypothetical capacity cases

CASE	C1	C2	C3	C4
Diameter(m)	5	5	5	5
Penetration depth (m)	25	7.5	25	7.5
Depth/Diameter ratio	5	1.5	5	1.5
Soil profile	Uniform clay	Uniform clay	Top and bottom clay	Top and bottom clay
Models	a, b, e	a, b, e	a, b, c, d, e	a, b, e

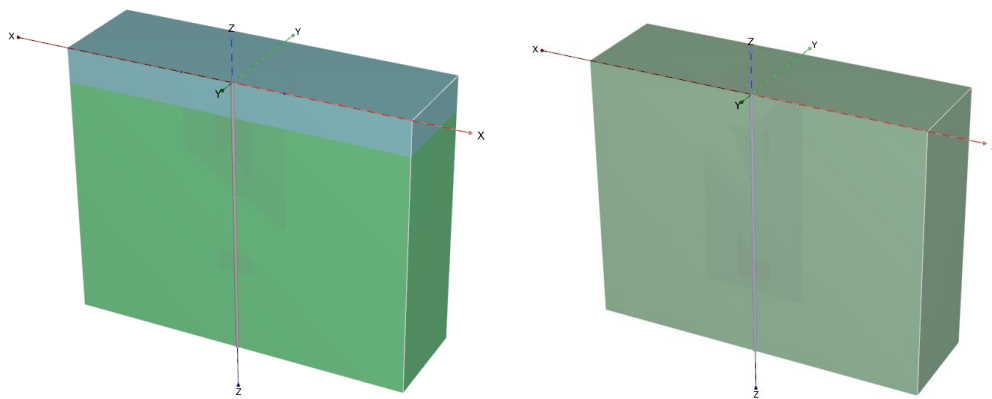
Considering this, most of the model properties can be described only once.

7.2.2 Description of the model

Input

The geometry of the project is $x_{\min} = -25$, $x_{\max} = 25$, $y_{\min} = 0$ and $y_{\max} = 15$. The soil properties are described in Table 13, in case of *Uniform clay* (C1 and C2), the soil has the same properties from $z = 0$ to $z = -40$. In C3 and C4, there is change of soil properties from *Top Clay* to *Bottom clay* at $z = -5$ as described in Table 13. In Figure 52 is shown model geometry and soil layers position for all cases.

Figure 52: Soil layers as used in C3 and C4 on the left and C1 and C2 on the right

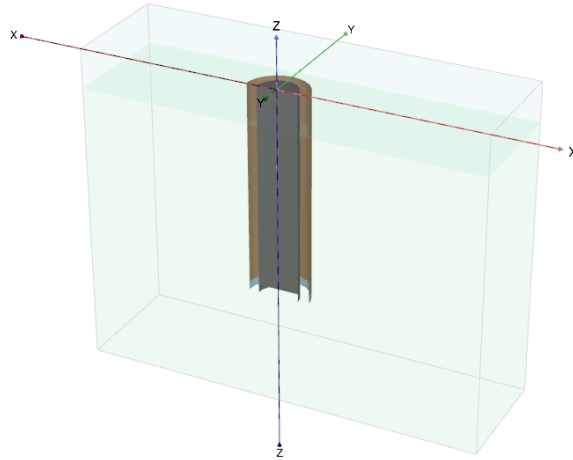


The borehole water head is set to 10 m.

The suction pile itself is modelled in *Structures* mode. The surface cross-section has a semicircular shape with radius 2.5 m and the middle in $[0, 0]$. The length of the pile downwards is 25 m in C1 and C3 and 7.5 m in C2 and C4.

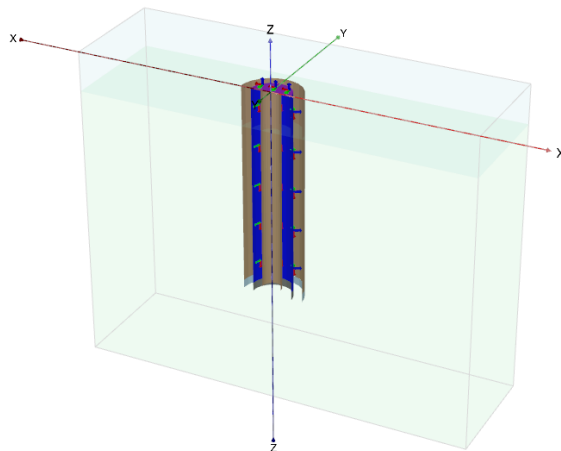
- 1) In the case of very stiff soil body and soil volume rigid body, the pile is modelled as soil body with *Plug* properties and positive interfaces around the pile. Here should be pointed out, that the interface strength factor is set to 0.65 for all soils. The interface elements are generated one meter below the tip of the pile to avoid numerical singularity and improve computational efficiency. The geometry is shown in Figure 53. For the stiff soil body *Point prescribed displacement* is defined at the center of the body $[x = 0, y = 0]$ in the horizontal plane and at the depth of optimal loading point, which position is different for every suction pile design and soil profile. At the same position is defined reference point of the soil rigid body.

Figure 53: The suction pile geometry of the models using soil body and soil rigid body



- 2) The second option is modelling the suction pile using plates and plate rigid bodies. The pile walls are modelled using *Steel anchor* material and for the top of the pile is used *Upper part of the anchor* material, both described in Table 14. Inside the anchor is a soil with the same properties as surrounding soil. The interfaces are modelled in the same manner as in first case with soil rigid bodies with addition of negative interfaces inside the pile with the same properties as positive interfaces. For suction pile made of plates *point prescribed displacement* is defined at the position of hypothetical pad-eye – it has to coincide with plate element. The position is $[x = 2.5, y = 0]$ and the depth depends on position of the optimal loading point. The reference point of rigid body is defined at the same place.

Figure 54: The suction pile geometry in models using plates and plate rigid bodies



Meshing

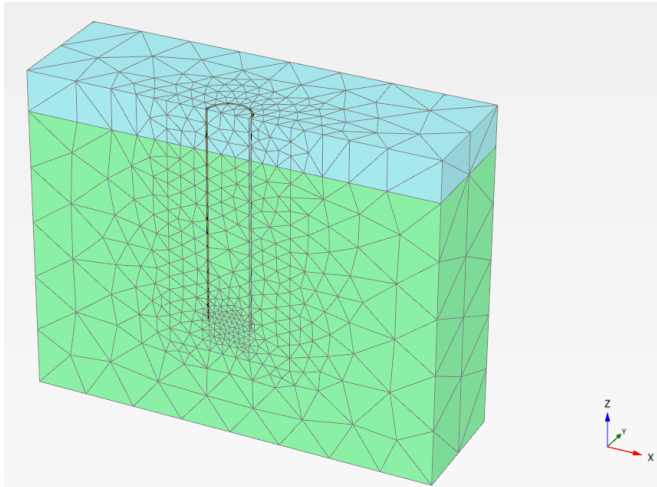
The overall coarseness was set to *Very coarse* with local changes in coarseness factor as following:

- The inside of the pile is set to 0.5
- The surrounding area of the pile with diameter 7.5 m and depth of 30 m (respectively x m) is set to 0.25

- The extension of the pile ranging 3 m below the pile is defined by coarseness factor 0.1

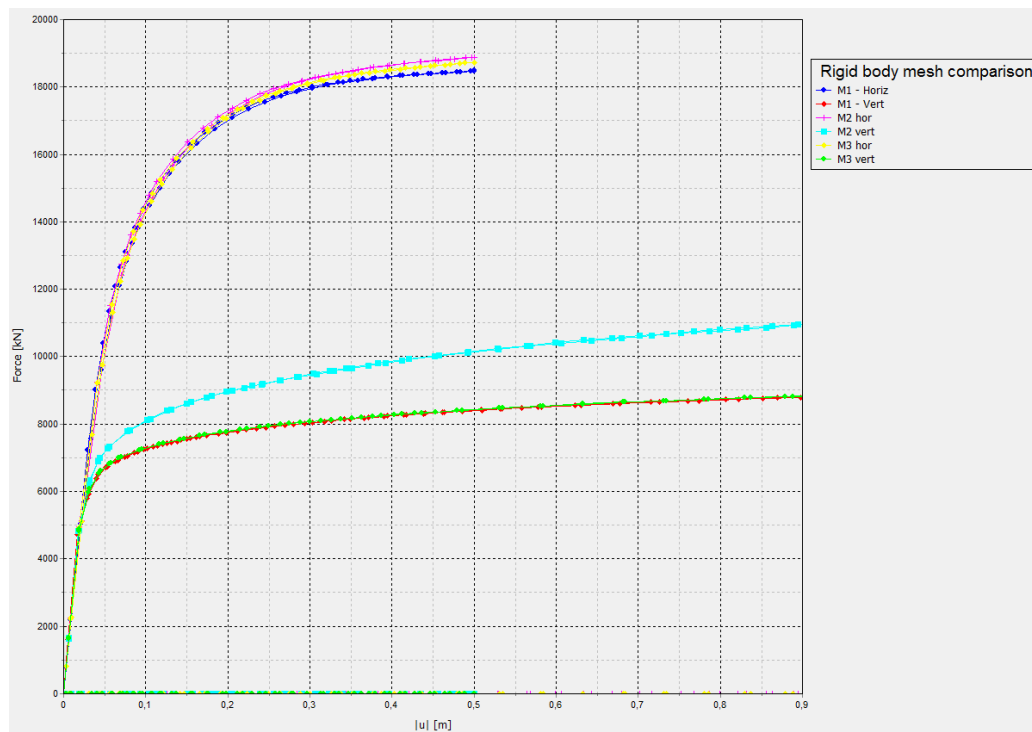
The final mesh contains 12 287 nodes and is shown in Figure 55.

Figure 55: Generated mesh



In order to investigate influence of mesh fineness on the results set of calculations was performed with different mesh coarseness.

Figure 56: Bearing capacity for different meshing, C3 case with soil rigid body

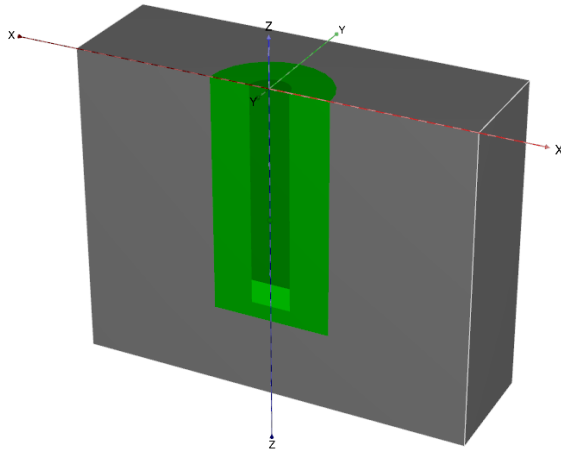


In the following parts of the model different coarseness factor was used:

- 1) The suction pile itself.
- 2) 3 m long prolongation of suction pile downwards.

3) Area around suction pile with radius 7.5 m and 5 m longer than suction pile.

Figure 57: Mesh coarseness factor changes



Three different meshing options were used, summarized in the Table 16.

Table 16: Mesh definitions – overall coarseness, coarseness factor (CF) and computation time

Name of generated mesh	Overall coarseness	Part 1 (CF)	Part 2 (CF)	Part 3 (CF)	Computation time of horizontal + vertical loading
M1	Coarse	0.5	0.1	0.25	22 min
M2	Very coarse	1	0.25	0.25	6 min
M3	Very coarse	1	0.1	0.25	8 min

To obtain all the results, many calculations had to be performed, as it was necessary e.g. for combined loading to run at least 15 simulations per model. To save computation time, comparison of mesh coarseness with computation time and bearing capacity was performed.

As expected, the lowest bearing capacity was obtained for the finest mesh (M1). The results for the same coarseness factor, but coarser *overall coarseness* (M3) showed almost identical results, but almost 3 times faster computation time. The coarsest mesh didn't show acceptable results, as the model was overestimating vertical bearing capacity significantly. Following this comparison, all simulations were performed for meshing option M3 with the best ratio *quality of the results/computation time*.

Staged construction

The aim of the calculations is to evaluate bearing capacity (vertical, horizontal and combined loading) and to find optimal loading point, i.e. the loading point, where is the vertical and horizontal bearing capacity the highest.

Phase 0: Initial conditions

The initial conditions are modelled using K_0 procedure with all soil clusters activated.

Phase 1: Anchor installation

In this stage construction of suction pile is simulated by plate or plate rigid body activation, respectively stiff soil body or soil rigid body. The rigid body has fixed displacement in y direction and fixed rotations around z and x axis, in the other directions is free to move. All interfaces are activated.

Phase 2: Loading

For plate and stiff soil body suction piles, point prescribed displacements are activated. For rigid bodies, the displacement is prescribed to the rigid body, fixities remains as in Phase 1.

The solver type is set to *Pardiso* and *Max load fraction per step* is set to 0.1.

7.2.3 Results

In this chapter are shown results of all models described in previous two chapters.

7.2.3.1 Optimal load attachment point

At first, it is necessary to find optimal load attachment point for all 4 hypothetical capacity cases (C1 – C4). The procedure consisted of prescribing 1.5 m vertical displacement, 1.0 m horizontal displacement or displacement in x and z direction with $|u|=1.2$ – combined loading. All the other displacements were fixed as well as rotations around z and x , only y rotation is free. The depth of the optimal load attachment point at the anchor wall will depend on the shear strength profile, the shear strength at the outside skirt wall, the load inclination and the depth to diameter ratio of the anchor.

Then, vertical, horizontal and combined bearing capacities were compared for different positions of load attachment point. The optimal load attachment point is the one with the highest bearing capacity.

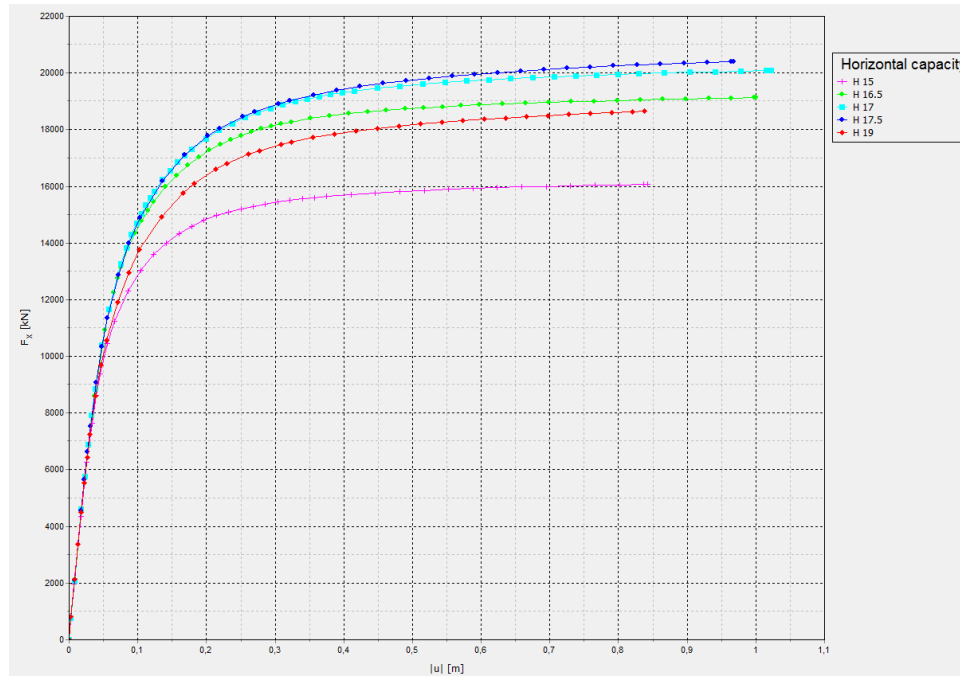
Optimal load attachment points for all the capacity cases are summarized in the following Table 17:

Table 17: Optimal load attachment point

Bearing capacity case	Position of the <i>optimal load attachment point</i> (depth in m)	Ratio <i>depth of an attachment point/suction pile length</i>
C1	17.5	0.7
C2	5.475	0.73
C3	17.5	0.7
C4	4.35	0.58

The example of obtained results for case C3 is shown in Figure 58, where horizontal bearing capacities for different load attachment points are compared:

Figure 58: Horizontal bearing capacity (C3)



7.2.3.2 Stiff soil body and soil volume rigid body – combined loading

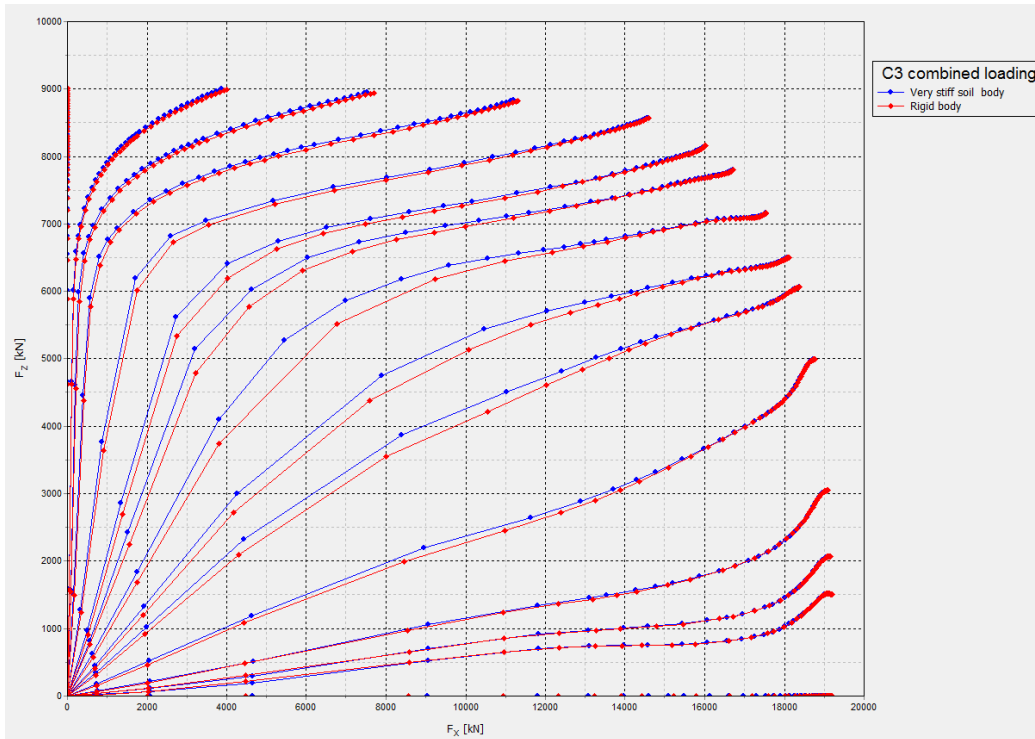
At the beginning, horizontal and vertical loading models were calculated, then, combined loading is carried out. The displacements u_x and u_z have prescribed ratio u_x/u_z changing in every calculation with constant value of $|u|=1.2\text{ m}$. In this way is carried out 15 calculations for rigid body and for stiff soil body. All the procedures are then repeated for every capacity case (C1 – C4). All the loading tests are summarized below:

- Horizontal loading, vertical loading, combined loading with u_x/u_z ratios: 1, 1.5, 2, 4, 10, 20, 40, 0.5, 0.25, 0.2, 0.1, 0.05 and 0.025.

For all of these test were created force/displacement curves and then combined together to form maximum bearing capacity curve in vertical reaction force F_z vs. horizontal reaction force F_x space.

At the end, Plaxis results for the rigid body and the stiff soil body were compared with each other. Example of this comparison for capacity case C3 is shown in Figure 59.

Figure 59: Combined loading of C3 case. In blue are shown results for very stiff soil body and in red for rigid body.



The resultant capacities coincide almost exactly for most of the cases with the biggest difference of 2% in F_x for nearly vertical loading, while difference in F_z is always below 1%.

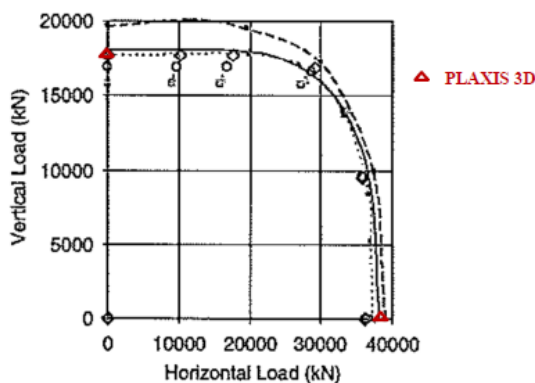
Then, both Plaxis results were compared with the results from numerous FEM studies published in (Andersen et al, 2005). Resultant bearing capacities are compared in following Table 18, while the results of Plaxis test are averaged to one number, as the difference is mostly insignificant. The results from (Andersen et al, 2005) are shown as an interval, as the article comprises many separate studies.

Table 18: Combined loading - comparison of Plaxis results and results from Andersen (2005).

Study case	Vertical loading (kN)	Horizontal loading (kN)
C1 Andersen	10300 - 11400	22000 – 23000
C1 Plaxis	10500	23000
C2 Andersen	2400 - 2700	1700 – 1800
C2 Plaxis	2460	1760
C3 Andersen	17500 - 18300	37000 – 39500
C3 Plaxis	18080	38400
C3 Plaxis plates	17500	39400
C4 Andersen	4000 - 4400	4000 - 4500
C4 Plaxis	4290	4410

For better representation, the Plaxis results of C3 case are compared with FEM capacity results published in (Andersen et al, 2005) in the Figure 60.

Figure 60: Comparison of Plaxis result with FEM results from (Andersen et al, 2005), C3 case.



7.2.3.3 Plate and plate rigid body - combined loading

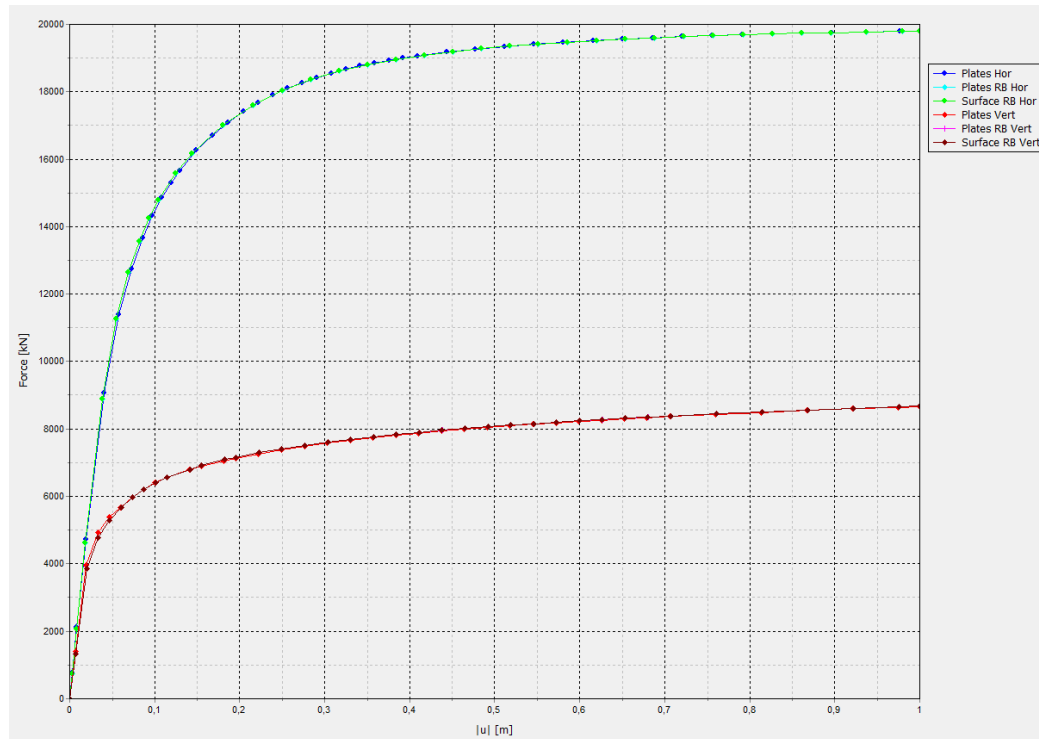
Horizontal, vertical and combined loading tests were carried out for C3 capacity case in the exactly same manner as in previous Chapter 7.2.3.2.

At first, it was necessary to compare results of rigid body defined from plates with rigid body defined from surfaces. The result is shown in Figure 61, where the curve for plate rigid body coincide exactly with the curve for surface rigid body, so it is almost impossible to see the latter one, as it is “behind” the plate rigid body curve.

Then, these results were compared with plate modelled suction pile with properties shown in Table 14. The biggest difference in ultimate bearing capacity between rigid body and plate suction pile is 20kN, while the bearing capacity ranges to 39 000 kN, so the difference is not

significant at all. The resultant bearing capacities are added in Figure 60 to results from (Andersen et al, 2005) and Plaxis model with soil volume rigid body.

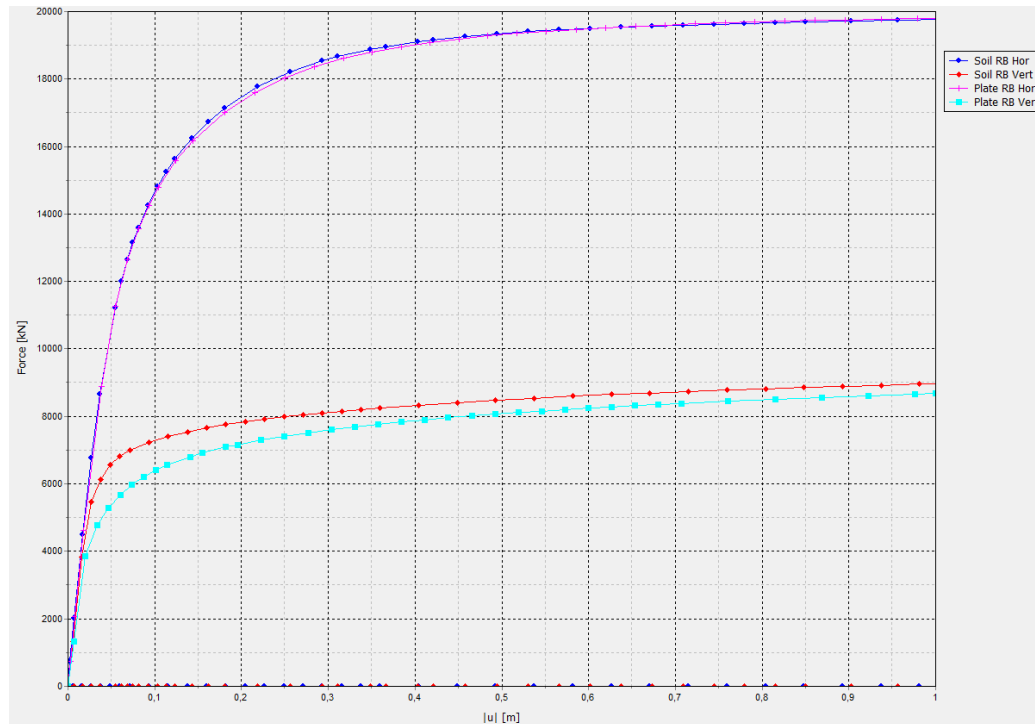
Figure 61: Plate/surface rigid body comparison with plate suction pile



The difference in ultimate bearing capacity between plate rigid body and soil volume rigid body is at first because the models are not corresponding to each other, as the reference points of the both models are in different positions in the suction pile. For the soil volume rigid body, the reference point is in the middle of the pile $[0, 0, z]$, so pure vertical displacement can be applied with no resulting rotation. This is not case of plate rigid body, where the reference point lies inside the plate (defined as rigid body in our case) at the position $[2.5, 0, z]$, which results in rotation even with pure vertical prescribed displacement.

To investigate it further, the model with soil and plate rigid body with the same reference point position was created. The results are shown in Figure 62. The horizontal capacity is the same, as during the horizontal pile movement, there is no activation on inner suction pile interfaces and no soil movement inside the pile. On the other hand, vertical capacity shows differences about 5% at ultimate state, as during the pull-out of the pile, inner interfaces are activated as the soil is “pulled out” off the pile.

Figure 62: Plate and soil rigid bodies with reference point at the same position.



7.3 CONCLUSION

At the beginning of this chapter were used models as simple as possible to allow verification by hand, for this purpose was used model of sliding block using Mohr-Coulomb criterion. Then after validation of behavior of interfaces the model was used to check the stability of the models with more rigid bodies, symmetry and comparison of plate, surface and soil volume rigid body. Then, all the basic calculation options used in Plaxis were verified for models with rigid bodies – plastic calculation, safety factor, consolidation and dynamics. All this verification examples were performed once for a model with very stiff structural elements and then for a model containing rigid bodies – then, the results were compared and in all cases same results were obtained.

After performing of basic validation, more complicated model was created. Because of the topic of the thesis, it was decided to use model of a suction pile with the results of bearing capacity of this particular suction pile and soil conditions obtainable in literature. Using this process it was possible to ensure, that the Plaxis kernel will be bug free for the case study of suction anchor described in Chapter 4, because the geometry and all the calculation processes were very similar.

At the beginning it was necessary to determine optimal load attachment point to find out ideal position of pad-eye to obtain highest possible bearing capacity. After that, combined horizontal and vertical loading was applied to the pile obtaining a bearing capacity locus in F_z vs. F_x space, then, these values were compared to results from literature. This procedure was used for soil volume, surface and plate rigid bodies, while all the results were compared to each other.

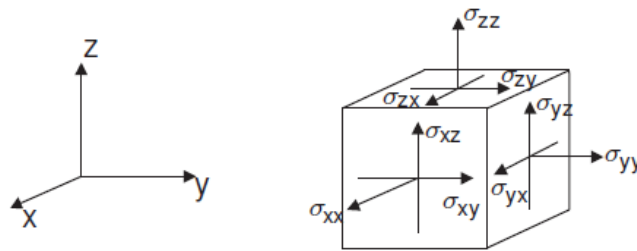
The first step was to obtain the same results as Andersen et al. (2004) for a Plaxis model with stiff structural elements, then, it was possible to compare all the Plaxis model to each other. Surface and plate rigid body models yielded exactly the same results as model using very stiff plates, in addition model with soil volume rigid body showed exactly the same results as very stiff soil volume. At the end these two models were compared and as it was expected they showed similar values for horizontal loading, but slightly different values for vertical loading, as the models were not corresponding to each other. The reason was, that in first case the whole suction pile with soil inside was modelled by rigid soil body and in second case suction anchor was modelled by plates with independent free to move soil inside.

8 APPENDIX B:

8.1 SIGN CONVENTION

Stresses computed in PLAXIS 3D are based on the Cartesian coordinate system shown in Figure 63. In all of the output data, compressive stresses and forces, including pore pressures, are taken to be negative, whereas tensile stresses and forces are taken to be positive. In Figure 63 are shown the positive stress directions.

Figure 63: Coordinate system and indication of positive stress components.



8.2 UNITS USED IN PLAXIS

The following Table 19 gives an overview of basic units used in Plaxis program.

Table 19: Basic units used in Plaxis.

Material properties		Forces and stresses	
Young's modulus	[kN/m ²]	Force	[N]
Cohesion	[kN/m ²]	Point loads	[kN]
Friction angle	[deg.]	Line loads	[kN/m]
Unit weight	[kN/m ³]	Distributed loads	[kN/m ²]
Permeability	[m/day]	Stresses	[kN/m ²]

8.3 GLOBAL ITERATIVE PROCEDURE USED IN PLAXIS

The equilibrium equation in discretized form is written as following:

$$\int B^T \Delta \sigma dV = \int N^T b^i dV + \int N^T t^i dS - \int B^T \sigma^{i-1} dV \quad (38)$$

The first term on the right-hand side together with the second term represent the current external force vector and the last term represents the internal reaction vector. The relation between stress increments and strain increments is usually non-linear. As a result, strain increments can generally not be calculated directly, and global iterative procedures are required to satisfy the equilibrium condition for all material points.

By substituting of the relationship between increments of stress and increments of strain:

$$\Delta\sigma = M \Delta\varepsilon \quad (39)$$

into equation (38) we obtain the formula for global iterative procedure:

$$K^i \Delta v^i = f_{ex}^i - f_{in}^{i-1} \quad (40)$$

In this equation K is a stiffness matrix, Δv is the incremental displacement vector, f_{ex} is the external force vector and f_{in} is the internal reaction vector. The superscript i refers the step number. As the relation between stress increments and strain increments is in the most cases non – linear, the stiffness matrix cannot be formulated exactly, but the global iterative procedure is required to satisfy both the equilibrium equation and the constitutive relation. The global iteration process can be written as:

$$K^j \delta v^i = f_{ex}^i - f_{in}^{j-1}$$

The superscript j refers to the iteration number. δv^i is a vector containing sub-incremental displacements, which contribute to the displacement of step i :

$$\Delta v^i = \sum_{j=1}^n \delta v^j$$

Where n is the number of iterations within step i . The stiffness matrix K represents the material behavior in an approximated manner. The more accurate the stiffness matrix, the fewer iterations are required to obtain equilibrium within a certain tolerance.

In its simplest form, K represents a linear – elastic response. In this case, the stiffness matrix can be formulated as:

$$K = \int B^T D^e B dV$$

Where D^e is the elastic material matrix according to Hooke's law and B is the strain interpolation matrix (Brinkgreve et al, 2013).

8.4 FINITE ELEMENT CALCULATION PROCESS BASED ON THE ELASTIC STIFFNESS MATRIX

The program starts with reading an input data, then, the stiffness matrix is formed:

$$K = \int B^T D^e B dV \quad (41)$$

Then, calculation procedure continues to the next step ($i \rightarrow i+1$), where new load vector (42) and reaction vector (43) are formed, the unbalance is calculated (44) and displacement increment is resented (45):

$$f_{ex}^i = f_{ex}^{i-1} + \Delta f_{ex} \quad (42)$$

$$f_{in} = \int B^T \sigma_c^{i-1} dV \quad (43)$$

$$\Delta f = f_{ex}^i - f_{in} \quad (44)$$

$$\Delta v = 0 \quad (45)$$

Then, in the new iteration ($j \rightarrow j+1$) the displacements are solved (46) and displacement increments are updated (47), then strain increments (48) and stresses (49) are calculated.

$$\delta v = K^{-1} \Delta f \quad (46)$$

$$\Delta v^i = v^{i-1} + \delta v \quad (47)$$

$$\Delta \varepsilon = B \Delta v, \delta \varepsilon = B \delta v \quad (48)$$

$$\sigma^{tr} = \sigma_c^{i-1} + D^e \delta \varepsilon \quad (49)$$

Then, the reaction vector is formed again (50) and from the result the unbalance is calculated (51).

$$f_{in} = \int B^T \sigma_c^{i-1} dV \quad (50)$$

$$\Delta f = f_{ex}^i - f_{in} \quad (51)$$

From the resultant force the error is calculated (52)

$$e = \frac{|\Delta f|}{|f'_{ex}|} \quad (52)$$

and the accuracy is checked: if resultant e from (52) has a higher value than $e_{tolerated}$, a new iteration is carried out and this whole procedure is repeated until the error is within the tolerance ($e < e_{tolerated}$).

9 CURRICULUM VITAE

PERSONAL INFORMATION

Name: **JAN JERMAN**
 Address: **FR. KOSÍKA 300, KLADNO 4, CZECH REPUBLIC**
 Telephone: **+420602651646**
 E-mail: **honza.jerman@gmail.com**

Nationality: Czech
 Date of birth: 29.7.1989

WORK EXPERIENCE

- Dates: February 2014 – June 2014
 - Name and address of employer: Plaxis BV, 2600 AN Delft, The Netherlands
 - Type of business or sector: Geotechnical software
 - Occupation or position held: Researcher – structural elements
 - Main activities and responsibilities: Development and verification of rigid body elements used in Plaxis 3D software
-

EDUCATION

- Dates: 2005 – 2009
- Name and type of organization providing education and training: Gymnasium Kladno
- Level in national classification: High school

- Dates: 2009 – 2012
- Name and type of organization providing education and training: Geology, Faculty of Science, Charles University in Prague, Czech Republic
 - Thesis: Modelling of soil asymptotic behavior using discrete element method (in *Czech*)
- Title of qualification awarded: BSc. (*summa cum laude*)

- Dates: 2012 – 2014
- Name and type of organization providing education and training: Applied Geology, Faculty of Science, Charles University in Prague, Czech Republic
 - Title of qualification awarded: MSc. (expected - 2014)

-
- Dates: 2013 – 2014
 - Name and type of organization providing education and training: Geomechanics, civil engineering and risks, Université Joseph Fourier, Grenoble France
 - Thesis: Evaluation of a rigid element for offshore application
 - Title of qualification awarded: MSc. (expected - 2014)
-

PERSONAL SKILLS AND COMPETENCIES

MOTHER TONGUE: **CZECH**

OTHER LANGUAGES:

- Skill level: **ENGLISH - FLUENT**
SPANISH – BASIC KNOWLEDGE
FRENCH – BASIC KNOWLEDGE
GERMAN – BASIC KNOWLEDGE
-

TECHNICAL SKILLS
AND COMPETENCIES: C++, Python – Basic knowledge
Plaxis – Experienced user

ADDITIONAL INFORMATION

Received scholarship for excellent study results during the whole bachelor's degree.

2nd place in „Geotechnical engineering bachelor's thesis in the Czech Republic, 2012“ organized by Fine and Mott MacDonald CZ with thesis *Modelling of soil asymptotic behavior using discrete element method.*